1992

Characteristics and applications of the short external cavity laser diode

Jin-Yong Kim
Iowa State University

INFORMATION TO USERS

This manuscript has been reproduced from the microfilm master. UMI films the text directly from the original or copy submitted. Thus, some thesis and dissertation copies are in typewriter face, while others may be from any type of computer printer.

The quality of this reproduction is dependent upon the quality of the copy submitted. Broken or indistinct print, colored or poor quality illustrations and photographs, print bleedthrough, substandard margins, and improper alignment can adversely affect reproduction.

In the unlikely event that the author did not send UMI a complete manuscript and there are missing pages, these will be noted. Also, if unauthorized copyright material had to be removed, a note will indicate the deletion.

Oversize materials (e.g., maps, drawings, charts) are reproduced by sectioning the original, beginning at the upper left-hand corner and continuing from left to right in equal sections with small overlaps. Each original is also photographed in one exposure and is included in reduced form at the back of the book.

Photographs included in the original manuscript have been reproduced xerographically in this copy. Higher quality 6" x 9" black and white photographic prints are available for any photographs or illustrations appearing in this copy for an additional charge. Contact UMI directly to order.

U·M·I

University Microfilms International
A Bell & Howell Information Company
300 North Zeeb Road, Ann Arbor, MI 48106-1346 USA
313/761-4700 800/521-0600

Order Number 9234825

Characteristics and applications of the short external cavity laser diode

Kim, Jin-Yong, Ph.D.

Iowa State University, 1992

U·M·I
300 N. Zeeb Rd.
Ann Arbor, MI 48106

Characteristics and applications of the short external cavity laser diode

by

Jin-Yong Kim

A Dissertation Submitted to the
Graduate Faculty in Partial Fulfillment of the
Requirements for the Degree of
DOCTOR OF PHILOSOPHY

Department: Electrical Engineering and Computer Engineering
Major: Electrical Engineering

Approved:

Signature was redacted for privacy.

In Charge of Major Work

Signature was redacted for privacy.

For the Major Department

Signature was redacted for privacy.

For the Graduate College

Iowa State University
Ames, Iowa

1992

TABLE OF CONTENTS

CHAPTER 1. INTRODUCTION

The word laser is an acronym for Light Amplification by Stimulated Emission of Radiation. A laser is a light amplifier which is capable of producing an intense beam of photons having identical scalar and vector properties. The ideas leading to the laser can be traced back to a theory of light emission proposed by Albert Einstein in 1917 [1]. However, the full implications of that work were not realized until much later. The principles of laser action were first described by Townes and Schawlow in 1958 [2]. The invention of the maser, which is the microwave equivalent device, by Charles Townes in 1959 stimulated a lot of research work. Finally, the first visible laser was demonstrated by Theodore Maiman in May 1960 [3] at Hughes Aircraft Corporation. Maiman's laser was small, consisted of a ruby rod, with its ends silvered to reflect light, which he placed inside a spring-shaped flashlamp. At room temperature, ruby is a three-level laser. In November 1960, Peter Sorokin and Mirek Stevenson of the IBM T. J. Watson Research Center succeeded in lasing uranium laser [4], which was the first four-level laser. The four-level approach avoids the need to depopulate the ground state, making the population inversion easier.

These successes were only a beginning. Many gas laser systems and solid-state lasers followed soon thereafter. Recent years have brought new systems like the tunable dye laser and short wavelength excimer laser. During the past three decades, laser technology has found a tremendous range of applications. Lasers are used in pure scientific research such as ultraprecise measurements of time and length. In industry lasers drill holes, cut metal and plastic, and perform welding, engraving, scribing, fusing, hardening, marking, and

melting. In medicine, lasers perform surgery, treat blindness caused by diabetes, and clean arteries. In stores, lasers read the striped symbols of the Universal Product Code. The range of applications for lasers continues to widen, not only in professional applications but in consumer electronics as well. The development of semiconductor lasers extends the application area remarkably.

In 1962, Robert Hall demonstrated the first gallium-arsenide injection lasers [5] at General Electric's Research and Development Laboratories. Shortly after Hall, three independent groups reported similar devices. Those early devices required cryogenic cooling even for pulsed operation. Continuous wave oscillation of a semiconductor laser at room temperature was achieved in 1970. By 1975, semiconductor lasers able to emit continuously reached the commercial market. Steady technical advances helped trigger a tremendous expansion in the semiconductor laser market that continues today.

Semiconductor lasers, also denoted as laser diodes, differ from other laser systems due to their small size and light weight, large gain per unit length, wide gain spectrum, low mirror reflectivities , and mass-productivity by the same photolithographic techniques as electronic circuits. These unique properties of the laser diodes make them widely used as key elements in diverse optoelectronic systems. Though specially designed heterojunction light emitting diodes (LEDs) are used as light sources in optical communication systems with modest requirements in terms of bandwidths and fiber link distances, the use of laser diodes in optical communication offers the broader opportunity for producing high-performance systems. The gas lasers used as light sources for the early laser printers and optical disk player

systems (such as video disk players) have been replaced by the small laser diodes. Recently, research and developments in strained-layer quantum well laser diodes, high power arrays, surface emitting laser diodes, and miniature visible wavelength laser diodes have been making steady progress, and will eventually produce a variety of new applications for laser diodes.

When a laser diode is operated in any kind of optical communication system, it is practically impossible to be free from the external optical feedback that takes place when a part of the output power is coupled back into the laser diode cavity after being reflected at an external surface. Operating characteristics of laser diodes are strongly affected by this external optical feedback. External feedback results in variations in threshold current, output power and output spectra of lasers.

Depending on the application, even a relatively small amount of feedback may cause either beneficial or harmful effects to the laser diode operation. It may provide advantages for a number of applications requiring greater spectral purity and frequency stability than can be obtained typically from a solitary laser diode (without feedback). External cavity laser diode configurations are sometimes used to induce short optical pulse generation. In this case, the external cavity contains a focusing lens, a mirror, and possibly a wavelength control filter to produce optical feedback. The device is then actively modelocked by applying a repetitive electrical pulse stream with a period equal to the laser roundtrip time. Understanding the optical feedback effect on the properties of laser diodes may lead to the building of a sensor system such as a laser diode radar, which detects the range and velocity of the object, or an optical disk head, which detects the difference in reflectivities of pre-recorded

bits on the optical disk. Long access times due to relatively heavy optical head have been a big problem for read-only optical disk drives and a potential problem for erasable optical memory. By adopting the external cavity configuration, an optical disk head can be fabricated with only a small assembly of a laser diode chip and a photo detector, so that access times can be reduced dramatically owing to the head's light weight. In laser feedback interferometry, the optical-path dependent phase of the feedback results in a modulation of the threshold current when a weakly reflecting target is included in the lasing system. The modulation of the threshold current manifests itself in variations in the optical power output and energy consumption of the laser. The laser itself becomes a phase-sensitive detector.

However, reflections from the optical components, e.g., coupling lenses or fiber endfaces, may sometimes contribute to deterioration of performance in optical communication systems. For an extreme example, under a certain feedback condition, laser linewidth may become enormously broadened to the order of 25 GHz and instabilities may occur, so practically laser diodes can not be used as a light source of the high performance communication system in this feedback regime.

Following the first analysis of Lang and Kobayashi [6], a number of theoretical and experimental studies of external optical feedback have been undertaken during the last decade so that the influence of feedback has been widely discussed. And it is in fact still such an active research area that dozens of research papers are published each year.

Much of the previous work has focussed on the laser diodes coupled to distant reflectors (long external cavity) in order to investigate the influence of

the reflections at optical interfaces such as lenses. Inherently, feedback level is usually low so that the multiple reflection effect can be ignored in the theoretical analysis for this case, as in Lang and Kobayashi's model. On the other hand, the short external cavity laser diodes are usually designed and formed intentionally for the purpose of stabilizing the mode characteristics or making laser diode sensors. Interestingly, this short external cavity case has been less extensively studied, even though it has more direct applications than the long external cavity laser configuration, partly because the strong coupling feature makes the dynamical model become too complicated to be analyzed.

In this dissertation work, we study the effect of optical feedback to the laser diode. We mainly focus on the laser diode coupled to a short external cavity by developing model equations appropriate to analyze this configuration. The stationary and dynamical characteristics are investigated as well as the chaotic behavior of the modulated external cavity laser diode. Special emphasis is placed on the ultra short external cavity case, for which little investigation has been made. Throughout this work, the ultra short external cavity implies the case of external cavity length $d \leq 20$ μm, where the optical output power shows extremely sensitive dependence on the change in the external cavity length, and the short external cavity covers 20 μm $\leq d \leq 5$ mm.

Chapter 2 presents a brief review of the previous work about the external cavity laser diodes, and gives a motivation for this work.

In Chapter 3, we derive our model equations which are used in later analyses. The rate equations are derived when the effective reflectivity due to

the external feedback causes an additional loss and phase change to the original rate equations of the solitary laser diode. The multiple reflection effect is included in the model as a form of infinite series of time-delayed terms. This model equation can generally be used to describe any kind of feedback configuration, either weak or strong, long or short. The effective reflectivity operator in the infinite series form is reduced to the closed form with a short external cavity length approximation.

Chapter 4 deals with the stationary solutions of our model equations, and discusses some of the basic properties of external cavity laser diodes. Also the open resonator model suited for the ultra short external cavity configuration is introduced. Based on the open resonator theory, we show that the coupling coefficient becomes a complex function of the external cavity length and the near field beam size of the laser diode.

In Chapter 5, the dynamical properties of the external cavity laser diode are discussed. The rate equations are solved numerically to show the time evolution of the laser parameters. An investigation of the instabilities and chaotic behavior of the autonomous external cavity system are also contained in this chapter.

Chapter 6 deals with the chaotic behaviors in the current-modulated external cavity laser diode. The subharmonic waveforms are obtained by numerical simulation. The bifurcation diagrams and the return maps are plotted for the various external cavity situations. It is shown for the first time that the period-doubling route to chaos is not the only route to chaos in this case.

Using the open resonator model derived in Chapter 4, the optical disk head is analyzed in Chapter 7. In order to make the external cavity optical disk head more practical, a large tolerance in flying height is preferred. The criterion for this tolerance which is useful for the design of the optical disk head is derived. The chapter also reports experimental results of the thermal bump distribution on metal coated glass, by configuring a laser diode and metal film as an external cavity laser diode sensor. This experiment is another good example of the external cavity laser diode as a displacement sensor, as well as helping in the understanding of the liftoff effect in the photoinductive method, which is one of the new techniques in the nondestructive evaluation area.

Finally, Chapter 8 presents the conclusions.

CHAPTER 2. REVIEW OF THE PREVIOUS WORK AND STATEMENT OF THE PROBLEM

Review of the Previous Work

With the progress of optoelectronics, there has been an increasing interest in sophisticated coherent optical communication systems. Such systems directly employ the optical frequency or phase as a carrier, so they need extremely stable and narrow spectral characteristics. The linewidth of a Fabry-Perot type or a DFB solitary laser emitting at $\lambda = 1.3$ μm is usually larger than 50 MHz. For optimum use in a coherent optical communication system, the spectral characteristics have to be improved considerably. In the search for a stable narrow-linewidth source, it has been shown that the spectrum of laser diodes may be reduced in width by optically coupling an external cavity to the laser [7-12]. A semitransparent Au-coated GRIN-rod lens and a short spherical reflector are used to build an external cavity configuration, which reduces the laser linewidth to submegahertz [12]. External cavity lengths of the order of 10 cm are used yielding spectral linewidths in the order of a few kHz [13], where a diffraction grating is used to make strong, frequency-selective feedback.

However, it is also well known that optical feedback from reflections at fiber end faces may generate intensity noise in regular laser diodes, and the laser linewidth may broaden or split under the influence of feedback if the phase of the feedback is not controlled [14-17]. Tkach and Chraplyvy [14] experimentally show that the weak feedback level (as small as - 71 dB) can reduce or broaden the laser linewidth according to the feedback phase in the long external cavity configuration with external cavity length $d = 40$ cm. A

successful external cavity design makes use of the constructive interference of light reflected back into the laser diode cavity to enhance one mode relative to the other modes within the gain bandwidth. The conditions for optimum design of an external cavity laser diode have been investigated to obtain a single mode source [18]. It is recommended that laser diode cavity length $L < 200\ \mu m$, and external cavity length $50\ \mu m < d < 200\ \mu m$ may be suitable for obtaining the single- longitudinal mode under high-speed modulation conditions. However, external cavity laser diodes are often sensitive to small current and temperature changes. By mounting the laser and external GaAs mirror chip on the same heatsink, temperature-stabilized external cavity laser diodes have been fabricated [19,20], and nowadays they are commercially available. It is shown that lasing mode may not hop in the usual temperature region (in a range of more than 46°C), and wavelength deviation is kept within 3 Å over 24°C for a certain configuration [20]. With the progress of integrated optic technology, monolithic external cavity lasers have been fabricated yielding a potential for economic production and providing better mechanical stability [21-24].

As mentioned before, laser properties may deteriorate if the feedback phase is not carefully chosen. Especially for a long distant external reflection, these detrimental effects become more pronounced. The low-frequency intensity fluctuation and the transient optical response were experimentally studied [16,25]. It was asserted that the observed low frequency fluctuations, the light intensity recovery after a sudden drop to zero in a stepwise manner, each corresponding to an external cavity roundtrip time occur due to an intrinsic instability (not a mechanical instability) of the external cavity

configuration [26]. For a long external cavity, in a time interval less than the roundtrip time of external cavity τ, the reflected feedback term may be considered as an injection of the stationary solution, since during such a short time, the reflected field can not respond to any changes. This coherent feedback assumption for a long external cavity was introduced first in Henry and Kazarinov [27]. It is referred to as the injection locking assumption [28], and used to show that the low frequency fluctuation is due to a bistability phenomenon, which accounts for the first sudden intensity drop. The subsequent intensity build-up is described as an iterative extension of the injection locking formalism.

The coherence collapse phenomena [29], which include a spectral broadening of the order of several 10 GHz, and a kink in the light output versus current characteristics, have been studied, and it is shown that it is not due to the quantum fluctuation noise, but due to the inherent dynamical properties of the external cavity laser diode. Tkach and Chraplyvy [30] experimentally classified the regimes of feedback effects into five different regions as a function of feedback power ratio and external cavity length. They showed that the coherence collapse region is bounded by the high feedback level and the low feedback level, i.e., coherence collapse may occur at moderate feedback level. But their investigation was limited to the long external cavity configuration.

Even though there were a lot of theoretical investigations in the 1970's, e.g., [31-33], Lang and Kobayashi's model [6] has commonly been used to analyze the external cavity laser diode exposed to weak or moderate feedback levels [34,35]. The model is obtained by adding a delayed feedback field to the

usual rate equation for the complex electric field of the solitary laser diode. The linewidth enhancement factor introduced by Henry [36] has been added to Lang and Kobayashi's original model to permit the inclusion of a gain-dependent frequency shift effect in analyses [28,37,38]. Slightly different forms of rate equations have been used in numerical and analytical studies [39-41], but basically they are just slight variations or rearrangements of Lang and Kobayashi's model. In the numerical work performed by Schunk and Peterman [41], it is found that the lasing mode with the minimum linewidth is most stable rather than the mode with minimum threshold gain. However, since these models neglect the multiple reflection effects, they are valid only for the weak feedback level.

Recently, a flying optical disk head has successfully demonstrated the capability to read and write signals to the phase-change optical recording medium [42,43], where the external cavity length between laser diode and recording surface is only several μm. Also, a very short external cavity laser diode has been used as a diode laser sensor [44,45] and studied for various applications [46,47]. In order to further investigate the properties of the short external cavity, the multiple reflection effect should be included in the model equations. The steady state lasing conditions of a short external cavity laser have been studied by approximating the external cavity as a simple Fabry-Perot plane resonator [48-50] taking into account the multiple reflections. A simple formula for the spectral linewidth of the external cavity laser diode is given in the literature [50]. A special feature introduced in Sato and Ohya [50] is that the effective reflectivity is treated as a function of the phase coherence time. It is asserted that the feedback wave cannot couple coherently with the field

inside the diode cavity when the external cavity roundtrip time is much longer than the phase coherence time. As an another attempt to improve the model, the divergence angle of the output beam is included as one of the variables, assuming an elliptical Gaussian beam is exiting from the laser facet [51]. In the recent work by Hui and Tao [52], light intensity and phase are treated as random variables in stationary stochastic process and develop the differential rate equations for external cavity laser diodes which are applicable to any amount of external feedback. The works cited above seem to be successful in explaining the observed tendency of property change in the short external cavity laser diode, but there are still many aspects that should be investigated. For example,the output power versus external cavity length characteristic shows a considerably different pattern for the very short external cavity, which takes place in optical disk head application. And none of previous work investigates the dynamical characteristics of the short external cavity laser diode. It is, therefore, highly desirable to have a model that can properly describe the coupling phenomenon in an ultrashort and short external cavity laser diode.

Statement of the Problem

The goal of this dissertation work is to study the stationary and nonlinear dynamic characteristics of the laser diode with optical feedback. Emphasis will be placed on the short external cavity and ultra short external cavity case throughout this work. It is because there has been little investigation for these feedback regimes, but there are much more benevolent applications in these

regions, such as a laser diode sensor, an optical disk head, and a temperature-stabilized single mode external cavity laser package. Various temporal and spectral characteristics will be investigated. And efforts will be made to find an optimum operating condition, (for example, optimum external cavity length) by comparing and discussing the properties as they vary the external feedback phase.

The most general governing dynamic equations will be derived, which include the multiple reflection effects. It is very important to set up any model to correctly describe what happens physically, but the solvability of the model can not be neglected. Our general model equations will be reduced to the forms which allow either analytical or numerical analysis of the short external cavity laser diode with appropriate approximations.

The stationary and dynamical properties will be investigated by solving developed model equations. A constant coupling factor will be used in most parts of the analysis, but for the ultra short external cavity, we will introduce the complex coupling coefficient in order to properly describe the coupling phenomenon [53] for the first time. This complex coupling coefficient has come from the inherent diffractive property of the open resonator, and is supported by new experimental results--the asymmetry in output power versus external cavity length characteristics [54]. This complex coupling -coefficient concept, which results from the open resonator model, is very useful and necessary for describing and analyzing the ultra short external cavity laser diode.

Dynamical characteristics will be studied both numerically and analytically to examine the transient waveform of the laser parameters. The dynamical

stability condition will be presented too. Chaotic behavior of the autonomous system will be discussed. And the route to chaos for the current-modulated nonautonomous system will be investigated in detail.

Finally some applications of this work will be given.

CHAPTER 3. DERIVATION OF MODEL EQUATIONS

In this chapter we derive the model equations used for the theoretical consideration in the following chapters. The theoretical investigations of the long external cavity laser diodes with weak feedback level have usually been based on the model developed by Lang and Kobayashi [6], which is obtained by adding a single delayed field term to the usual rate equation for the solitary laser diode. Here, we will present our basic model equations, which can describe the characteristics of the short external cavity laser diode better.

Effective Reflectivity Operator considering Multiple Reflections

A laser diode of length L coupled to an external cavity of length d is shown in Figure 3.1(a). Here ρ_1 and ρ_2 are the field amplitude reflectivities of the laser diode facets, and ρ_m is that of the external reflector. The equivalent laser diode is shown in Figure 3.1(b), where the influence of the external cavity is integrated in an expression for the effective facet field amplitude reflectivity ρ_e. P_1 and P_2 represent the power output at each facet. We will describe the optical field $\beta(t)$ of the laser as

$$\beta(t) = E(t) \exp(j\omega_0 t) \tag{3.1}$$

where E(t) is the slowly varying complex amplitude function, and ω_0 is the angular frequency of the solitary laser diode. Note that the solitary laser diode is assumed to oscillate in a single longitudinal mode. Also, we will neglect the

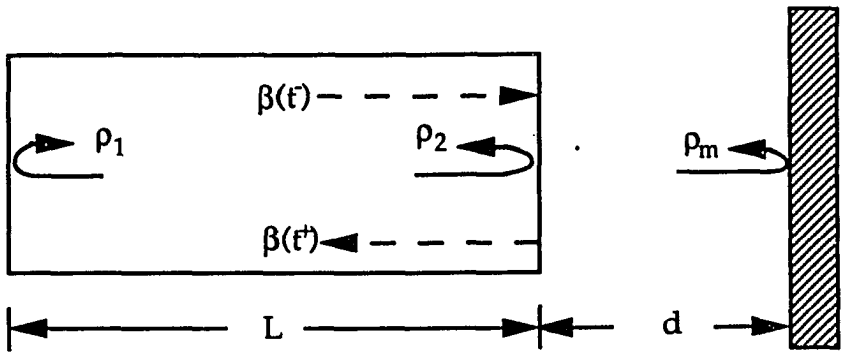

(a)

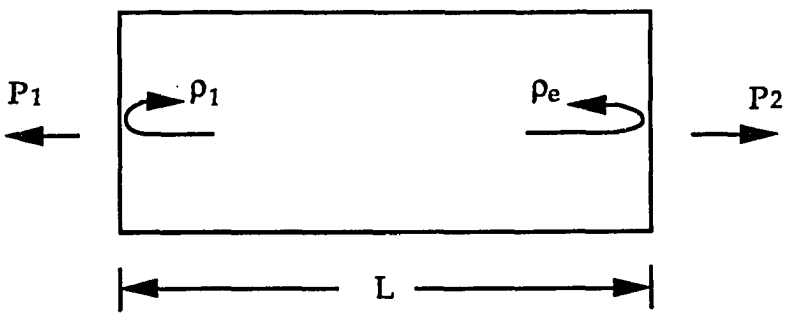

(b)

Figure 3.1. (a) Configuration of an external cavity laser diode

(b) The equivalent laser diode

spatial dependence of the optical mode. The complex amplitude E(t) can be expressed in terms of two real quantities: photon density S(t) and phase $\Phi(t)$

$$E(t) = \sqrt{S(t)}\, \exp[j\Phi(t)] \tag{3.2}$$

Consider that the optical field $\beta(t^-)$ has arrived at the facet 2 at time t^-. At time t^+, $\beta(t^+)$ can be expressed as the sum of the reflected field from facet 2 and the multiple injected field due to the external reflector,

$$\beta(t^+) = \rho_2\, \beta(t^-) - \frac{1-R_2}{\rho_2} \sum_{n=1}^{\infty} [\, c_n\, \beta(t^- - n\tau)\, (-\rho_2\rho_m)^n \,] \tag{3.3}$$

where the power reflectivity of the laser diode facet

$$R_2 = |\rho_2|^2 \tag{3.4}$$

and the roundtrip time in the external cavity is given as

$$\tau = \frac{2d}{c} \tag{3.5}$$

The coupling coefficient c_n represents the fractional amount of coupled field into the laser diode at the n-th reflection. Now, the effective field amplitude reflectivity ρ_e can be expressed as

$$\rho_e \equiv \frac{\beta(t^+)}{\beta(t^-)} = \rho_2 - \frac{1-R_2}{\rho_2} \sum_{n=1}^{\infty} \left[c_n \frac{\beta(t-n\tau)}{\beta(t)} (-\rho_2\rho_m)^n \right] \tag{3.6}$$

Let's define a normalized feedback factor Z(t) as

$$Z(t) \equiv \frac{\rho_e}{\rho_2} \tag{3.7}$$

then, Z(t) can be written using Eq.(3.1), (3.2) and (3.6) as,

$$Z(t) = 1 - \frac{1-R_2}{R_2} \sum_{n=1}^{\infty} \left[c_n \sqrt{\frac{S(t-n\tau)}{S(t)}} (-\rho_2\rho_m)^n \exp\{-j(n\omega_0\tau + \Phi(t) - \Phi(t-n\tau))\} \right] \tag{3.8}$$

Derivation of Rate Equations for a Solitary Laser Diode

The interchange of energy between electrons and photons in a laser diode is governed by spontaneous and stimulated emission processes. The rate of energy transfer between electrons and photons is described by rate equations. The linewidth enhancement factor α was introduced by Henry [36] in order to explain the measured linewidth, which was about 50 times greater than that predicted by the modified Schawlow-Townes formula. The linewidth enhancement factor

$$\alpha = \frac{\Delta\mu'}{\Delta\mu''} \tag{3.9}$$

is the ratio of the changes in the real and imaginary parts of the refractive index with change in carrier density. In AlGaAs and InGaAsP lasers α is about 4 - 7 [36, 37] . We will first derive the rate equations for the solitary laser following Henry [36]. The wave equation for the electric field is

$$\frac{\partial^2}{\partial z^2} E_T(z,t) = \frac{1}{c^2} \frac{\partial^2}{\partial t^2} \{ \varepsilon_r E_T(z,t) \} \tag{3.10}$$

The solution can be written as

$$E_T(z,t) \approx \beta(t) \exp(-jkz) + c.c. \tag{3.11}$$

where $\beta(t)$ is the time dependent term represented as Eq.(3.1) and k is the wave number. To take into account that the change in the dielectric constant ε_r due to dispersion, which is caused by the time dependence of E(t), we may write,

$$\omega' = \omega_0 - j \frac{\dot{E}}{E} \tag{3.12}$$

where ω' denotes the effective angular frequency, and

$$\dot{E} = \frac{\partial}{\partial t} E$$

Therefore ε_r at ω' is

$$\varepsilon_r(\omega') \equiv \varepsilon_r(\omega_0) - j\,\frac{\dot{E}}{E}\,\frac{\partial}{\partial\omega}\varepsilon_r \tag{3.13}$$

Substitution of Eq.(3.11) and (3.13) into (3.10) will give the following first order differential equation, if we neglect the higher order derivative terms.

$$\frac{2j\omega_0}{c^2}\left(\varepsilon_r + \frac{\omega_0}{2}\,\frac{\partial}{\partial\omega}\varepsilon_r\right)\dot{E}(t) = \left(\frac{\omega_0^2}{c^2}\varepsilon_r - k^2\right)E(t) \tag{3.14}$$

This approximation may be expressed as a "slow varying approximation", since it is assumed

$$\omega_0\,\dot{E}(t) >> \ddot{E}(t)$$

The dielectric constant ε_r is complex and can be written as

$$\varepsilon_r = (\mu' - j\,\mu'')^2 \tag{3.15}$$

where μ' and μ'' are a real and an imaginary part of the refractive index respectively. The imaginary part μ'' determines the net gain according to

$$g - \alpha_r = -\frac{2\omega_0}{c}\,\mu'' \tag{3.16}$$

where g is the gain per unit length, and α_r is the loss, including facet losses, which are usually approximated as uniformly distributed over the cavity. At threshold $g = \alpha_r$, ε_r is real and ω_0 is chosen so that

$$\frac{\omega_0}{c}\mu' = k \tag{3.17}$$

Changes in electron density will cause μ' and μ'' to deviate from the threshold values, and ε_r becomes

$$\begin{aligned}\varepsilon_r &= [\,(\mu'+\Delta\mu') - j\,(\mu''+\Delta\mu'')\,]^2 \\ &\cong (\mu')^2 - 2j\mu'\Delta\mu''(1+j\alpha)\end{aligned} \tag{3.18}$$

since $\mu'' \approx 0$ around the threshold. Here, α is the linewidth enhancement factor as defined in Eq.(3.9). The bracketed term on the left side of Eq.(3.14) is related to the group velocity v_g:

$$\begin{aligned}\varepsilon_r + \frac{\omega_0}{2}\frac{\partial}{\partial\omega}\varepsilon_r &\cong (\mu')^2 + \frac{\omega_0}{2}\cdot 2\mu'\cdot\frac{\partial}{\partial\omega}\mu' \\ &= \mu'\left[\,\mu' + \omega_0\frac{\partial\mu'}{\partial\omega}\,\right] = \mu'\cdot\frac{c}{v_g}\end{aligned} \tag{3.19}$$

Substituting Eq.(3.17), (3.18) and (3.19) into (3.14) gives

$$\begin{aligned}\dot{E}(t) &= -\frac{\omega_0}{c}\,v_g\,\Delta\mu''\,(1+j\alpha)\,E(t) \\ &= \frac{(g-\alpha_r)}{2}\,v_g\,(1+j\alpha)\,E(t)\end{aligned} \tag{3.20}$$

The gain per unit length is related to the stimulated emission coefficient G (can be called the gain per unit time) as

$$G = g \cdot v_g \tag{3.21}$$

and similarly the loss per unit length is related to the photon lifetime τ_{ph} as

$$\frac{1}{\tau_{ph}} = \alpha_r \cdot v_g \tag{3.22}$$

If we define the net gain per unit time ΔG as

$$\Delta G = G - \frac{1}{\tau_{ph}} = (g - \alpha_r) v_g \tag{3.23}$$

the final equation for E is

$$\dot{E}(t) = \frac{1}{2} \Delta G \, (1+j\alpha) \, E(t) \tag{3.24}$$

For later use, we redefine the loss term α_r as [55]

$$\alpha_r = \alpha_s + \frac{1}{L} \ln \left(\frac{1}{\rho_1 \rho_2} \right) \tag{3.25}$$

where α_s accounts for any optical loss within the laser cavity which does not yield a generation of carriers within the active layer, as for example scattering losses, and facet losses represented by the second term. Throughout this work, ρ_1 and ρ_2 are considered as real values, and the power reflectivities of laser facets are defined as;

$$R_i = | \rho_i |^2, \quad (i = 1, 2) \tag{3.26}$$

Lax and Louisell [56, 57] showed that, starting with a fully quantum mechanical model of a laser, the quantum problem can be transformed into a classical problem of calculating the statistical properties of a fluctuating wave field. The laser, like many classical systems having several variables fluctuating in time, satisfies a set of first-order ordinary differential equations that include random Langevin forces. The role of the Langevin force is to account for how the statistical distribution of the variable changes in time. In the laser diode, the Langevin noise force is arising from spontaneous emission [55] and should be added to Eq. (3.24). However, in our discussion, the noise effect due to the Langevin forces will be neglected. Further discussion about the Langevin noise can be found in several papers [37, 58, 59].

In addition to Eq. (3.24), a rate equation for the carriers is required, yielding for the carrier density N(t):

$$\dot{N}(t) = \frac{J(t)}{q \cdot d_{act}} - \frac{N(t)}{\tau_s} - G(N)\, S(t) \tag{3.27}$$

where J(t) is the current density injected into the active region (supplied by the bias current) with thickness d_{act} , q is the electron charge, τ_s is the carrier lifetime, G(N) is the stimulated emission coefficient as defined in Eq. (3.21), and S(t) is the photon density. Note that the stimulated emission coefficient G(N) is a function of the carrier density N, and can be expressed as

$$G(N) = G_N (N - N_o) \tag{3.28}$$

where G_N is the gain constant, and N_o is the carrier density at transparency. However, if we include the nonlinear gain compression effect , G_N can be modeled as

$$G_N(\text{nonlinear}) = G_N (1 - \kappa S) \tag{3.29}$$

where κ is the gain compression coefficient [55], which is zero in the linear gain model. Since a net gain is zero at threshold, Eq. (3.23) and (3.28) give

$$G(N_{th}) = G_N (N_{th} - N_o) = \frac{1}{\tau_{ph}} \tag{3.30}$$

Model Equations for the General External Cavity Laser Diode

Since Lang and Kobayashi [6] suggested that external feedback may be described by adding a time-delayed term $\kappa_f E(t-\tau)$ to the standard laser equation (where κ_f is a feedback coefficient), a lot of work has used a similar model to analyze the behavior of the external cavity laser with weak feedback. Henry [37] included the effect of an α - parameter, and gave the expression as following:

$$\dot{E}(t) = \frac{1}{2} \Delta G (1+j\alpha) E(t) + \kappa_f E(t-\tau) \exp[-j\omega_0\tau] \tag{3.31}$$

where

$$\kappa_f = \frac{(1-R_2)}{\tau_{in}} \frac{\rho_m}{\rho_2} \tag{3.32}$$

τ_{in} is the roundtrip time in the laser diode cavity, and

$$R_m = |\rho_m|^2 \tag{3.33}$$

is the power reflectivity of the external reflector.

In the case of the long external cavity laser, Eq. (3.31) has been working well in describing its characteristics with little variation in its expression, according to the authors [28, 40, 41, 60-62]. Evidently, Eq. (3.31) is valid only for weak feedback levels. The purpose of this section is to present a derivation of a similar rate equation valid for the short external cavity laser in which the feedback level is generally strong.

There have been a lot of efforts to include the multiple reflection effects in analyzing the short external cavity laser [48,51,52,63]. The concept of an additional loss caused by an external cavity was introduced [51] and added to the rate equation intuitively [52] without proper derivation. Following the same steps used in the previous section, we can obtain the rate equation which is universally applicable to any kind of external cavity laser.

The normalized feedback factor Z(t), which is shown in Eq. (3.8), is a complex function. We will define

$$Z(t) = |Z| \cdot \exp[j\theta_Z] \tag{3.34}$$

The effective loss per unit length with external feedback α_{rf} becomes a complex function:

$$\alpha_{rf} = \alpha_s + \frac{1}{L} \ln\left(\frac{1}{\rho_1 \rho_2 Z}\right)$$

$$= \alpha_r - \frac{1}{L} \ln Z \tag{3.35}$$

where a real value α_r is defined in Eq. (3.25). The net gain equation of Eq. (3.16) is changed into

$$g - \mathrm{Re}[\alpha_{rf}] = g - \alpha_r + \frac{1}{L} \ln|Z| = -\frac{2\omega_0}{c} \mu'' \tag{3.36}$$

and the wave number equation of Eq. (3.17) is also altered to

$$\frac{\omega_0}{c} \mu' = k - j\frac{\theta_Z}{2L} \tag{3.37}$$

Using Eq. (3.36) and (3.37) instead of (3.16) and (3.17) will yield the following differential equation:

$$\dot{E}(t) = \left[\frac{\Delta G}{2}(1+j\alpha) + \frac{1}{\tau_{in}} \ln\{Z(t)\}\right] E(t) \tag{3.38}$$

where

$$\ln \{ Z(t)\} = \ln |Z| + j\,\theta_Z \tag{3.39}$$

and we use the relationship of

$$\tau_{in} = \frac{2L}{v_g} \tag{3.40}$$

Eq. (3.38) holds for any case, since Z as defined in Eq. (3.8) has no approximation. Now from Eq. (3.38) we may generate two coupled differential equations with the real valued variables S(t) and $\Phi(t)$. Considering

$$S(t) = E(t) \cdot E^*(t) \tag{3.41}$$

$$\Phi(t) = \frac{j}{2} [\, \ln E^*(t) - \ln E(t) \,] \tag{3.42}$$

we can easily yield the rate equations for the photon density and phase easily by differentiating Eqs. (3.41) and (3.42) and sustituting Eq. (3.38)

$$\dot{S}(t) = \left[\Delta G + \frac{2}{\tau_{in}} \ln |Z(t)| \right] S(t) \tag{3.43}$$

$$\dot{\Phi}(t) = \frac{\alpha}{2} \Delta G + \frac{1}{\tau_{in}} \theta_Z(t) \tag{3.44}$$

Again, we want to mention that we ignore all noise terms including the spontaneous emitting noise power.

Slow Varying and Short External Cavity Length Approximation

We can make the form of the normalized feedback factor Z(t) in Eq. (3.8) easy to handle with some approximation. The first approximation we will use is:

$$c_n = r^n \tag{3.45}$$

This approximation implies that the reflectivity of the external reflector reduces to $r\rho_m$ due to absorption or coupling losses. In many cases r may be assumed as a constant [64] or modeled to be a function of external cavity length d [51]. More rigorous analysis shows that r is also a function of n [53], which will be discussed in the next chapter. But, except for the ultra short external cavity case, Eq. (3.45) is a fine approximation. The parameter r can be treated as an experimentally-measured factor.

The following approximation can be justified in the case of short external cavity length:

$$S(t-n\tau) \cong S(t) - n\tau \dot{S}(t) \tag{3.46}$$

$$\Phi(t-n\tau) \cong \Phi(t) - n\tau\dot{\Phi}(t) \tag{3.47}$$

The external cavity roundtrip time τ is only 1 psec at d = 150μm. Considering the $(-\rho_2\rho_m)^n$ term in Eq. (3.8), the effect of the n-th reflections for n>10 is small enough to be neglected. Therefore, within the interested time scale (order of nsec, considering the speed of the photodetector), the approximation

made in Eq. (3.46) and (3.47) is valid up to d = several cms. The last assumption we will make in this section is the slow varying amplitude approximation for S(t). Actually this is the basic assumption used to yield our rate equation in Eq. (3.14). Therefore the following assumption automatically holds, once the rate equation can be successfully applied.

$$\sqrt{\frac{S(t-n\tau)}{S(t)}} \cong \sqrt{1 - n\tau \frac{\dot{S}(t)}{S(t)}} \cong 1 - \frac{n\tau}{2} \frac{\dot{S}(t)}{S(t)}$$
$$\cong \left[1 - \frac{\tau}{2} \frac{\dot{S}(t)}{S(t)} \right]^n \tag{3.48}$$

Substituting Eq. (3.45), (3.47) and (3.48) into (3.8) yields

$$Z_a(t) = \frac{1 + \frac{r\rho_m}{\rho_2} \left(1 - \frac{\tau}{2} \frac{\dot{S}(t)}{S(t)} \right) \cdot \exp\left[-j\{\omega_0 + \dot{\Phi}(t)\}\tau\right]}{1 + \rho_2 (r\rho_m) \left(1 - \frac{\tau}{2} \frac{\dot{S}(t)}{S(t)} \right) \cdot \exp\left[-j\{\omega_0 + \dot{\Phi}(t)\}\tau\right]} \tag{3.49}$$

where subscript a in $Z_a(t)$ implies that it is an approximated value.

With definitions of

$$U(t) \equiv \frac{\dot{S}(t)}{S(t)} \tag{3.50}$$

$$\Omega(t) \equiv \omega_0 + \dot{\Phi}(t) \tag{3.51}$$

$Z_a(t)$ can be rewritten into

$$Z_a(U,\Omega) = \frac{1 + \frac{r\rho_m}{\rho_2}\left(1 - \frac{\tau}{2}U\right)\cdot \exp\left[-j\Omega\tau\right]}{1 + \rho_2\left(r\rho_m\right)\left(1 - \frac{\tau}{2}U\right)\cdot \exp\left[-j\Omega\tau\right]} \tag{3.52}$$

and the rate equations in Eq. (3.43) and (3.44) become

$$U(t) = \Delta G(N) + \frac{2}{\tau_{in}} \ln\left|Z_a(U,\Omega)\right| \tag{3.53}$$

$$\Omega(t) = \omega_0 + \frac{\alpha}{2}\Delta G(N) + \frac{1}{\tau_{in}}\theta_{Z_a}(U,\Omega) \tag{3.54}$$

where

$$Z_a(t) = \left|Z_a\right| \cdot \exp\left[j\theta_{Z_a}\right] \tag{3.55}$$

CHAPTER 4. STATIONARY SOLUTIONS AND BASIC PROPERTIES OF EXTERNAL CAVITY LASER DIODES

In this chapter, we consider the stationary solutions of our model equations derived in the previous chapter, and we discuss some basic properties of them. Due to the presence of an external cavity, the stationary solution (the phase and amplitude condition) is modified compared to the solitary laser diode. The influence of an external cavity has been widely explored theoretically as well as experimentally [48,50,62,65-68] . Numerous papers have focussed on analyzing the long and weak external cavity, since the reflection from the optical fiber ends or other optical components such as lenses, and beam splitters can change the properties of a laser diode dramatically [10,14,15,69-72].

A short external cavity laser diode can be used as a phase sensor [73], and in some cases, can improve the spectral characteristics of a solitary laser diode. Therefore, the characteristics of the short external cavity laser have been also the subject of many studies [18,49,51,74,75]. The properties of external cavity laser diodes are governed essentially by the external cavity length d and the strength of feedback level. It is impossible to find model equations which can explain all phenomena and can be applied to all external cavity configurations. The following section will consider the stationary solutions and several features of external cavity laser diodes, mainly laying stress on the short external cavity. The second section will deal with the special case, the ultra short cavity case, in which the open resonator model will be introduced.

Stationary Solutions and their Characteristics

We have three coupled differential equations, Eqs. (3.27), (3.43) and (3.44). for the carrier density, photon density and phase. A set of stationary solutions can be defined as

$$\begin{aligned} S(t) &= S_s \\ \Phi(t) &= \Delta\omega_s \cdot t \\ N(t) &= N_s \end{aligned} \tag{4.1}$$

where the subscript s implies the stationary solution. $\Delta\omega_s$ is the stationary shift in angular frequency due to the external cavity. Now, we obtain from Eqs. (3.50) and (3.51)

$$U(t) = 0 \tag{4.2}$$

$$\Omega(t) = \omega_0 + \Delta\omega_s \equiv \Omega_s \tag{4.3}$$

for the stationary solution, where Ω_s is the angular frequency of the external cavity laser diode. If we use the slow varying and short external cavity length approximation we discussed in the chapter 3, Eqs. (3.52), (3.53), (3.54) and (3.27) are reduced to in the stationary case:

$$Z_{as}(0, \Omega_s) = \frac{1 + \frac{r\rho_m}{\rho_2} \exp[-j\Omega_s\tau]}{1 + \rho_2(r\rho_m) \exp[-j\Omega_s\tau]} \tag{4.4}$$

$$0 = \Delta G(N_s) + \frac{2}{\tau_{in}} \ln \mid Z_{as}(0,\Omega_s) \mid \tag{4.5}$$

$$\Omega_s = \omega_0 + \frac{\alpha}{2}\Delta G(N_s) + \frac{1}{\tau_{in}} \theta_{Z_{as}}(0,\Omega_s) \tag{4.6}$$

$$0 = \frac{J_b}{q \cdot d_{act}} - \frac{N_s}{\tau_s} - G(N_s)\, S_s \tag{4.7}$$

where J_b denotes the bias current density. Equation (4.5) gives a threshold gain condition for the external cavity laser diode,

$$\Delta G(N_s) = G(N_s) - \frac{1}{\tau_{ph}} = G_N (N_s - N_{th})$$

$$= -\frac{2}{\tau_{in}} \ln |Z_{as}(0,\Omega_s)| \tag{4.8}$$

where N_{th} is the threshold carrier density for a solitary laser diode. Without external reflection (i.e. $\rho_m = 0$), $N_s = N_{th}$. When the external feedback is introduced, the required gain for the threshold is either reduced or increased depending on the phase $\Omega_s\tau$, and shows a quasi-periodic function of τ, in other words, a function of d.

A phase condition is obtained by substituting Eq. (4.5) into Eq. (4.6):

$$\Omega_s\tau = \omega_0\tau + \frac{\tau}{\tau_{in}} [\, \theta_{Z_{as}}(0,\Omega_s) - \alpha \ln |\, Z_{as}(0,\Omega_s)|\,] \qquad (4.9)$$

Rigorously speaking, the actual phase condition should add the multiple of 2π to the right hand side of the equation. Without feedback, $Z_{as} = 1$, $\theta_{Zas} = 0$, and $\ln |\, Z_{as}\,| = 0$. Therefore Ω_s is simply equal to ω_0. With feedback, the shifted Ω_s can be calculated from Eq. (4.9). A graphical representation of Eq. (4.8) and (4.9) can give the qualitative explanation about spectral properties of the external cavity laser diodes. This method has been well-developed for the weak coupling case [62,66] . Once Ω_s is determined from Eq. (4.9), N_s and S_s will be easily calculated from Eqs. (4.7) and (4.8).

For later use, let's define some functions of angular frequency ω, as

$$L(\omega) \equiv \ln \sqrt{\frac{1 + \dfrac{(r\rho_m)^2}{\rho_2^2} + \dfrac{2r\rho_m}{\rho_2}\cos(\omega\tau)}{1 + \rho_2^2 (r\rho_m)^2 + 2r\rho_2\rho_m \cos(\omega\tau)}} \qquad (4.10)$$

$$C(\omega) \equiv 1 + (r\rho_m)^2 + \frac{r\rho_m}{\rho_2}(1+\rho_2^2)\cos(\omega\tau) \qquad (4.11)$$

$$D(\omega) \equiv \frac{r\rho_m}{\rho_2}(\rho_2^2 - 1)\sin(\omega\tau) \qquad (4.12)$$

Then, we obtain

$$\ln |\, Z_{as}(0,\Omega_s)| = L(\Omega_s) \qquad (4.13)$$

$$\theta_{Z_{as}}(0,\Omega_s) = \tan^{-1}\frac{D(\Omega_s)}{C(\Omega_s)} \tag{4.14}$$

Our gain and phase condition, Eqs. (4.8) and (4.9) will be reduced to the conditions for weak feedback [28, Eq. 7] in the limit of small $r\rho_m$. Therefore, we assert that our threshold condition is applicable both to weak and strong feedback. It is interesting that though our derivation assumes a short external cavity, the resulting threshold condition is reduced to the same as those which are used for the long external cavity case.

Function L, C, and D, defined as Eqs. (4.10), (4.11), and (4.12), are plotted in Figures 4.1, 4.2, and 4.3 respectively. The abscissa represents a phase $\omega\tau$, and the ordinate represents the function value. In the legend, the external reflectivity is expressed as

$$R'_m \equiv r^2 R_m \tag{4.15}$$

where R'_m includes the effect of coupling losses as defined in Eq.(3.45).

Now, we are ready to discuss the graphical solving method for the phase (oscillating frequency change) condition. Equation (4.9) can be rewritten as

$$\Omega_s\tau - \omega_0\tau = \frac{\tau}{\tau_{in}}\left[\tan^{-1}\frac{D(\Omega_s)}{C(\Omega_s)} - \alpha\, L(\Omega_s)\right] \tag{4.16}$$

Figure 4.4 shows an example of the graphical method. The abscissa represents a phase $\Omega_s\tau$, and the ordinate shows a calculated value of Eq. (4.16). The straight line shows the left hand side (LHS) of Eq. (4.16) and the curve with high Q

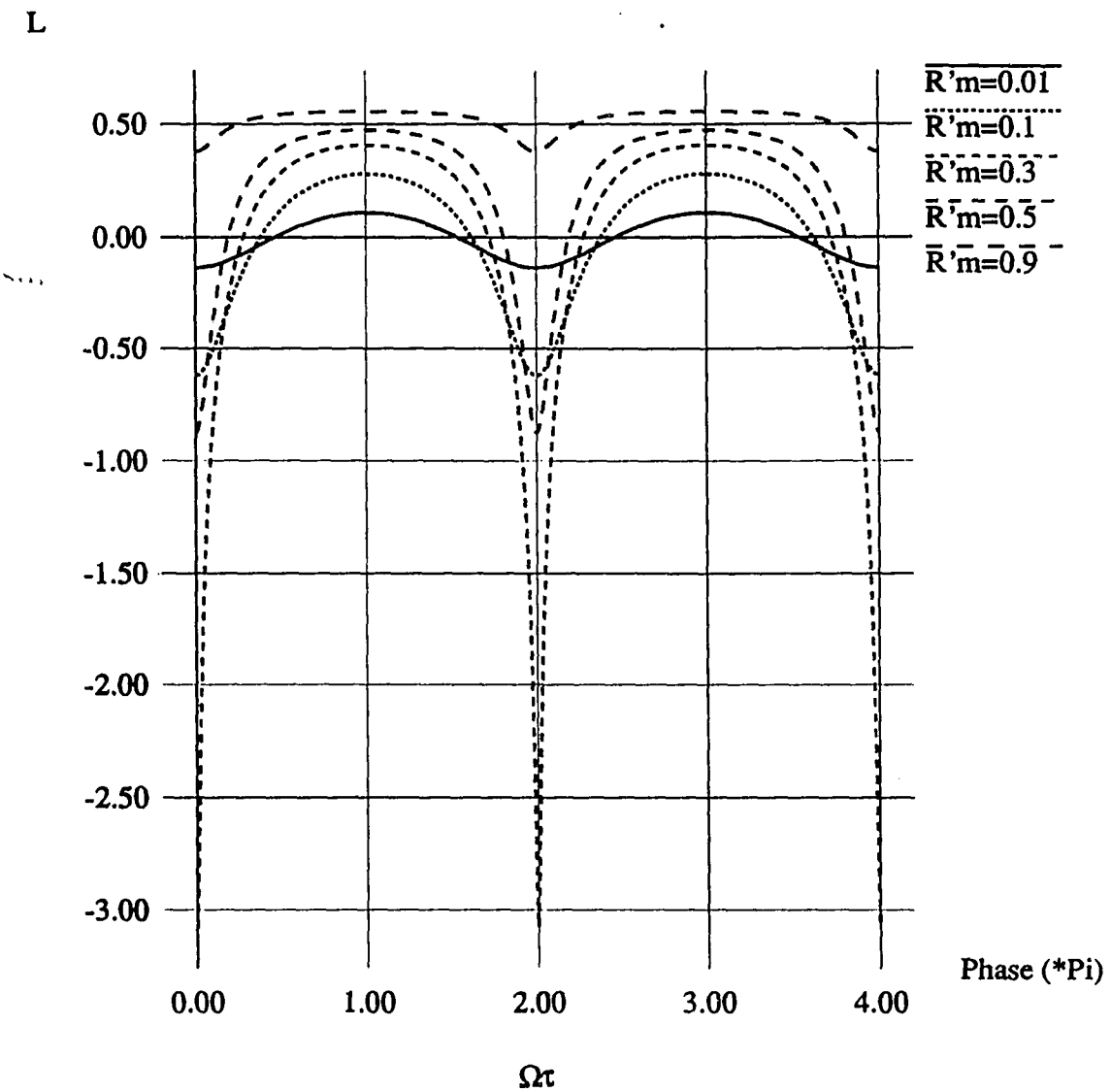

Figure 4.1. Function L

C

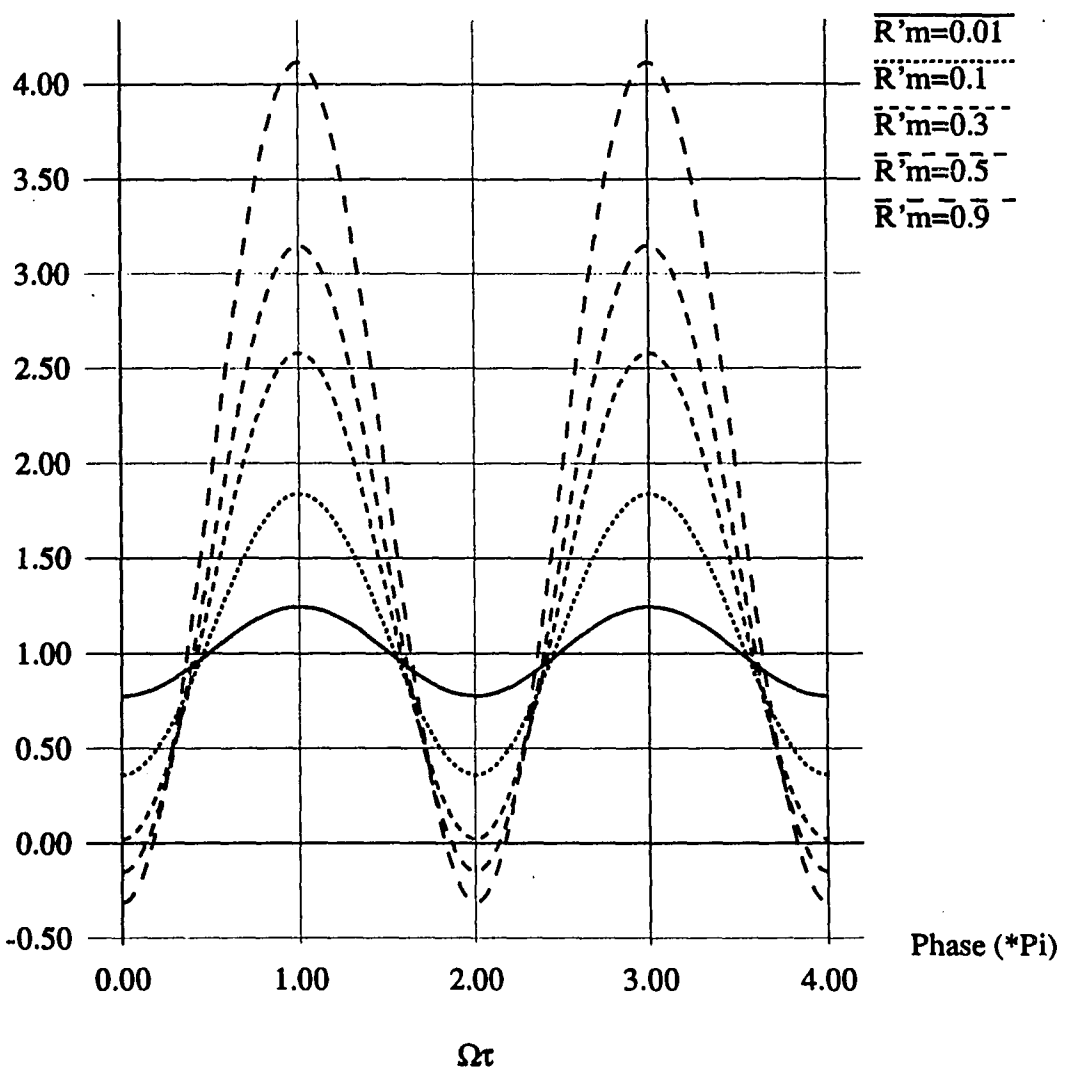

Figure 4.2. Function C

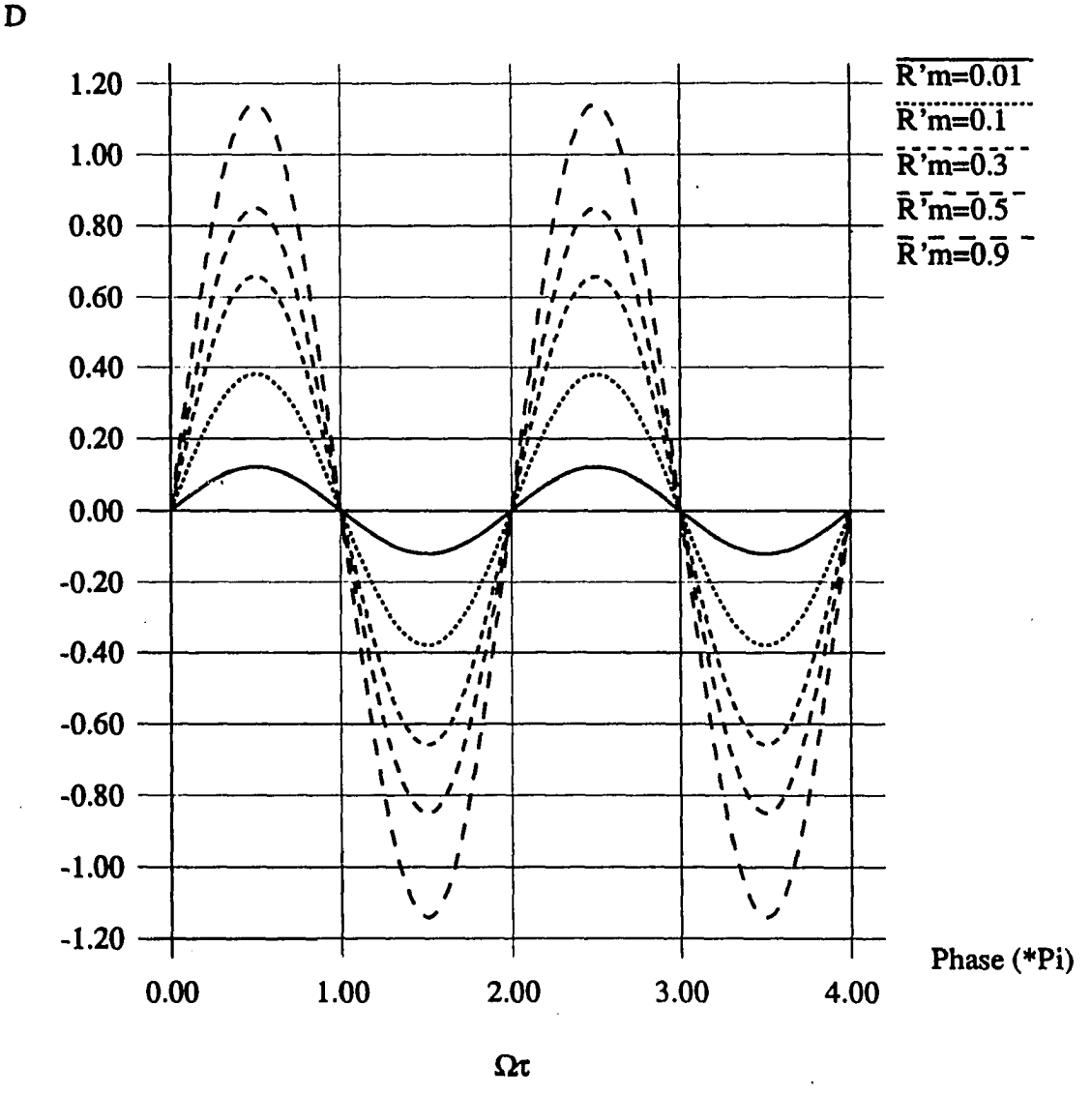

Figure 4.3. Function D

factor represents the right hand side (RHS) of Eq. (4.16). The sinusoidal curve represents the equation obtained with the weak coupling approximation [28, Eq.7]. In the legend μ_e represents the effective refractive index of the gain medium. The zero crossing point of the straight line is $\omega_0\tau$. The intersecting point of the straight line and the curve meets the new phase condition for the external cavity laser, and the oscillating frequency is changed to Ω_s from ω_0. The frequency of the solitary laser ω_0 can easily be tuned as temperature changes or bias current changes. The roundtrip time τ is also easily controlled by increasing or reducing the external cavity length d. Therefore, the point $\omega_0\tau$ may be moved between 0 and 2π by controlling one of the following factors: temperature, bias current, or external cavity length d.

As $\omega_0\tau$ moves, the straight line moves parallel to the previous one, and the oscillating frequency of the external cavity laser Ω_s changes correspondingly. Since the reflectivity of the external reflector is relatively high, $R'_m = 0.2$, a considerable difference between our model and that of the weak coupling approximation can be noticed. The difference may be more significant in the situation shown in Figure 4.5. The external cavity length d is now increased to 300 μm. Since the RHS of Eq. (4.16) is proportional to τ, the amplitude of the curve becomes larger compared to the case in Figure 4.4. As a result, we have three intersecting points, which means there is a possibility to support three external cavity modes (the stability of these modes will be discussed later) . However, if we use the phase condition derived from the weak coupling approximation (using the sinusoidal curve), we still end up with only one possible lasing mode.

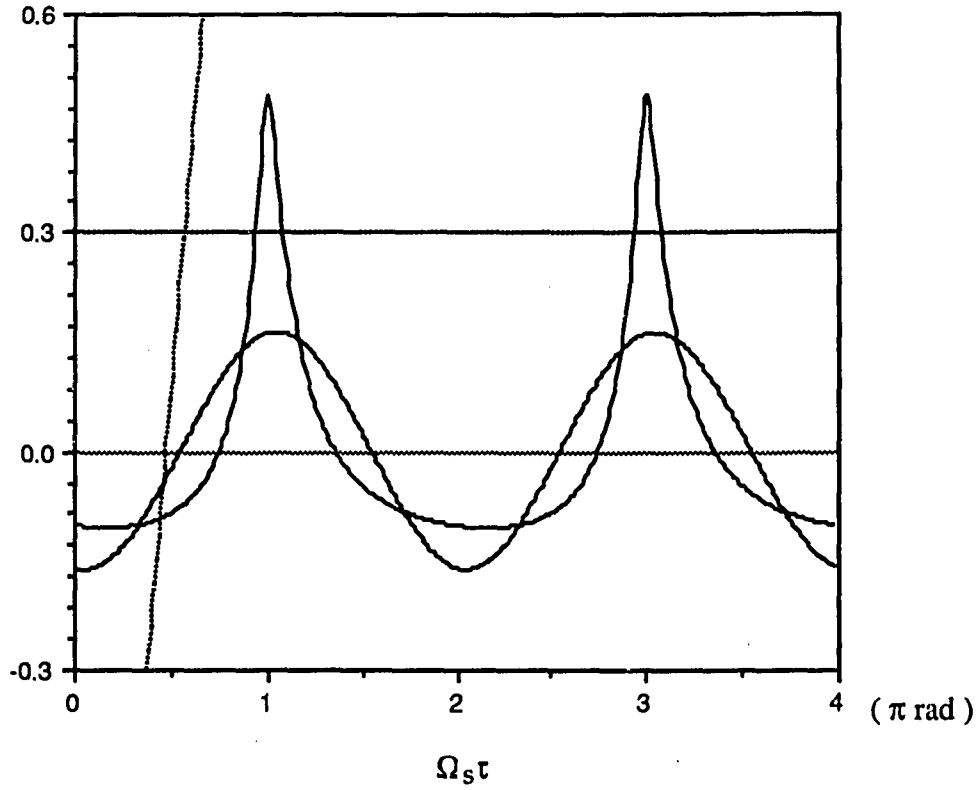

Figure 4.4. Graphical solving method for the phase condition, where the straight line shows the left hand side of Eq.(4.16), the curve with high Q factor represents the right hand side of Eq. (4.16), and the sinusoidal curve represents the equation obtained with the weak coupling approximation : The parameters used are d = 50 μm, L = 250 μm, μ_e = 4.5, R_2 = 0.32, R'_m = 0.2 and α = 6

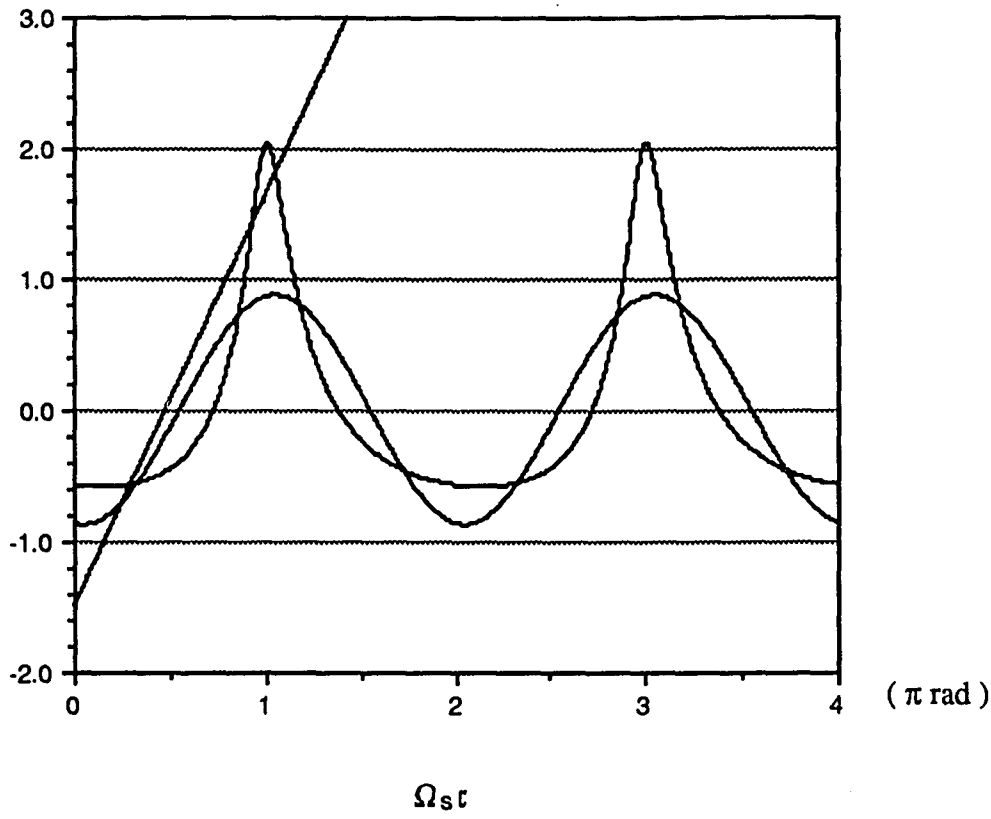

Figure 4.5. Graphical solving method for the phase condition, where the straight line shows the left hand side of Eq.(4.16), the curve with high Q factor represents the right hand side of Eq. (4.16), and the sinusoidal curve represents the equation obtained with the weak coupling approximation : The parameters used are d = 300 μm, L = 250 μm, μ_e = 4.5, R_2 = 0.32, R'_m = 0.2 and α = 6

In Figure 4.6, we show a totally different type of function (RHS of Eq. (4.16)) compared to the sinusoidal curve in the case of $R'_m > R_2$. A gradual change of the shape of RHS is plotted in Figure 4.7 as R'_m is increased.

Now, we will include the gain modulation effect of Eq. (4.8) in our discussion of lasing mode. Let's define the mode spacing of the laser diode cavity

$$\delta f \equiv \frac{1}{\tau_{in}} = \frac{c}{2\,\mu_e\,L} \tag{4.17}$$

and the mode spacing of the external cavity

$$\delta f_e \equiv \frac{1}{\tau} = \frac{c}{2\,d} \tag{4.18}$$

and the laser gain bandwidth of the gain curve due to the stimulated emission defined in Eq. (3.21) as

$$\Delta f_{gain} \equiv \text{FWHM of material gain curve of solitary laser} \tag{4.19}$$

For GaAs,

$$\frac{1}{40} > \frac{\Delta f_{gain}}{f_0} > \frac{1}{70} \tag{4.20}$$

for the nominal carrier density level [55], where

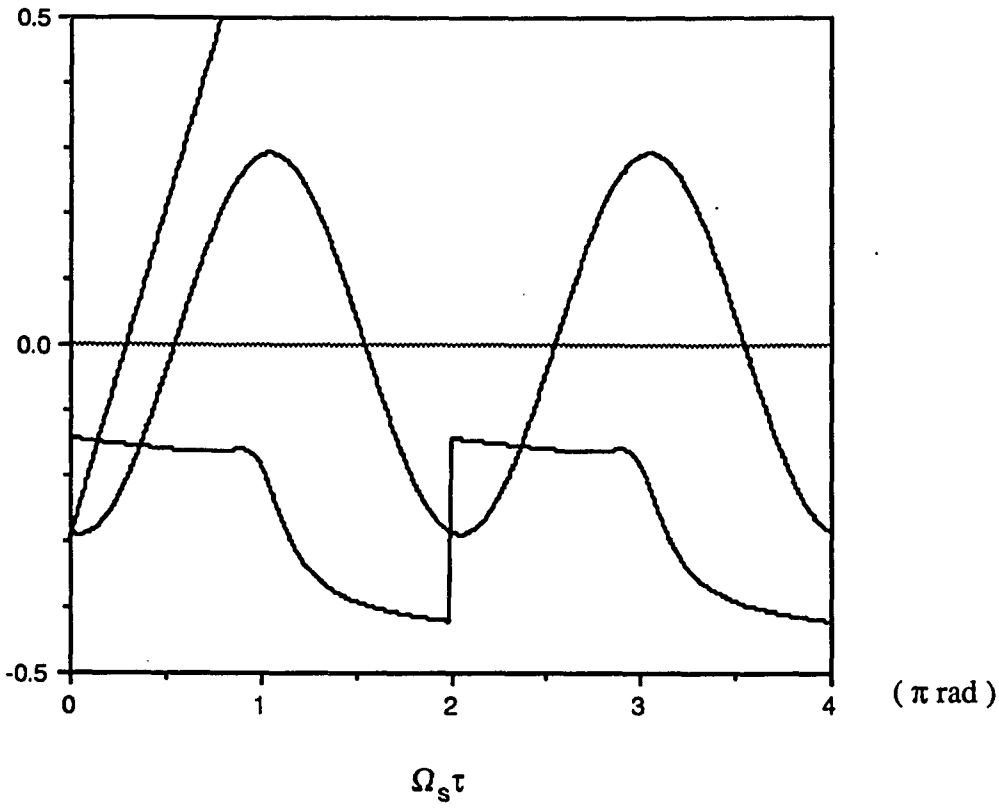

Figure 4.6. Graphical solving method for the phase condition, where the straight line shows the left hand side of Eq.(4.16), the curve with rather square form represents the right hand side of Eq. (4.16), and the sinusoidal curve represents the equation obtained with the weak coupling approximation : The parameters used are d = 50 μm, L = 250 μm, μ_e = 4.5, R_2 = 0.32, R'_m = 0.8 and α = 6

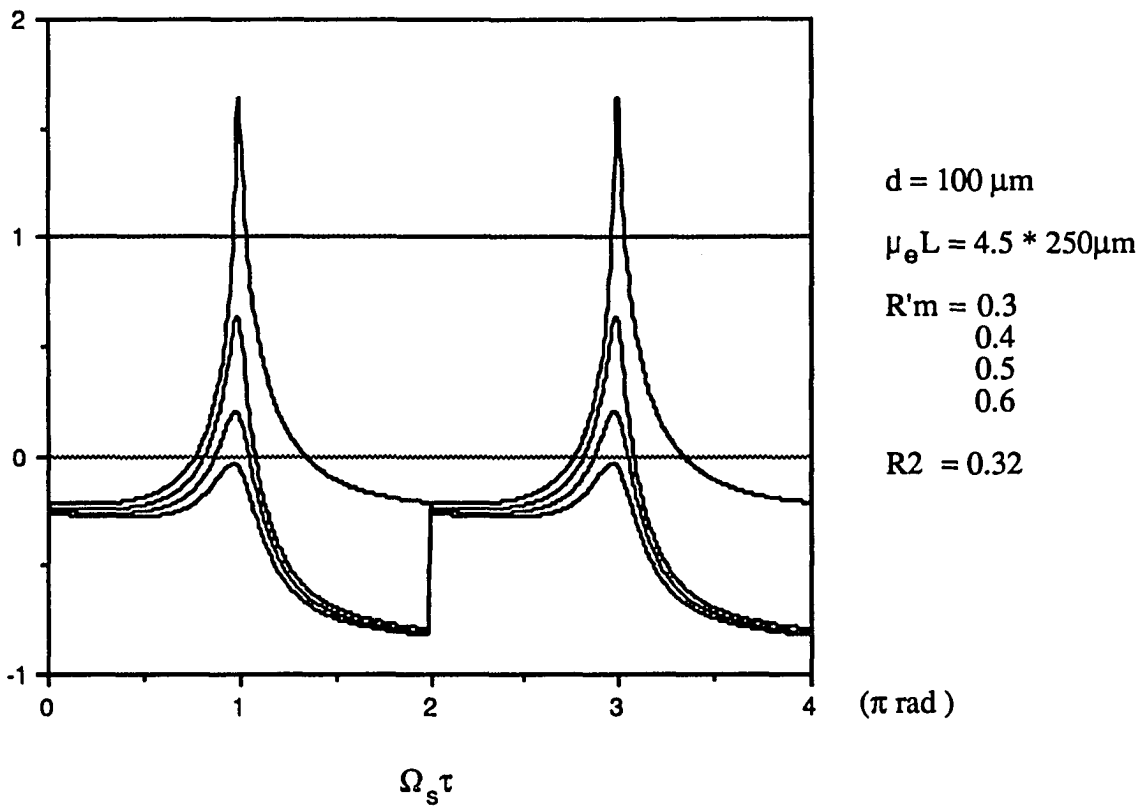

Figure 4.7. Gradual change of the shape of RHS of Eq.(4.16) as R'_m is varied

$$f_0 = \frac{\omega_0}{2\pi} \tag{4.21}$$

If we choose ordinary values of L=300μm and μ_e =4.5, then $\delta f = 1.1 \times 10^{11}$ Hz, which gives

$$\frac{\delta f}{f_0} \cong \frac{1}{3600} \tag{4.22}$$

for the wavelength of the solitary laser diode λ_0 = 0.75 μm. And it can be easily shown that

$$\frac{\delta f_e}{f_0} = \frac{\lambda_0}{2d} = \frac{0.375}{d\ (\text{in } \mu m)} \tag{4.23}$$

For the short external cavity, external mode spacing δf_e is big and Eq. (4.23) has a larger value than the long external cavity.

First, consider an extremely short external cavity, say, d=1.5μm. Then from Eq.(4.23), $\delta f_e = f_0/4$. Therefore, the external cavity mode spacing is far greater than either the mode spacing of the solitary laser or the medium gain bandwidth. Consequently, once the solitary laser shows a single mode characteristic, the external cavity laser also shows single mode with shifted frequency according to phase condition of Eq.(4.9). If the amount of shifted frequency is big enough to make the net gain in Eq.(4.8) for that mode become greater than the net gain of the adjacent possible mode, the mode hopping effect occurs to change the lasing frequency by approximately δf. However, the frequency shift effect is small in the case of an ultra short external cavity,

so those mode hopping phenomena does not occur. As d increases to several tens of micrometers, the mode hopping effect described above starts to occur. When the external cavity mode spacing δf_e becomes comparable to the solitary laser mode spacing δf, both modes start to compete against each other. At another extreme case of the long external cavity, the external cavity mode spacing is reduced to a very small value, and multiple modes start to lase.

These situations are illustrated in Figure 4.8 for the short external cavity and in Figure 4.9 for the long external cavity. So, unless we are considering the very long external cavity, which may cause the multiple external mode lasing situation, our assumption for a single mode rate equation can be justified. Otherwise, we should set up the equations for the multiple mode equations. Most of this work will deal with the single mode case; the single mode for a solitary laser will produce the single external cavity mode.

The single mode condition may be easily obtained from Eq.(4.16). Graphically, the slope of the curve representing RHS of Eq.(4.16) should be smaller than the slope of the straight line representing LHS of Eq.(4.16). So we obtain

single mode condition

$$\frac{1}{\tau_{in}}\left[\frac{1}{1+\left(\frac{D}{C}\right)^2}\frac{d}{d\Omega_s}\left(\frac{D}{C}\right)-\alpha\frac{dL}{d\Omega_s}\right]<1 \qquad (4.24)$$

or

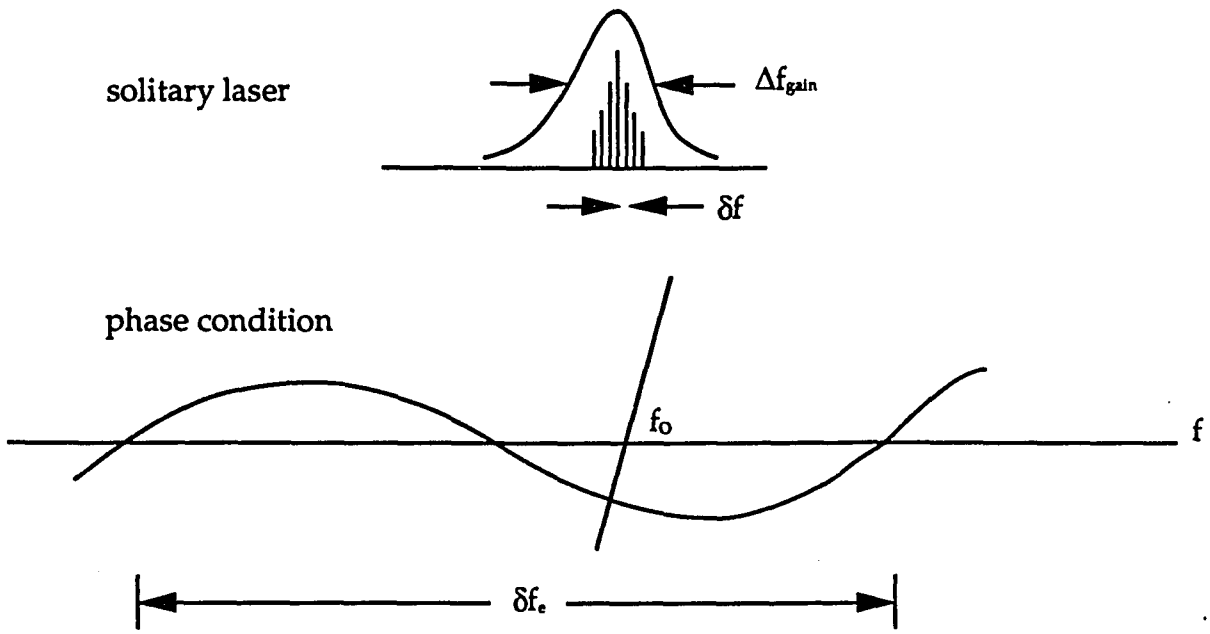

Figure 4.8. Phase condition for the short external cavity laser diode

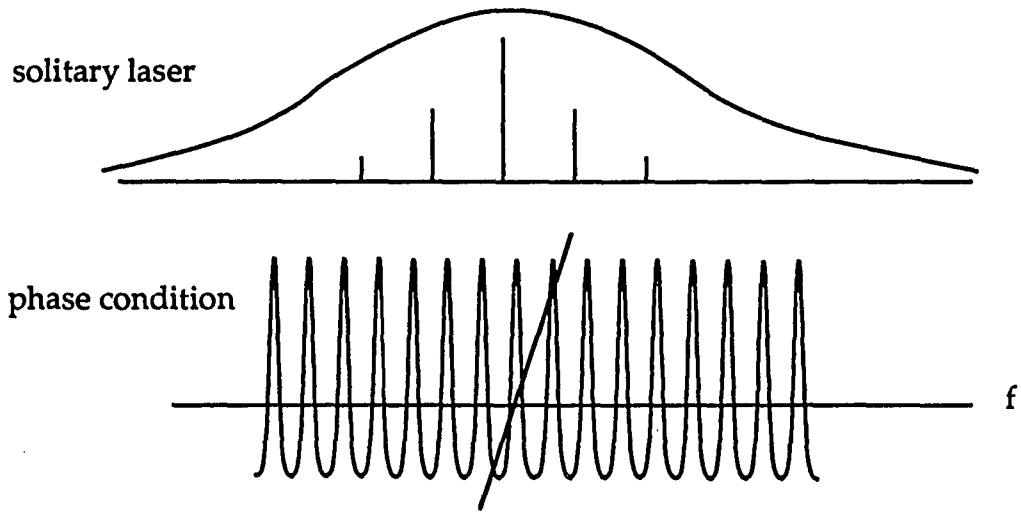

Figure 4.9. Phase condition for the long external cavity laser diode

$$\frac{d\omega_0}{d\Omega_s} = 1 + \frac{1}{\tau_{in}}\left[\alpha\frac{dL}{d\Omega_s} - \frac{d}{d\Omega_s}\theta_{Z_{as}}(0,\Omega_s)\right] > 0 \qquad (4.25)$$

This single mode condition is plotted in Figure 4.10. The RHS of Eq.(4.25) is calculated as external reflectivity changes. The lasing wavelength is assumed as $\lambda = 0.78\mu m$, and $R_2 = 0.32$, and $\alpha = 6$ are used. Since the derivative of function L has large magnitude only around $\Omega_s\tau = 2m\pi$, as clearly shown in Figure 4.1, RHS of Eq. (4.25) does not vary much from 1 at d = 7.6 μm ($\Omega_s\tau$ is close to an odd multiple of π) . Therefore, around d = 7.6 μm, the external cavity laser shows a single mode characteristic for all R_m. As d becomes close to 7.8 μm ($\Omega_s\tau=40\pi$), RHS of Eq. (4.25) deviates from 1 around $R'_m = 0.32$ (which is the same as facet reflectivity). Figure 4.10 shows that the external cavity laser may support multiple modes if R'_m is close to R_2 at d=7.799 μm. After the external cavity length d exceeds 7.8μm, namely at d = 7.801 μm, RHS of Eq. (4.25) always becomes greater than 1, which can be expected since the derivative of function L changes its sign at $\Omega_s\tau = 2m\pi$, as can be seen in Figure 4.1.

The above description is illustrated in Figure 4.11. The single mode condition (RHS of Eq.(4.25)) is plotted as a function of external cavity length for fixed $R'_m = 0.31$. For d<6 μm, the external cavity laser always operates as a single mode. As d increases, a multiple mode regime starts to exist as shown in Figure 4.5. In Figure 4.12, a similarly calculated plot is shown. All parameters used in the calculation are the same as for the case of Figure 4.11, except we use $\alpha = 1$ in Figure 4.12. The larger the linewidth enhancement factor α is, the greater the chance for multiple mode oscillation.

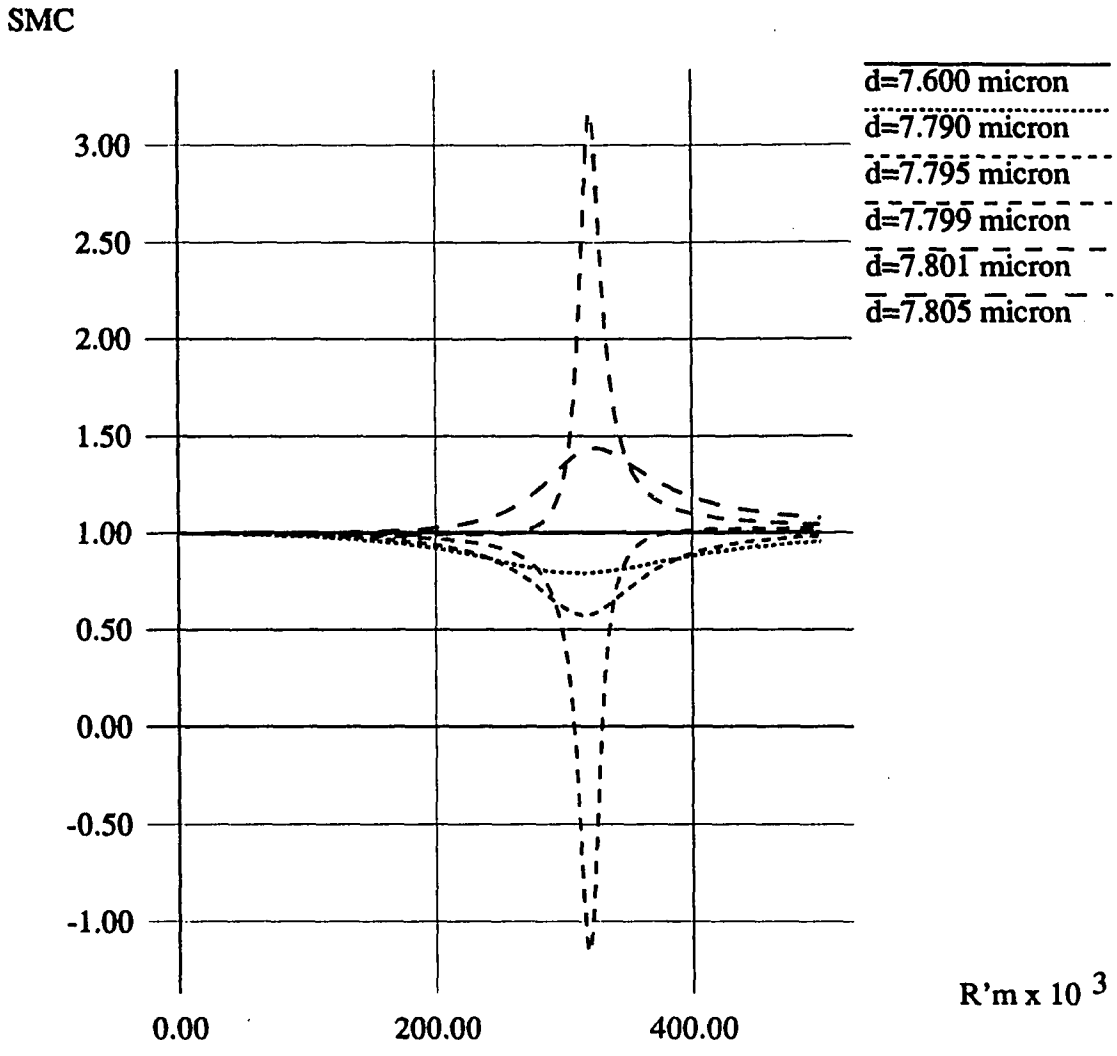

Figure 4.10. Plot of single mode condition, where the negative value denotes the multi mode lasing

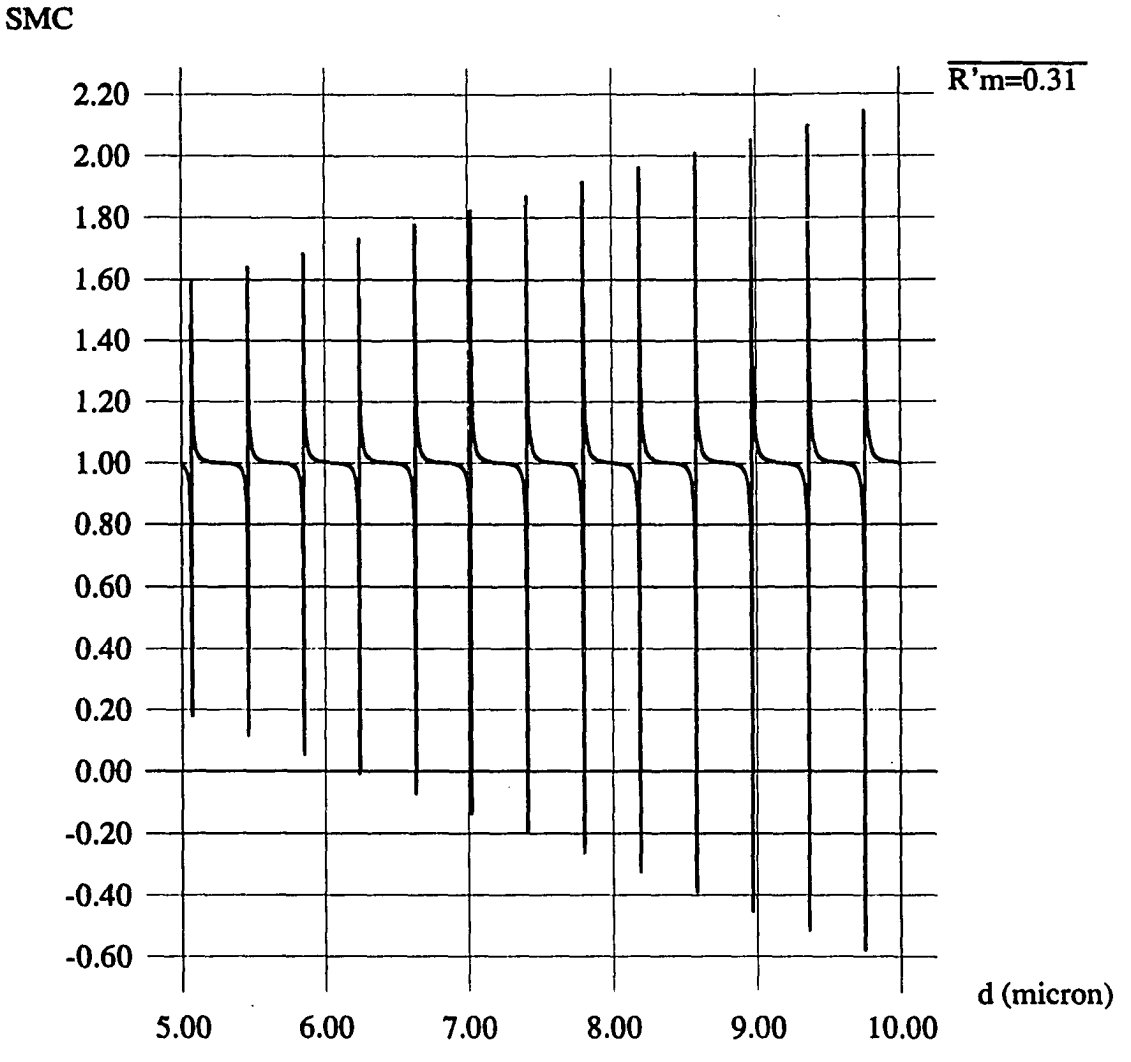

Figure 4.11. Single mode condition calculated when $R'_m = 0.31$, and $\alpha = 6$

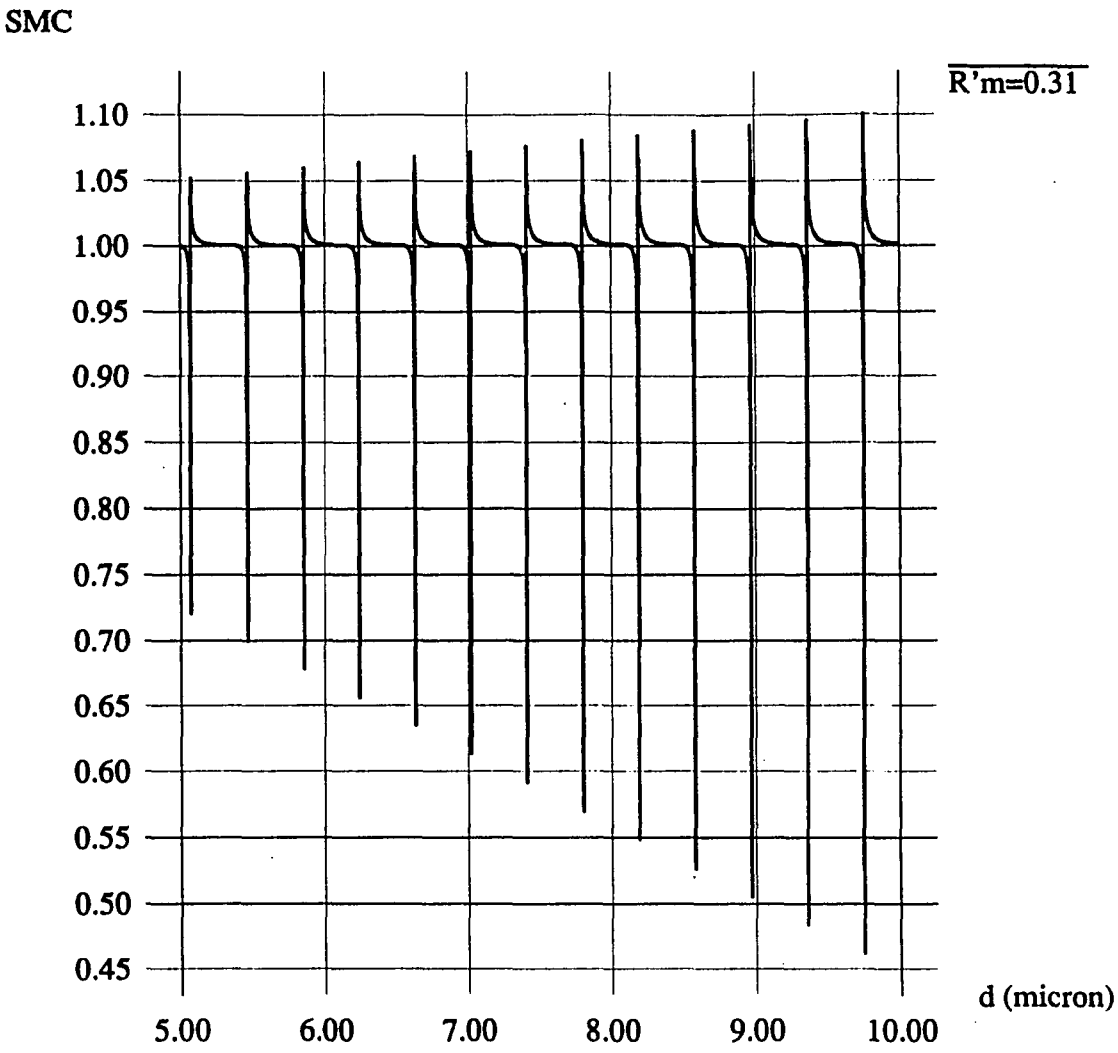

Figure 4.12. Single mode condition calculated when $R'_m = 0.31$, and $\alpha = 1$

We can conclude that a single mode condition will be met more likely for the short external cavity laser and for the external reflectivity well below or beyond the facet reflectivity. The behavior of RHS of Eq. (4.25) around $\Omega_s\tau = 2m\pi$ will be more investigated in more detail in Appendix A.

In Figure 4.13, we plot the frequency of the external cavity laser as changing the external cavity length d. The ordinate represents the fractional amount of change in frequency. For small R'_m , the frequency shift is only on the order of 10^{-4} , which is smaller than the value obtained in Eq.(4.22). This means that there is no mode jumping phenomena as external cavity length varies. However, for large R'_m , especially in the case where R'_m is close to R_2 , the amount of frequency shift can exceed the mode spacing of the solitary laser δf around $\Omega_s\tau = 2m\pi$, which will cause mode jumping as external cavity length varies.

Open Resonator Model for Ultra Short External Cavity

This section is concerned with the development of a method of analysis that is particularly suitable for analyzing the output power characteristics of an ultra short external cavity laser diode by constructing an appropriate model of the complex coupling factor with the aid of open - resonator theory [76] . This model should describe properly the effect of multiple reflection as well as the dependency on the size of the near field pattern of the laser diode. The model under consideration is described in detail in following subsection. Numerical illustration of the output power characteristics of the external cavity laser diode is also presented and compared with experimental observations.

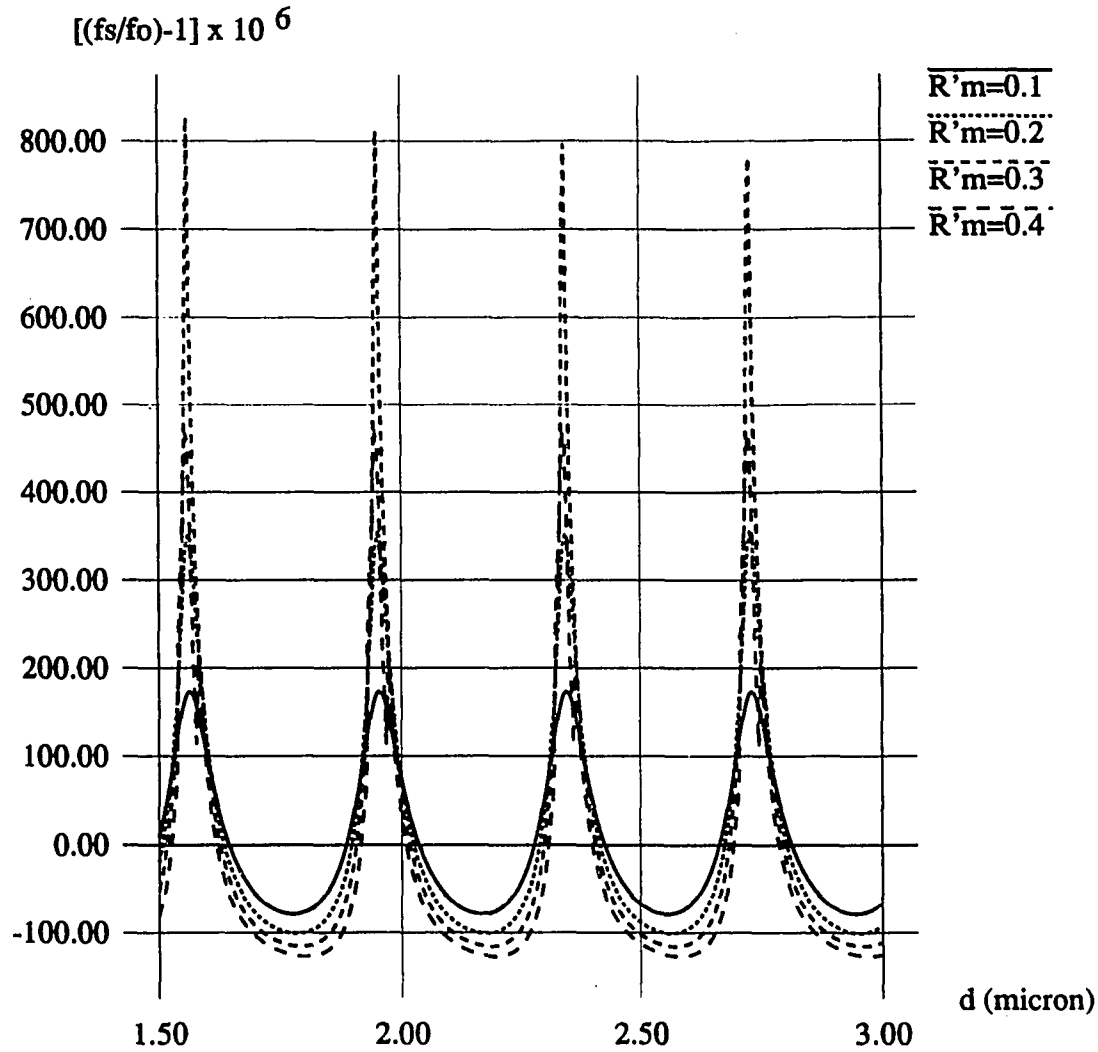

Figure 4.13. Lasing frequency shift versus external cavity length

Open resonator formed by rectangular mirrors

An open resonator formed by two parallel rectangular mirrors at $-a < x < a$, $-b < y < b$, $z = \pm d$ is shown in Figure 4.14. A quantitative theory of open resonators with plane mirrors was first given in a paper by Fox and Li [77], where they calculated resonator modes by solving the diffraction integral equation iteratively. Vainshtein [76] gave a theory of natural vibrations for open resonators based on a rigorous theory of diffraction at the open end. The two mirrors represent a waveguide in which waves are propagated by multiple reflections parallel to the mirror surfaces. The rays are almost parallel to the z axis and for resonance we have

$$\frac{2d}{\cos\theta} = q\frac{\lambda}{2} \qquad q = 1,2,3\cdots \qquad (4.26)$$

where a small angle θ represents the angle between the z axis and ray propagation direction. In this section, since we are mainly dealing with the ultra short external cavity, we assume the lasing frequency of the external cavity is same as that of the solitary laser diode, and we simply define the wavelength of laser as λ. This assumption can be justified from the discussion of previous section. At the open end the wave is diffracted. Part of the energy may be turned through the angle 2θ, which results in the formation of a reflected wave. Using the free space wave number $k = \omega / c$, Eq.(4.26) can be rewritten as

$$k d = \pi (q/2 + p) \qquad (4.27)$$

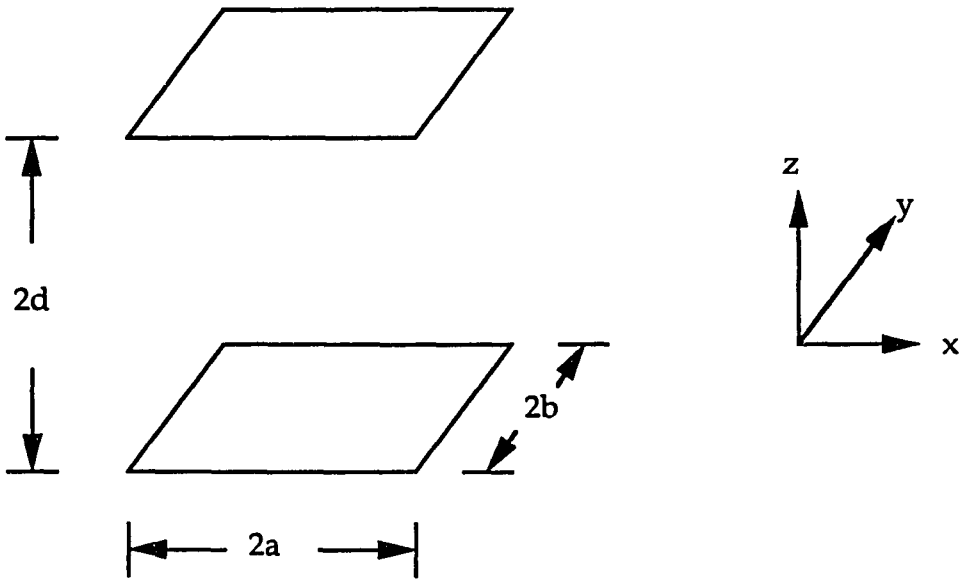

Figure 4.14. An open resonator formed by two parallel rectangular mirrors

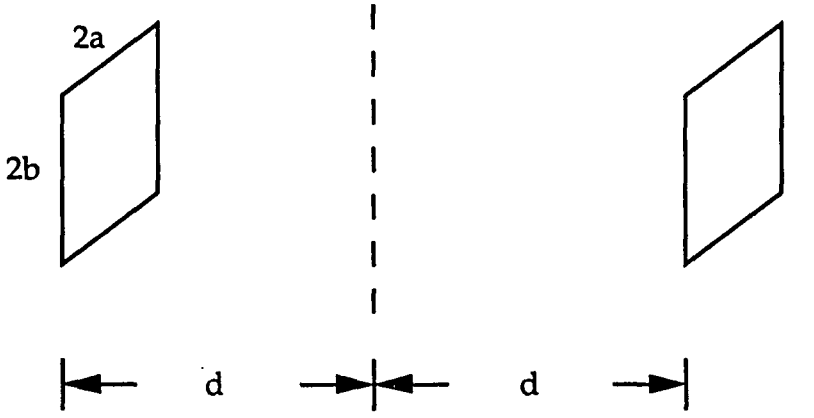

Figure 4.15. An unfolded equivalent open resonator model of the external cavity

where q is a large integer (for practical purposes $q > 3$) and p is small correction within a range of $|p| < 1/2$. In case of small θ, the x and y components of k are negligible, i.e.,

$$k_x << k, \qquad k_y << k \tag{4.28}$$

then, the quasi-mode amplitude eigenfunctions in the x-y plane can be put in the form of a product

$$f(x,y) = f_a(x) \cdot f_b(y) \tag{4.29}$$

where, in the fundamental mode

$$f_a(x) = \cos\left\{ \frac{\pi x}{2a\,[\,1 + \beta(1+i) / M_a\,]} \right\} \tag{4.30}$$

$$f_b(x) = \cos\left\{ \frac{\pi x}{2b\,[\,1 + \beta(1+i) / M_b\,]} \right\} \tag{4.31}$$

$$M_a = \sqrt{\frac{2ka^2}{d}}, \qquad M_b = \sqrt{\frac{2kb^2}{d}} \tag{4.32}$$

$$\beta = -\zeta(0.5) / \sqrt{\pi} = 0.824 \tag{4.33}$$

and $\zeta(z)$ is the zeta function of Riemann.

The correction term p in Eq.(4.27) is given by

$$\tilde{p} = p_a + p_b \tag{4.34}$$

where

$$p_a = \frac{\pi}{4} (M_a + \beta + i\beta)^{-2} \tag{4.35}$$

$$p_b = \frac{\pi}{4} (M_b + \beta + i\beta)^{-2} \tag{4.36}$$

for the fundamental mode, or in the real and imaginary form

$$p_a = p_a' - ip_a'' \tag{4.37}$$

$$p_a' = \frac{\pi}{4} \frac{M_a (M_a + 2\beta)}{[(M_a + \beta)^2 + \beta^2]^2} \tag{4.38}$$

$$p_a'' = \frac{\pi}{2} \frac{\beta (M_a + \beta)}{[(M_a + \beta)^2 + \beta^2]^2} \tag{4.39}$$

and similar equations can be obtained for p_b.

The frequency $\omega = \omega' - i\omega''$ of the oscillation is complex. Quantities p' and p" have the following meanings. In the time of $t = 2d/c$, there is an additional phase shift

$$\Delta = 2\pi p' = 2\pi (p_a' + p_b') \tag{4.40}$$

and the fractional decrease of the energy

$$\Lambda = 1 - \exp(-4\pi p'') = 1 - \exp[-4\pi(p_a''+p_b'')] \tag{4.41}$$

For later use, let us connect M_a and M_b with the Fresnel zone number introduced in [77]

$$N_a = \frac{a^2}{2d\lambda}, \quad N_b = \frac{b^2}{2d\lambda} \tag{4.42}$$

by the simple relations

$$M_a = \sqrt{8\pi N_a}, \quad M_b = \sqrt{8\pi N_b} \tag{4.43}$$

Complex coupling coefficient

The external cavity of length d in Figure 3.1 can be considered as an open resonator in the following manner. In the most experimental situation, beam size on the external reflector is much smaller than the size of the reflector itself. Therefore, we can describe the problem by the unfolded equivalent open resonator formed by the emitting area of the laser diode (2a x 2b) and separated by 2d as shown in Figure 4.15 [31]. In the case of a very short external cavity length ($0 < d < 5$ μm), the near field spot size does not vary practically [78], and the field pattern maintains its Gaussian distribution property. Fox and Li's iterative solution [77] shows that the steady state field distribution has a Gaussian-like shape for the fundamental mode when a uniform plane wave is used as an initially launched wave. The approximate analytic solutions shown

in Eq.(4.29), (4.30), and (4.31) also show similar spatial characteristics. A condition in Eq.(4.28) is also satisfied for the external laser diode configuration. Now we assume that the guided modes inside the laser diode are smoothly matched to the eigenmodes of the external open cavity so that we can use the above properties of the open cavity to calculate the coupling coefficient. The effective field amplitude reflectivity defined in Eq.(3.6) can be reduced for the stationary case as,

$$\rho_e = \rho_2 - \frac{1-R_2}{\rho_2} \sum_{n=1}^{\infty} c_n \left[-\rho_2 \rho_m \exp(i\psi) \right]^n \tag{4.44}$$

where the phase delay due to the external cavity

$$\psi = \omega\tau = \frac{4\pi d}{\lambda} \tag{4.45}$$

Equations (4.40) and (4.41) suggest that we should consider the nth coupling coefficient c_n to be a complex quantity of the following form:

$$c_n = \exp(-i2\pi p_n) \equiv \exp(-\delta_n)\cdot\exp(-i\Delta_n) \tag{4.46}$$

where

$$p_n = p_{na} + p_{nb} = (p_{an}' + p_{bn}') - i\,(p_{an}'' + p_{bn}'') \tag{4.47}$$

It should be noted that c_n consists of an amplitude - reduction factor, $\exp(-\delta_n)$, and a phase - modification factor, $\exp(-i\Delta_n)$. The amplitude - reduction parameter δ_n and the phase - modification parameter Δ_n are given, respectively, as

$$\delta_n = \pi^2 \left\{ \frac{\beta\,(M_a(n)+\beta)}{[\,(M_a(n)+\beta)^2+\beta^2\,]^2} + \frac{\beta\,(M_b(n)+\beta)}{[\,(M_b(n)+\beta)^2+\beta^2\,]^2} \right\} \tag{4.48}$$

$$\Delta_n = \frac{\pi^2}{2} \left\{ \frac{M_a(n)\,(M_a(n)+2\beta)}{[\,(M_a(n)+\beta)^2+\beta^2\,]^2} + \frac{M_b(n)\,(M_b(n)+2\beta)}{[\,(M_b(n)+\beta)^2+\beta^2\,]^2} \right\} \tag{4.49}$$

where M_a, M_b, and N_a, N_b are defined in Eqs. (4.42) and (4.43).

It should be noted that since δ_n and Δ_n are the functions of the Fresnel zone numbers, the coupling coefficient depends on the distance d and the near field beam size of the laser diode.

The variation of parameters δ_n and Δ_n with the Fresnel zone number $N=N_a=N_b$ is illustrated in Figure 4.16 for the case of a=b. We observe that δ_n decreases monotonically with N while Δ_n has a maximum value of 0.58 at $N\approx0.015$. At a large value of N, which is the case where the external open resonator length for the n-th reflection (2 x nd) is small, parameters δ_n and Δ_n both approach zero as N approaches infinity so that c_n approaches unity, which is to be expected. As N decreases (i.e., the external cavity length d increases), Δ_n increases to give a larger phase - modification and δ_n increases to reduce the amplitude of the coupling coefficient. On the other hand, in the limit of

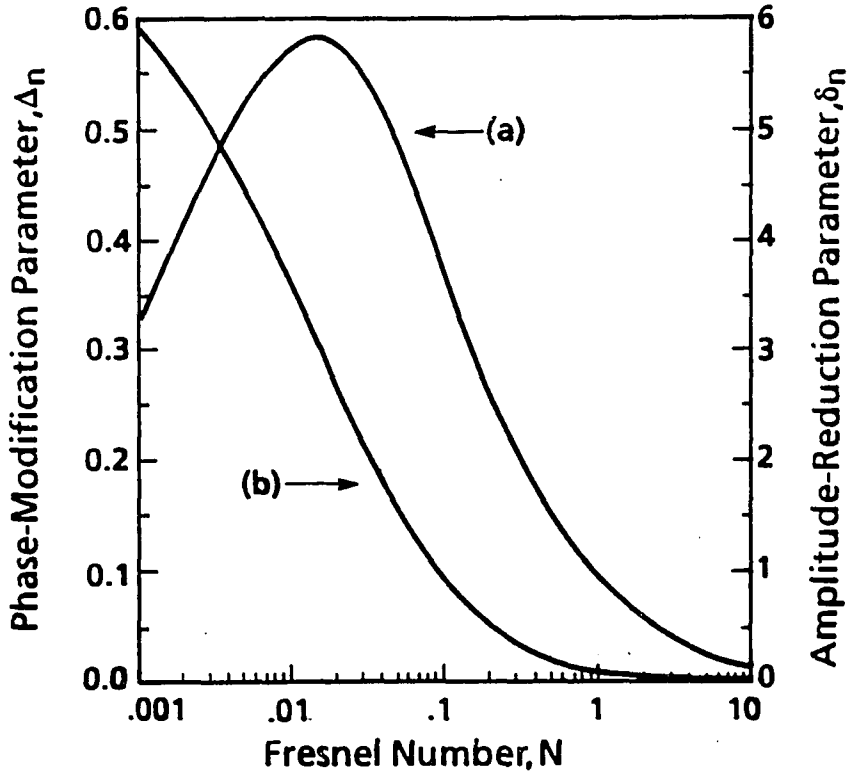

Figure 4.16. Variation of the amplitude - reduction parameter δ_n and the phase - modification parameter Δ_n with Fresnel zone number N

small N, Δ_n starts to decrease at N=0.015 as N is decreased and approaches zero as N -> 0. However, δ_n has a finite value of $0.5(\pi/\beta)^2$ at N=0, which gives $c_n=7\times10^{-4}$.

It should be pointed out that in the range N<0.015 our model could pose some problems because physically, as d approaches to infinity, N approaches to zero, and δ_n remains at a finite large value rather than approaches infinity as we would expect in order to meet the condition of zero coupling in this case.

However, in considering the ultrashort external cavity case, a large value of 2 x nd can occur only when n is a very large integer (after many reflections). Since the net change in ρ_e is proportional to $c_n[\rho_2\rho_m]^n$, the amount of amplitude loss goes practically zero with a large value of n.

Therefore, our model can work well especially for the ultra short external cavity configuration. Since δ_n is a monotonically decreasing function of N, we observe that, as expected, the amplitude of coupling coefficient $|c_n|=\exp(-\delta_n)$ will be reduced if the cavity length d is increased. On the other hand, the Δ_n is a positive - definite quantity and represents the amount of phase - angle modification of the n-th reflection introduced by the coupling process at the laser facet in addition to the conventional phase shift $n\psi$ in Eq.(4.44) that was produced by the multiple reflection. This phase - modification effect, which, to our knowledge, is reported for the first time [53], is due to the inherent characteristics of the open resonator and should be considered when the external cavity laser diode is used as a phase sensor [45,73] or when the frequency characteristics are investigated [55] . The amplitude - reduction parameter δ_n for Eq.(4.48) agrees with Voumard et al.'s coupling coefficient ε_n

[31] (which, in our notation, is $\exp(-\delta_n)$) in the limit of $N_a >> 1$ and $N_b >> 1$ [79].

Threshold current and output power characteristics

In this subsection we give some calculated examples of threshold current and L-I characteristics by using simple linearized equations. Once the effective field reflectivity ρ_e is obtained, the threshold current of the laser diode can be written as

$$I_{th} = K_{th}\left[\alpha_s + \frac{1}{L} \ln \frac{1}{\sqrt{R_1 R_e}} \right] \tag{4.50}$$

where K_{th} is a constant determined by the physical parameters, α_s is the internal loss inside the laser diode cavity as defined in Eq.(3.25). The total output power characteristics above threshold can be written in terms of the normalized driving current $I_N = I/I_{th}$ as

$$P_1 + P_2 = 2\,\eta_{ex}\, I_{th}\,(I_N - 1) \tag{4.51}$$

where P_1 and P_2 are the power output at each facets shown in Figure 3.1, and η_{ex} is the external quantum efficiency. The factor of 2 is introduced in Eq.(4.51) because usually only one of the output power relationships is used to define the external quantum efficiency. Also, it is well known that if different laser facets with different reflectivities are used, the emitted powers are related by [80],

$$r_p \equiv \frac{P_1}{P_2} = \sqrt{\frac{R_e}{R_1}} \left(\frac{1 - R_1}{1 - R_e} \right) \tag{4.52}$$

and give the equations

$$P_1 = \frac{2\, r_p}{1 + r_p} \eta_{ex} I_{th} (I_N - 1) \tag{4.53}$$

$$P_2 = \frac{2}{1 + r_p} \eta_{ex} I_{th} (I_N - 1) \tag{4.54}$$

In most cases, the power output, which is detected by an external photodetector, is P_1. The calculated result of the variation of the effective power reflectivity R_e, the threshold current I_{th}, and the output power P_1 of the laser diode with the length of external cavity d is illustrated in Figure 4.17, for the case of typical values of the parameters $R_1 = R_2 = 0.32$, $R_m = 0.6$, $\lambda = 0.78$ μm and $2a = 0.35$ μm, and $2b = 4$ μm (Hitachi CSP type laser diode [73]) . The multiple reflection effects are considered round trips up to 20 in obtaining the plots of Figure 4.17. In the plots shown in Figure 4.17 the solid - line curves represent the result in which the effect of the presence of the phase - modification parameter Δ_n is included while the dashed - line curves represent the case where Δ_n is set equal to zero. (i.e., the effect of Δ_n is neglected). For the calculation of output power characteristics the bias current $I_b = 1.3\, I_{tho}$ is used, where I_{tho} is the free - running threshold current with no external reflector

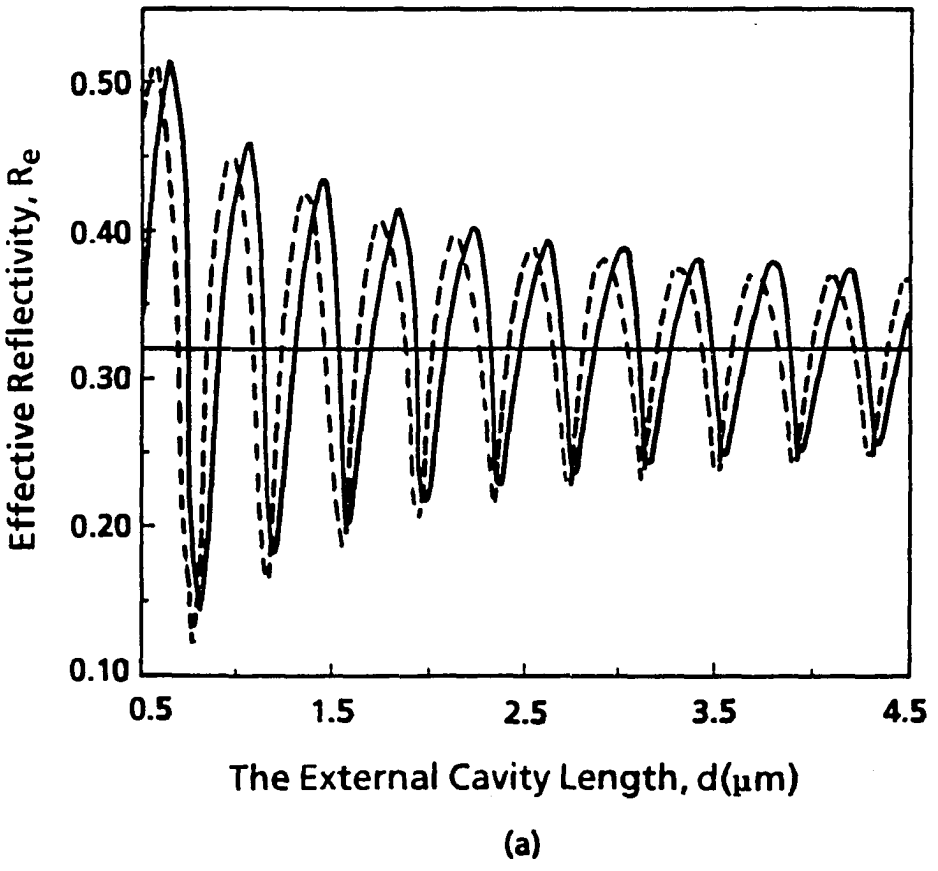

Figure 4.17. Variations of the parameters with external cavity length d for the case $R_1 = R_2 = 0.32$, $R'_m = 0.6$, $\lambda = 0.78$ μm, $2a = 0.35$μm, and $2b = 4$μm, where the solid lines and the dashed lines represent the plots for the case of nonzero and values of Δ_n, respectively, and the straight line represents the case of no external reflector; (a) the effective reflectivity R_e vs. external cavity length d

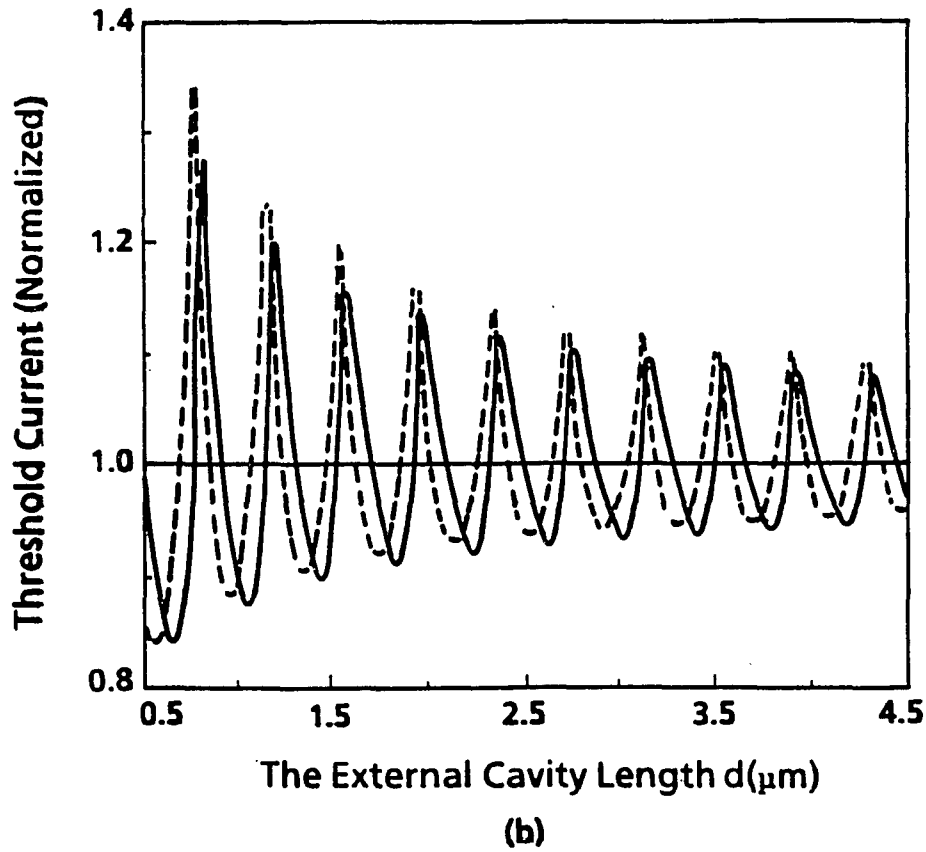

Figure 4.17. (continued); (b) the normalized threshold current vs. the external cavity length d

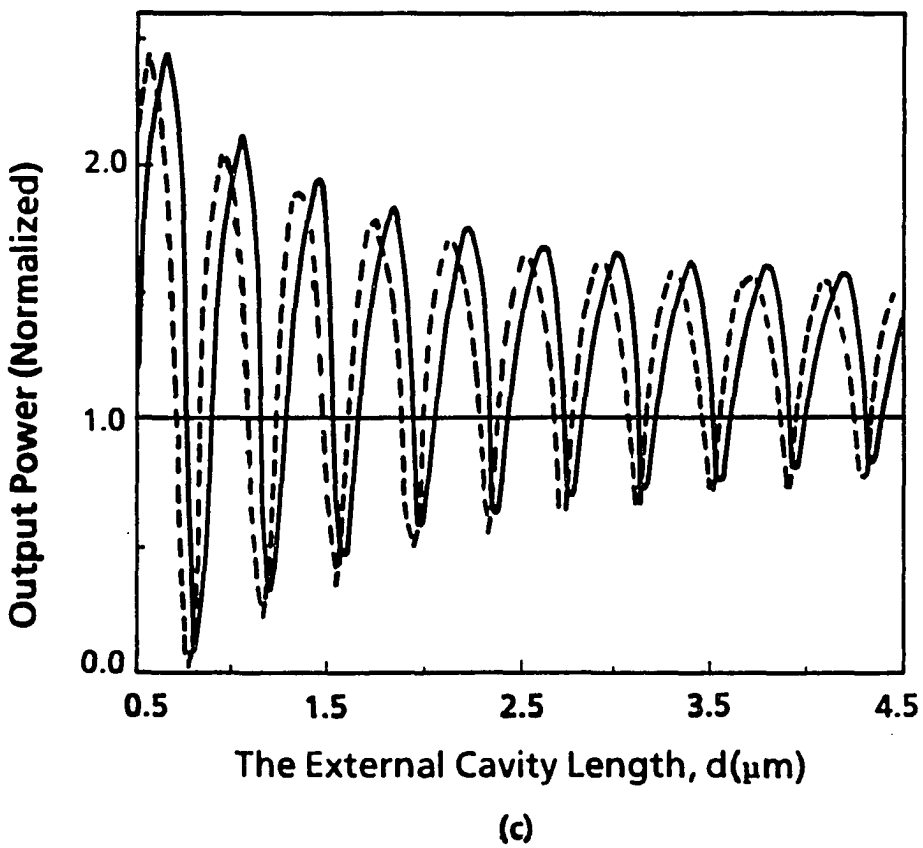

Figure 4.17. (continued); (c) the normalized output power vs. the external cavity length d

($R_m = 0$). The straight lines in Figure 4.17 represents the case of no external reflector.

It is interesting to observe that because of the effect of phase modification introduced by the parameter Δ_n, the positions of peaks and valleys of the plot are shifted from those for the case where the effect of Δ_n is neglected. Furthermore, the spacing between two adjacent peaks is no longer a constant of $\lambda/2$ but changes with the range of d under consideration. In particular, in the range of small d, peaks and valleys show an exponential-like decay pattern, which agrees qualitatively with our experimental result shown in Figure 4.18 (the starting position d_o is not exactly measured and thought to be less than 10 μm). For this experiment, a Mitsubishi ML-4402 laser diode is used. The encapsulation of the laser diode package was removed to allow the formation of a short external cavity. Since the starting position is not exactly known it is difficult to compare with our model directly. However, it can be seen clearly from Figure 4.17 (c) that the shape of the output power curve between two adjacent valleys exhibits some degree of asymmetry, which will be discussed in next subsection. This asymmetry is also influenced by the effect of the presence of Δ_n; for example, it becomes more pronounced for the case of $\Delta_n \neq 0$ (see the solid - line curve of Figure 4.17(c)) than for the case of $\Delta_n = 0$ (i.e., the dashed - line curve of Figure 4.17(c)).

<u>Asymmetry in the optical output power characteristics</u>

We have shown that the coupling coefficient c_n, representing the fractional amount of coupled field into the laser diode at the n-th reflection, becomes a complex function of the external cavity length and the near field

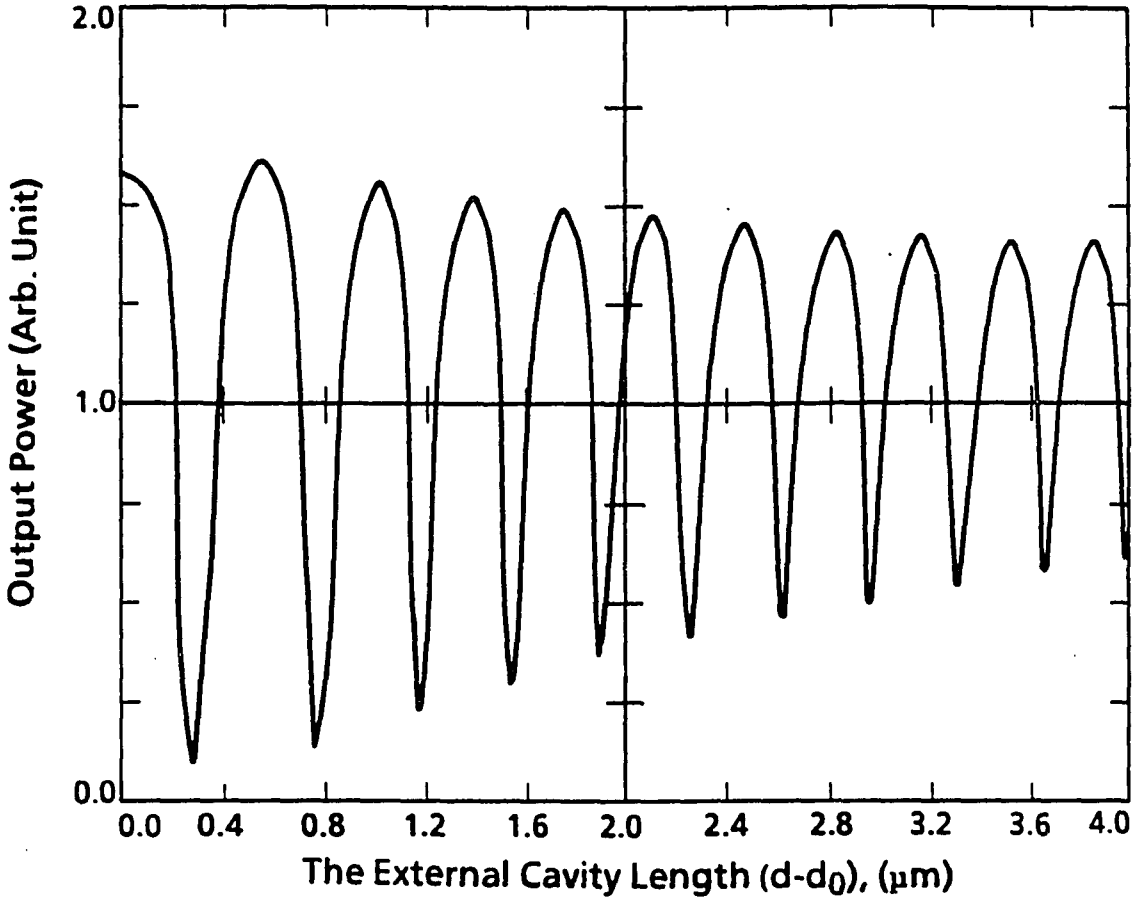

Figure 4.18. Experimental result of output power versus external cavity length for the case of $\lambda = 0.78$ μm, where the starting position is not exactly measured

beam size of the laser diode. This subsection gives the experimental evidence supporting our complex coupling coefficient model - the asymmetry in output power versus external cavity length characteristics [54].

The single mode AlGaAs laser (Mitsubishi ML4402, $\lambda = 0.78$ μm) was mounted on a temperature stabilized platform by means of a Peltier device. The encapsulation of the laser package was also removed to allow the formation of a short external cavity. The external reflector was placed on a voice coil motor to vary the external cavity length. The tilt angle was minimized by 5-axis positioner. In Figure 4.19, the output power detected by the monitoring photo detector located at the rear facet is shown when the 45% reflector mounted on the voice coil motor is oscillating. The laser diode was biased at 1.5 I_{tho} . The 83 Hz triangular waveform shows the current being applied to the voice coil motor. The horizontal axis represents a time axis. The velocity of the voice coil motor may be approximated as a constant around the central portion of the linear waveform, while the coil movement slows down around the current peak values. This effect can be seen in the output power characteristics in which time duration between adjacent peaks becomes longer as the current waveform reaches its peaks, while the distance between adjacent peaks should remain $\lambda/2$. There are about 60 peaks within a half period of the applied current waveform, and this implies that the external cavity length is increased about 23 μm during this period. The external cavity length d_o at the middle position is measured to be about 20 μm. This experimental curve also illustrates an exponential-like power decay pattern in the small d range, due to the amplitude-reduction parameter δ_n. In Figure 4.20,

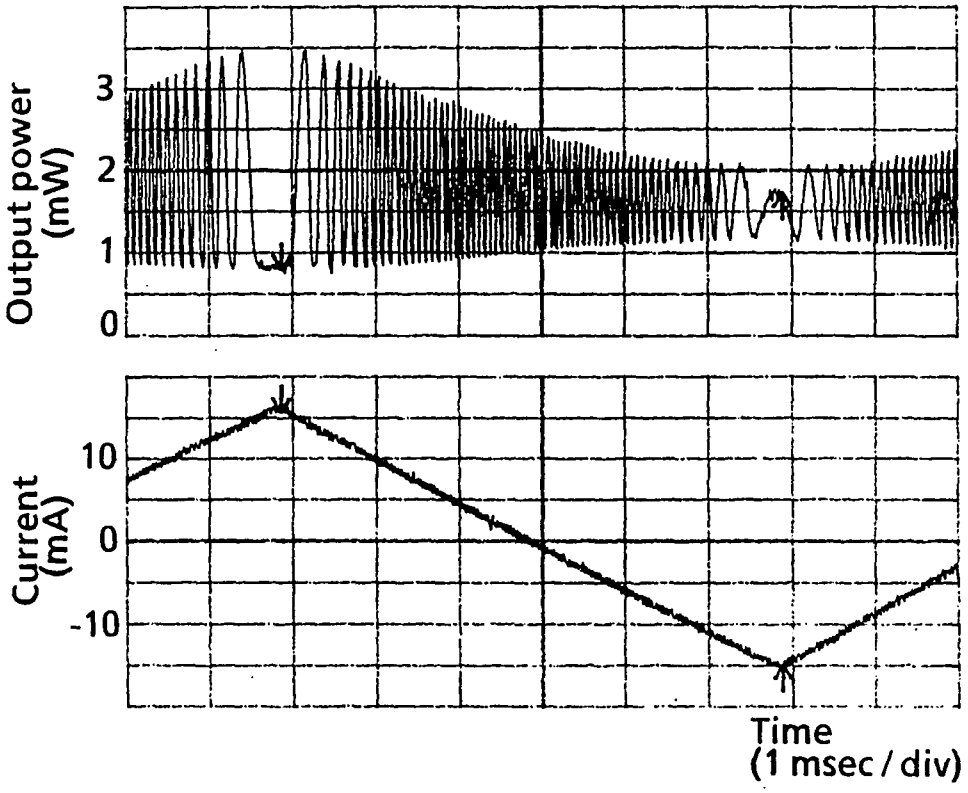

Figure 4.19. Oscillograms showing the applied current to the voice coil motor where the 45 % reflector is mounted for vibration, and resulting optical power variation detected by monitoring photodiode

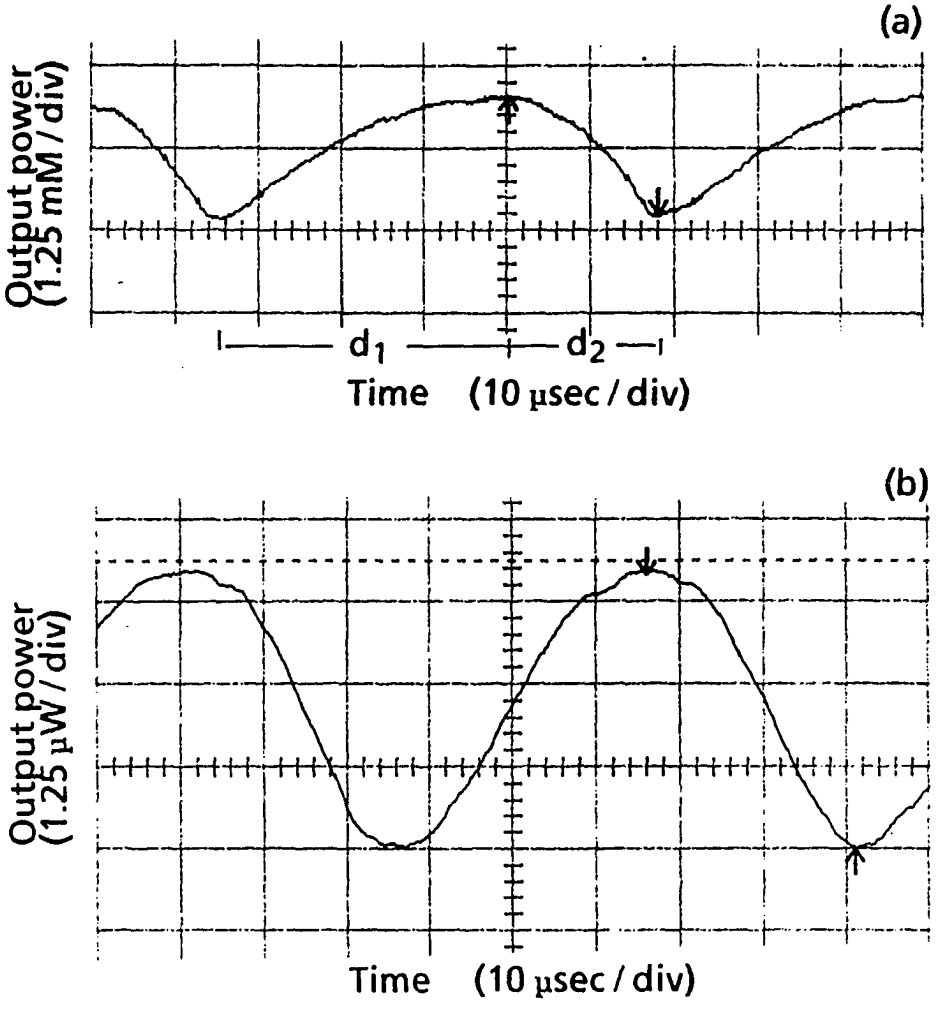

Figure 4.20. Oscillograms of P - d curve on an expanded scale to show a big asymmetry in (a) $R_m = 0.95$ and a small asymmetry in (b) $R_m = 0.04$

the laser output power around the center of the linear waveform of the driving current is illustrated on an expanded scale. We can consider these experimental curves as output power versus external cavity length (P - d) characteristics. A 95% external reflector was used to get the result shown in Figure 4.20(a), and a 4% reflector was used for Figure 4.20(b). The asymmetry in P - d characteristics is clearly shown especially for the high external reflectivity. An asymmetry factor is defined as

$$AF \equiv \frac{d_1}{d_2} \tag{4.55}$$

where, d_1 is the distance from the valley to the adjacent peak in P - d curve, and d_2 is the distance from the peak to the adjacent valley.

Since the threshold gain has its peak values at valleys of $|\rho_e|$ and vice versa, the peaks and valleys in the P - d curve coincide with those in the R_e - d curve, so that the two curves have the same AF value. Using Eqs.(4.44) - (4.49) AF is numerically calculated as a function of R_m, and compared with the experimental data in Figure 4.21. The emitting area used for calculation is 2.1 μm x 0.7 μm, the typical value given in the Mitsubishi data book, and $R_1 = R_2 = 0.32$, $d_o = 20$ μm. It can be seen that AF varies with d in the very small range of d, but becomes insensitive to d if d is greater than a few μm. From Figure 4.22 it can be seen that AF is also a function of the emitting area. On calculation, the parameter 2a = 2.1 μm is used, and 2b is varied from 0.55 to 1.05 μm. The experimental data were obtained using three laser diodes each with different far field radiation angles, which are converted to the near field beam size. In Figures 4.21 and 4.22, the experimental results show qualitative

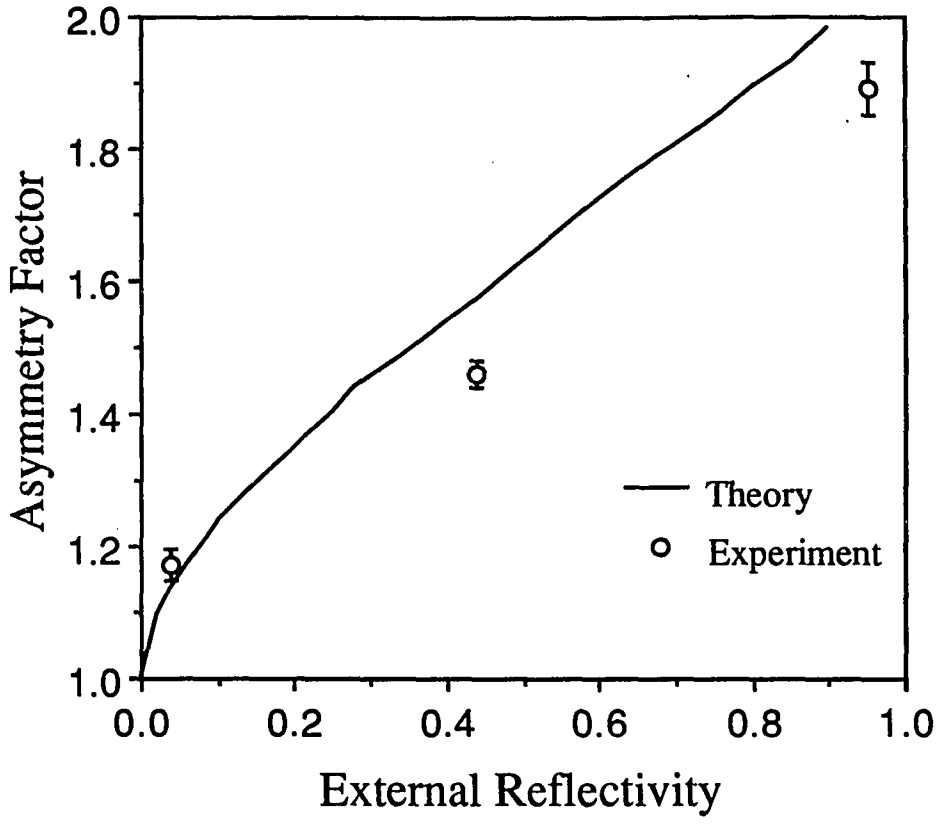

Figure 4.21. Asymmetry factor as a function of external reflectivity, where open circles represent the experimental data obtained at $d_o \approx 20$ μm

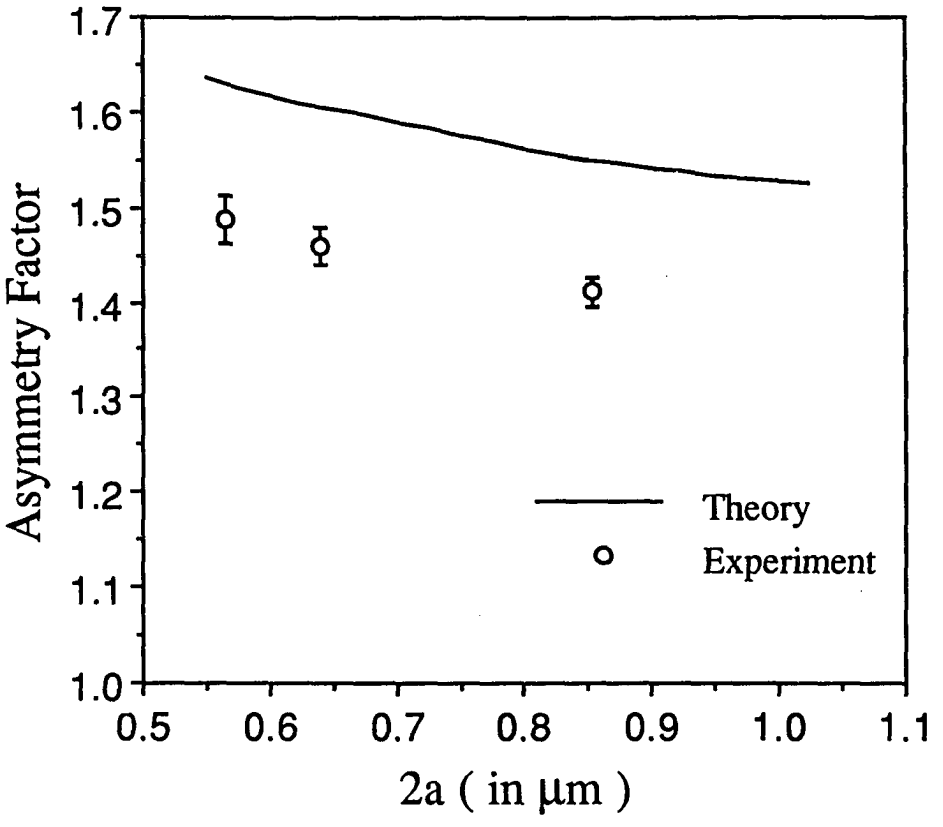

Figure 4.22. Asymmetry factor as a function of near field beam size, where open circles represent the experimental data obtained at $d_o \approx 20$ μm: Beam sizes are converted from the far - field radiation angles given by manufacturer

agreement with the calculated values. Once a real coupling coefficient is used for calculation, it is found that no asymmetry, i.e., AF=1, occurs at the range of d greater than a few μm. Even considering ρ_m as a complex number as for a metal reflector does not make any difference. While, if a complex constant is given to the coupling coefficient as

$$c_n \equiv \exp(-i\Delta) \tag{4.56}$$

where Δ is a constant, the peak/valley condition is easily obtained by finding zeroes of the first derivative of R_e with respect to d as

$$\sin(\psi - \Delta) = \frac{2\rho_2\rho_m \sin\Delta}{1 + R_2 R_m} \tag{4.57}$$

which shows AF=1 for the real coupling coefficient ($\Delta = 0$), but asymmetry will take place for the imaginary coupling coefficient ($\Delta \neq 0$). This simplified analysis supports our assertion: the asymmetry in the P - d curve can be seen as an evidence of a complex coupling coefficient. Equation (4.57) also suggests that AF is increased as ρ_m or $\sin\Delta$ is increased. These effects are shown in Figures 4.21 and 4.22 where it can be seen that a smaller emitting area causes a greater diffraction loss, so that the phase - modification parameter Δ_n becomes larger. The discrepancy between theory and experiment shown in Figures 4.21 and 4.22 seems to be caused by the overestimation of Δ_n at the range d>10 μm of our model discussed in the preceding subsection.

So far, we have assumed a single lasing frequency. However, it is well-known that lasing frequency is shifted or sometimes shows mode - jumping to

the adjacent mode. In short external cavity, as shown in Figure 4.8, the external - cavity mode spacing is much greater than the longitudinal mode spacing of solitary laser diode, and it is usually much greater than the gain profile bandwidth. Therefore mode jumping effects tend to be suppressed. In case of $d \approx 20\ \mu m$, the external cavity mode spacing becomes $\delta f_e \approx f_o / 100$ according to Eq.(4.23), which is the similar order of the laser gain profile bandwidth (see Eq.(4.20)). Assuming the worst case, the frequency may be shifted to the edge of the gain profile (i.e., about $100\delta f$ shift, which can hardly occur). In other words, the maximum wavelength shift within a $\lambda/2$ change in d is less than 2% of λ, which can also cause asymmetry in the P - d curve. It can be easily shown by following similar analysis used to get Eq.(4.57), that AF due to a 2% change in λ is less than 1.05, much smaller than our experimental data. In addition, it can be easily seen that the Doppler λ - shift in our experiment is negligibly small. In conclusion, we have shown that the asymmetry in the P - d curve observed in the short external cavity laser diode can be explained only by considering a complex coupling coefficient. This proves the validity of our open resonator model for the short external cavity laser diode derived in the previous subsections.

The asymmetry has practical importance in laser - diode sensor application [45,73] . Usually, the short external cavity configuration coupled to a flat mirror is used as a phase sensor. The operating position should be carefully controlled since the maximum sensitivity ($| \partial P/\partial d |$) can be changed once the operating position is moved to the opposite slope in the P - d curve. Also, the AF measurement may allow an estimate of the near field beam size of the laser diode. From our model, it is expected that $d_1 + d_2 > \lambda/2$ at ultra short

external cavity length ($d < 1\ \mu m$). This kind of experiment was hardly possible with our setup, but one of the previously published results for the optical disk head showed this tendency (Figure 13 in [42]). More discussion will be followed in Chapter 7 about the application of external cavity laser diodes.

CHAPTER 5. DYNAMICAL PROPERTIES AND CHAOS

In this chapter, we consider the dynamical properties of the external cavity laser diode from our model equations. From a practical point of view, it is very important to study the dynamical properties of the laser diode system, since in high-speed optical communication, it is modulated up to the frequencies comparable to the relaxation oscillation frequencies. The rate equations are solved numerically to show the time evolution of laser parameters. Also, with some approximation, they are solved analytically by linearized small signal expansion to give a simple expression for the relaxation oscillation frequency.

Dynamical stabilities are investigated for the stationary solutions obtained in Chapter 4. Since we do not consider the limit cycle solutions (periodic solutions of nonlinear differential equations) [81] of our rate equation set, the stability study is focussed on the equilibrium points.

The optical feedback introduces the time delay terms as shown in Eq.(3.3). When such delay terms are included in the nonlinear differential rate equations, laser parameters may show the chaotic behavior. Lenstra et al. [29] showed that with relatively strong feedback, the spectral linewidth is suddenly broadened on the order of 25 GHz. Since the coherence length of the laser light has then collapsed from about 10 m without feedback to about 10 mm with feedback, they called this feedback region "coherence collapse". Tkach and Chraplyvy [30] classified the regimes of feedback effects as a function of feedback power ratio and external cavity length, but only for the cases where external cavity length is longer than several cm. In a wide intermediate region between very low feedback level and very high feedback region, the laser

linewidth is observed to be several GHz, which corresponds to the coherence collapse region. Understanding of this deleterious effect on the laser diode has practical importance in designing optical communication systems, since it helps to reduce the noise level and improve the system performance by preventing from operating laser diodes in such regions. Therefore, the chaotic dynamics and bistabilities have been an active research field, and a lot of papers [16,82-90] investigate the bistable and chaotic behaviors of the external cavity laser diode. However, most of them considered long external cavity configuration and used the basic equations of Lang and Kobayashi [6]. Recently, stability analysis for the short external cavity configuration has been performed numerically [91] and analytically [92], and it shows that a laser remains stable for any feedback level without any coherence collapse if the external cavity length is shorter than about 5 mm. However, they still use the weak coupling model similar to Lang and Kobayashi's, so their analysis can not be directly adapted to the ultra short external cavity case. We will discuss the chaotic behavior in detail in the last part of this chapter.

Normalized Rate Equations

In this section, we will modify the form of our model equations to a set of simultaneous differential equations with the variables of S, N, and Ω, which are easier to handle. The normalized feedback factor Z(t) defined in Eq.(3.7) is approximated as $Z_a(t)$ in Eq.(3.49) with slow varying and short external cavity assumptions. Simple algebra will lead to

$$\ln|Z_a|$$

$$= \ln\sqrt{\frac{1+\frac{(r\rho_m)^2}{\rho_2}\left(1-\frac{\tau}{2}\frac{\dot{S}}{S}\right)^2+\frac{2r\rho_m}{\rho_2}\left(1-\frac{\tau}{2}\frac{\dot{S}}{S}\right)\cos(\Omega\tau)}{1+(\rho_2 r\rho_m)^2\left(1-\frac{\tau}{2}\frac{\dot{S}}{S}\right)^2+2\rho_2 r\rho_m\left(1-\frac{\tau}{2}\frac{\dot{S}}{S}\right)\cos(\Omega\tau)}} \qquad (5.1)$$

Using the slow varying approximation discussed in Chapter 3 which implies

$$\tau\frac{\dot{S}}{S} << 1 \qquad (5.2)$$

we can obtain

$$\ln|Z_a| \cong L(\Omega) + \ln\sqrt{\frac{1-\tau\frac{\dot{S}}{S}A(\Omega)}{1-\tau\frac{\dot{S}}{S}B(\Omega)}} \qquad (5.3)$$

where

$$A(\Omega) \equiv \frac{\frac{(r\rho_m)^2}{R_2}+\frac{r\rho_m}{\rho_2}\cos(\Omega\tau)}{1+\frac{(r\rho_m)^2}{R_2}+\frac{2r\rho_m}{\rho_2}\cos(\Omega\tau)} \qquad (5.4)$$

$$B(\Omega) \equiv \frac{R_2(r\rho_m)^2 + \rho_2(r\rho_m)\cos(\Omega\tau)}{1 + R_2(r\rho_m)^2 + 2\rho_2(r\rho_m)\cos(\Omega\tau)} \tag{5.5}$$

and $L(\Omega)$ is defined in Eq.(4.10). Functions A and B are plotted in Figures 5.1 and 5.2, respectively. Function B always has finite value, while Function A blows up for $\Omega\tau = 2\pi$, and $r\rho_m = -\rho_2$. Once the following conditions are satisfied,

$$\tau \frac{\dot{S}}{S} A(\Omega) << 1 , \quad \tau \frac{\dot{S}}{S} B(\Omega) << 1 \tag{5.6}$$

Eq.(5.3) can be further reduced as

$$\ln|Z_a| \cong L(\Omega) - \frac{\tau}{2}\frac{\dot{S}}{S}[A(\Omega) - B(\Omega)] \tag{5.7}$$

which is a reasonable approximation except both $\Omega\tau = 2\pi$ and $r\rho_m = -\rho_2$ are satisfied.

Substituting Eq.(5.7) into Eq.(3.53) gives

$$\dot{S}(t) = \frac{G_N(N - N_{th}) + \frac{2}{\tau_{in}} L(\Omega)}{1 + \frac{\tau}{\tau_{in}}[A(\Omega) - B(\Omega)]} S(t) \tag{5.8}$$

Similarly, the phase of $Z_a(t)$ is

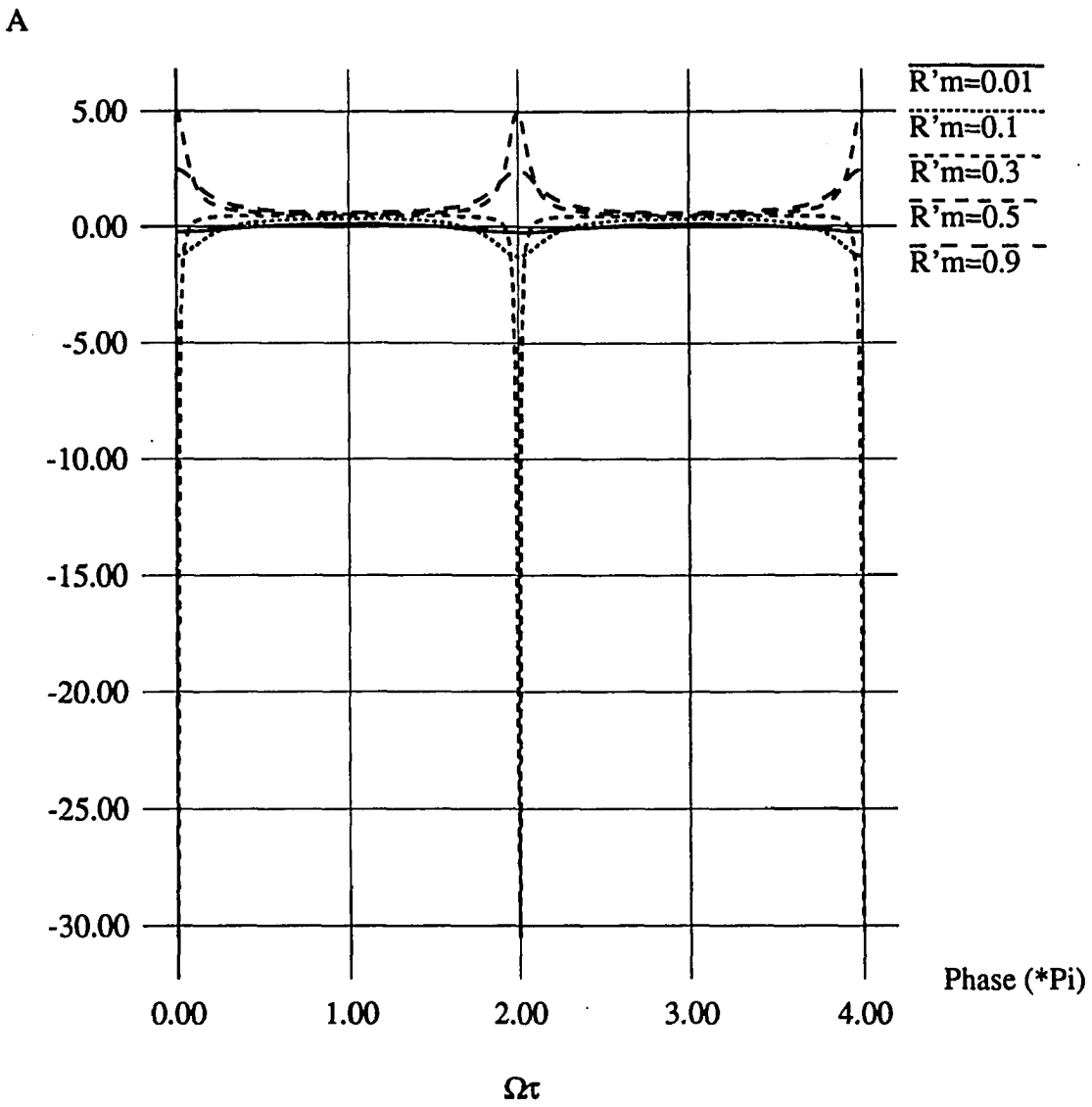

Figure 5.1. Function A

B

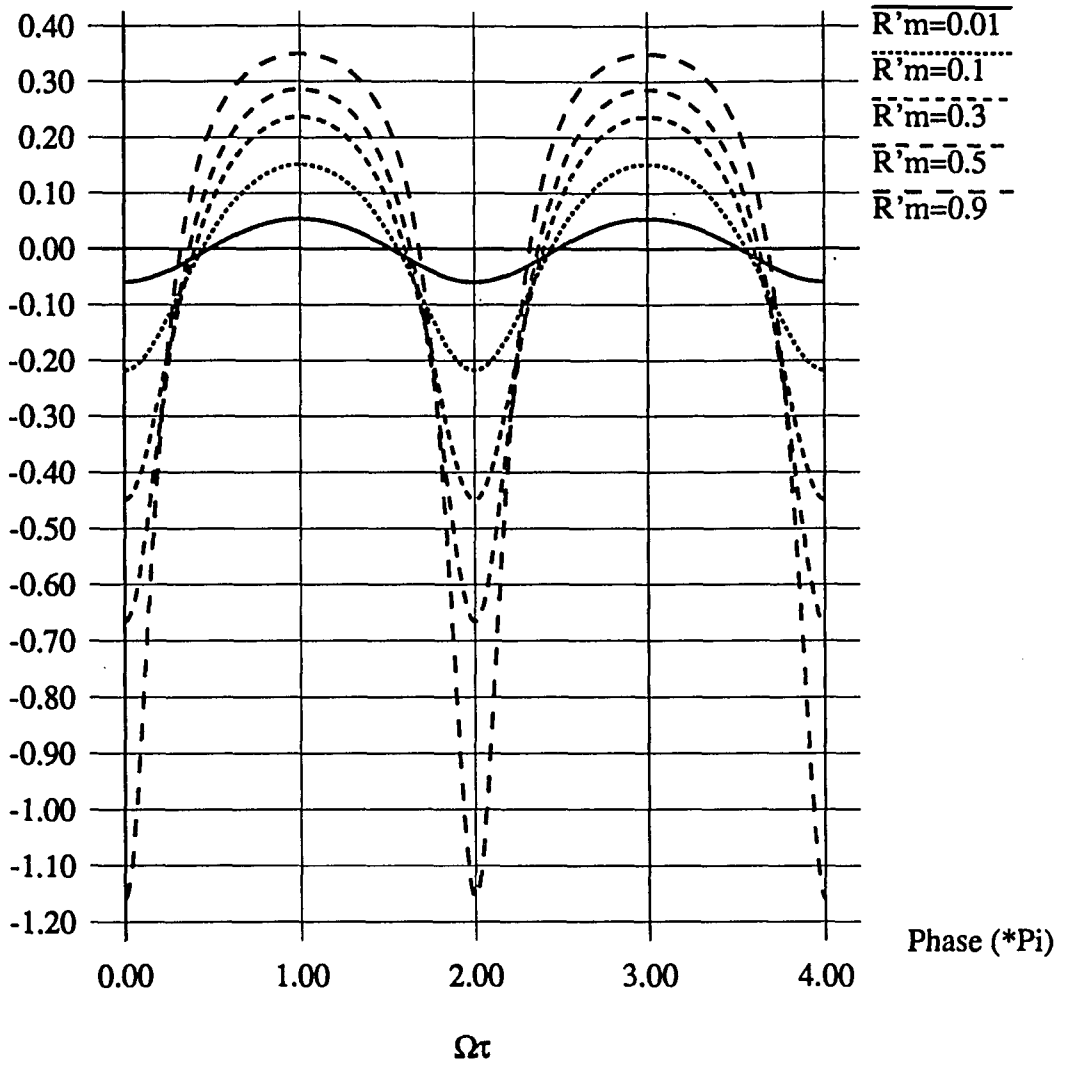

Figure 5.2. Function B

$$\theta_{Z_a}(t) = \frac{\frac{r\rho_m}{\rho_2}(R_2-1)\sin(\Omega\tau)\left[1-\frac{\tau}{2}\frac{\dot{S}}{S}\right]}{1+(r\rho_m)^2\left(1-\frac{\tau}{2}\frac{\dot{S}}{S}\right)^2+\frac{r\rho_m}{\rho_2}(1+R_2)\cos(\Omega\tau)\left[1-\frac{\tau}{2}\frac{\dot{S}}{S}\right]} \tag{5.9}$$

which can be reduced to

$$\theta_{Z_a}(t) \cong \frac{D(\Omega)}{C(\Omega)+\frac{\tau}{2}\frac{\dot{S}}{S}\left[1-(r\rho_m)^2\right]} \tag{5.10}$$

if we assume the slow varying photon density approximation shown in Eq.(5.2). Here, functions C and D are defined in Eqs. (4.11) and (4.12) respectively. Now, let us define function δ, which represents the difference in $\theta_{Za}(t)$, and compare it to the stationary $\theta_{Za}(\Omega_s)$ defined in Eq.(4.14) as

$$\delta(S,\dot{S}) \equiv \frac{\tau}{2}\frac{\dot{S}}{S}\left[1-(r\rho_m)^2\right] \tag{5.11}$$

which will give the simple form

$$\theta_{Z_a}(t) = \frac{D(\Omega)}{C(\Omega)+\delta(N,\Omega)} \tag{5.12}$$

Here, we use Eq.(5.8) to change the variables of δ in Eq.(5.11) into

$$\delta(N,\Omega) = \frac{\tau}{2}\left[1-(r\rho_m)^2\right]\frac{G_N(N-N_{th})+\frac{2}{\tau_{in}}L}{1+\frac{\tau}{\tau_{in}}(A-B)} \tag{5.13}$$

Now, we transform Eq.(3.54) into regular first order differential equation form by differentiating both sides of Eq.(3.54) with respect to t and using Eq.(5.12),

$$\dot{\Omega}(t) = \frac{\frac{\alpha}{2}G_N+\frac{1}{\tau_{in}}\frac{\partial\theta_{Z_a}}{\partial N}}{1-\frac{1}{\tau_{in}}\frac{\partial\theta_{Z_a}}{\partial\Omega}}\dot{N} \tag{5.14}$$

where

$$\frac{\partial\theta_{Z_a}}{\partial N} = \frac{\tau}{2}\left[(r\rho_m)^2-1\right]\frac{D}{(C+\delta)^2+D^2}\cdot\frac{G_N}{1+\frac{\tau}{\tau_{in}}(A-B)} \tag{5.15}$$

$$\frac{\partial\theta_{Z_a}}{\partial\Omega} = \frac{(C+\delta)\frac{\partial D}{\partial\Omega}-D\left(\frac{\partial C}{\partial\Omega}+\frac{\partial\delta}{\partial\Omega}\right)}{(C+\delta)^2+D^2} \tag{5.16}$$

Now, we have three coupled first order differential equations, Eq. (3.27), (5.8) and (5.14), which have the form

$$\frac{dX_i}{dt} = F_i(X_1, X_2, X_3) + f_i(t) \tag{5.17}$$

where X_i's represent S, N, Ω, and forcing term $f_i(t)$ exists due to the injected current density J(t). Equation (5.14) can also be transformed into the form of Eq.(5.17) by substituting Eq.(3.27) into Eq.(5.14).

If the time t does not appear explicitly in the RHS of Eq.(5.17) (i.e., constant current or DC biasing in our case), the set of equations is called autonomous. In contrast, if the time t appears explicitly, the system is referred to as nonautonomous [93].

For convenience and for ensuring the accuracy in numerical calculation, we will normalize the variables as follows:

$$\Omega_R \equiv \frac{\Omega}{\omega_0}$$

$$N_R \equiv \frac{N}{N_{th}}$$

$$T_R \equiv \frac{t}{\tau_{ph}} \qquad (5.18)$$

$$S_R \equiv G_N \cdot \tau_{ph} \cdot S$$

$$J_R \equiv \frac{J}{J_{th}}$$

where

$$J_{th} \equiv \frac{N_{th}}{\tau_s} \cdot q \cdot d_{act} \qquad (5.19)$$

Note that all variables in Eq.(5.18) S_R, N_R, Ω_R, T_R, and J_R are unitless quantities. The three coupled rate equations are now transformed into

$$\dot{S}_R(t) \equiv F_1(S_R, N_R, \Omega_R) = \frac{k_N (N_R - 1) + \frac{2\tau_{ph}}{\tau_{in}} L(\Omega_R)}{1 + \frac{\tau}{\tau_{in}} [A(\Omega_R) - B(\Omega_R)]} S_R \tag{5.20}$$

$$\dot{N}_R(t) \equiv F_2(S_R, N_R, \Omega_R) = \frac{\tau_{ph}}{\tau_s} [J_R - N_R] - \left[N_R - 1 + \frac{1}{k_N} \right] S_R \tag{5.21}$$

$$\dot{\Omega}_R(t) \equiv F_3(S_R, N_R, \Omega_R) = \frac{\frac{\alpha}{2} k_N + \frac{\tau_{ph}}{\tau_{in}} \frac{\partial \theta_Z}{\partial N_R}}{\omega_0 \tau_{ph} \left[1 - \frac{1}{\omega_0 \tau_{in}} \frac{\partial \theta_Z}{\partial \Omega_R} \right]} \dot{N}_R \tag{5.22}$$

where

$$k_N \equiv G_N \cdot N_{th} \cdot \tau_{ph} \tag{5.23}$$

With these definitions, the stationary solutions can be written as

$$\Omega_{RS} = \frac{\Omega_S}{\omega_0} \tag{5.24}$$

which can be determined by solving Eq.(4.16) and

$$N_{RS} = \frac{N_S}{N_{th}} = 1 - \frac{2}{k_N} \frac{\tau_{ph}}{\tau_{in}} L(\Omega_{RS}) \tag{5.24}$$

$$S_{RS} = G_N \tau_{ph} S = \frac{1}{N_{RS} - 1 + \frac{1}{k_N}} \frac{\tau_{ph}}{\tau_s} [J_R - N_{RS}]$$

$$= k_N \frac{\tau_{ph}}{\tau_s} \frac{J_R - 1 + \frac{2}{k_N} \frac{\tau_{ph}}{\tau_{in}} L(\Omega_{RS})}{1 - 2 \frac{\tau_{ph}}{\tau_{in}} L(\Omega_{RS})} \qquad (5.26)$$

Relaxation Oscillation and Damping Characteristics

When the laser diode is driven by a step-current-pulse, a damped ringing of optical power, with the relaxation resonance frequency f_{rx}, occurs, yielding upper limits for the attainable modulation frequency. These relaxation oscillations result from well-known interplay between photon density and carrier density with their respective lifetimes τ_{ph}, τ_s [55]. In order to study this phenomenon, it is useful to investigate the rate equations by linearized small signal analysis. For simplicity, we assume the lasing frequency is fixed and will use the set of two rate equations for the photon density and carrier density, i.e., Eqs. (5.20) and (5.21).

A laser diode is considered with modulation of the injection current around the mean current $\langle J_R \rangle$ according to

$$J_R(t) = \langle J_R \rangle + \Delta J_R \qquad (5.27)$$

where a small modulation amplitude $|\Delta J_R| << \langle J_R \rangle$ is assumed. The rate equations may be linearized yielding the variations of the carrier density and the photon density around their mean values $\langle N_R \rangle$ and $\langle S_R \rangle$, respectively,

$$N_R(t) = \langle N_R \rangle + \Delta N_R \tag{5.28}$$

$$S_R(t) = \langle S_R \rangle + \Delta S_R \tag{5.29}$$

Now, inserting Eqs. (5.27) - (5.29) into the original rate equations (5.20) and (5.21), and linearizing them by choosing the linear terms only, we can obtain

$$\Delta \dot{S}_R(t) = \frac{k_N \cdot \Delta N_R \cdot \langle S_R \rangle + \left[k_N (\langle N_R \rangle - 1) + \frac{2\tau_{ph}}{\tau_{in}} L \right] \Delta S_R}{1 + \frac{\tau}{\tau_{in}} [A - B]} \tag{5.30}$$

$$\Delta \dot{N}_R(t) = \frac{\tau_{ph}}{\tau_s} [\Delta J_R - \Delta N_R] - \Delta N_R \langle S_R \rangle - \left[\langle N_R \rangle - 1 + \frac{1}{k_N} \right] \Delta S_R \tag{5.31}$$

Combining these two equations will give the second order differential equation

$$\Delta \ddot{S}_R + \left[\langle S_R \rangle + \frac{\tau_{ph}}{\tau_s} \right] \Delta \dot{S}_R + \frac{\langle S_R \rangle [1 + k_N(\langle N_R \rangle - 1)]}{1 + \frac{\tau}{\tau_{in}} (A - B)} \Delta S_R$$

$$= k_N \cdot \langle S_R \rangle \cdot \frac{\tau_{ph}}{\tau_s} \cdot \Delta J_R \tag{5.32}$$

To derive Eq.(5.32), we use the stationary solution Eq.(5.25). Equation (5.32) may be written into a form of driven oscillator of resonance frequency ω_{rx} and damping coefficient a_d as follows:

$$\Delta\ddot{S}_R + 2\cdot a_d\cdot\Delta\dot{S}_R + \omega_{rx}^2\cdot\Delta S_R = k_N\cdot\langle S_R\rangle\cdot\frac{\tau_{ph}}{\tau_s}\cdot\Delta J_R \tag{5.33}$$

Here

$$\omega_{rx} = 2\pi f_{rx} = \left[\frac{\langle S_R\rangle\left\{1-\frac{2\tau_{ph}}{\tau_{in}}L\right\}}{1+\frac{\tau}{\tau_{in}}(A-B)}\right]^{0.5} \tag{5.34}$$

and

$$a_d = \frac{1}{2}\left[\langle S_R\rangle + \frac{\tau_{ph}}{\tau_s}\right] \tag{5.35}$$

Then, the solution to Eq.(5.32) has the form

$$\Delta S_R \propto \exp[-a_d t]\cdot\exp\left[j\omega_{rx}\cdot\sqrt{1-\frac{a_d^2}{\omega_{rx}^2}}\cdot t\right] \tag{5.36}$$

Following the same procedure, we can easily show that the second order differential equation for the photon density becomes in the case of the solitary laser diode (i.e., no feedback),

$$\Delta\ddot{S}_R + \left[\langle S_R \rangle + \frac{\tau_{ph}}{\tau_s} \right] \Delta\dot{S}_R + \langle S_R \rangle \Delta S_R = k_N \cdot \langle S_R \rangle \cdot \frac{\tau_{ph}}{\tau_s} \cdot \Delta J_R \qquad (5.37)$$

Equation (5.32) will reduce to Eq.(5.37) if we use $\langle N_R \rangle = 1$ (this is the case for the solitary laser diode around the threshold level) and $\tau = 0$.

Comparing Eq.(5.32) to Eq.(5.37) gives some implications about the change in damped relaxation oscillation due to external feedback. First, damping coefficient a_d is not changed from that of the solitary laser diode. Since $\langle S_R \rangle$ is also inversely proportional to τ_s, as shown in Eq.(5.26), the envelope of the oscillations is such that the oscillations decay in a period of time on the order of the carrier lifetime. Also, the higher the optical power, the shorter the decay time. The angular resonant frequency ω_{rx} in Eq.(5.34) has a multiplicative factor which is the function of A,B, and L, compared to $\omega_{rx} = \langle S_R \rangle^{0.5}$, the resonant frequency of the solitary laser diode.

In Table 5.1, the set of physical parameters and their numerical values which will be used in our calculation is summarized. Some of those values are quoted from the literature [28].

From Figures 4.1, 5.1, and 5.2, we can see the resonance frequency becomes higher around $\Omega\tau = 2\pi$, and R'_m becomes closer to R_2. Also, as the external cavity length increases (assuming R'_m can be maintained), (i.e., τ increases) resonance frequency decreases.

Table 5.1. Physical parameters and their numerical values

Parameter	Symbol	Value
Gain constant	G_N	$1.1 \cdot 10^{-12}$ m^3/sec
Carrier density at transparency	N_0	$1.1 \cdot 10^{24}$ $/m^3$ [a]
Carrier lifetime	τ_s	0.5 nsec
Photon lifetime	τ_{ph}	2 psec
Laser cavity roundtrip time	τ_{in}	9 psec [b]
Linewidth enhancement factor	α	6
Active region volume	V	10^{-16} m^3
Active layer thickness	d_{act}	0.2 μm

[a] Therefore

$$N_{th} = N_0 + \frac{1}{G_N \tau_{ph}} = 1.55 \cdot 10^{24} / m^3$$

[b] $\mu_e = 4.5$, $L = 300$ μm

The influence of weak optical feedback on the relaxation oscillation was discussed in the literature [60]. In this section we derived a simple expression for the relaxation oscillation frequency and damping coefficient which can be applied for both strong and weak feedback in a short external cavity configuration. This expression may be useful for designing an external cavity laser diode to give high relaxation oscillation frequency, so that it can be modulated at very high frequency.

In order that ΔS_R does not grow exponentially in Eq.(5.36), ω_{rx}^2 should have a positive value. It gives the simple stability condition

$$1 + \frac{\tau}{\tau_{in}} (A - B) > 0 \qquad (5.38)$$

since

$$1 - \frac{2\,\tau_{ph}}{\tau_{in}} L(\Omega) > 0 \qquad (5.39)$$

is always satisfied.

Dynamical Stability Condition

Consider the autonomous nonlinear differential equation set of Eq.(5.17). The time evolution of $X_i(t)$ (i=1,2,3) can be completely determined if we have three initial conditions $X_i(0)$ (i=1,2,3). In the case of nonlinear systems, the concept of stability is not clear-cut in comparison with the linear time-invariant systems. Gibson[94] mentions that there are 28 different classes of stability in current use. Some of the important features of nonlinear systems are as follows:

1. The stability of an unforced system can be very dependent upon the initial state $X_i(0)$.
2. The stability is dependent upon the input. For example, an unforced system may be stable, but the same system, subject to a step input, may be diverged.

We shall restrict ourselves to nonlinear systems subject to constant inputs (constant current density) only, in this chapter. Actually the stability theory for systems subject to arbitrary inputs is still very underdeveloped. And we will consider the local stability in this section. Assume that Eq.(5.17) has an equilibrium point (or a fixed point stationary solution) $\mathbf{X^0}$. The system is said to be locally stable if, when subject to a sudden small perturbation, it tends to remain within a small specified region R surrounding $\mathbf{X^0}$. It should be noted that stability in the above sense does not require the state to return eventually to $\mathbf{X^0}$. Since we are concerned with the dynamics in the immediate neighborhood of the equilibrium point, we can linearize the variables around that point. By introducing the deviation vector $\delta\mathbf{X}$, defined by

$$\delta \mathbf{X} \equiv \mathbf{X} - \mathbf{X}^0 \tag{5.40}$$

and by defining the Jacobian matrix

$$\mathbf{J} \equiv \begin{bmatrix} \frac{\partial F_1}{\partial X_1} & \frac{\partial F_1}{\partial X_2} & \frac{\partial F_1}{\partial X_3} \\ \frac{\partial F_2}{\partial X_1} & \frac{\partial F_2}{\partial X_2} & \frac{\partial F_2}{\partial X_3} \\ \frac{\partial F_3}{\partial X_1} & \frac{\partial F_3}{\partial X_2} & \frac{\partial F_3}{\partial X_3} \end{bmatrix} \tag{5.41}$$

We can obtain the following linear vector differential equation valid in the immediate neighborhood of $\mathbf{X}^0$:

$$\dot{\delta \mathbf{X}} \equiv \mathbf{J} \cdot \delta \mathbf{X} \tag{5.42}$$

The stability of this system depends entirely upon the nature of the eigenvalues obtained from the equation [95]

$$| s\mathbf{I} - \mathbf{J} | = 0 \tag{5.43}$$

The system is locally stable if and only if none of the three eigenvalues of **J** is located in the RHS of the s-plane. If some of the eigenvalues coincide, it may be necessary to include extra functions depending on the number of independent eigenvectors belonging to the multiple eigenvalues.

Following this procedure starting from Eqs.(5.20) - (5.22), we obtain the dynamic stability condition

Stability Condition

$$\frac{1+\dfrac{\alpha\dfrac{dL}{d\Omega_R}-2H(\Omega_R)}{\omega_0[\tau_{in}-\tau M(\Omega_R)]+H(\Omega_R)}}{1+\dfrac{\tau}{\tau_{in}}(A-B)}>0 \tag{5.44}$$

where

$$H(\Omega_R)\equiv\frac{\dfrac{\tau}{\tau_{in}}[1-(r\rho_m)^2]D\dfrac{dL}{d\Omega_R}}{(C^2+D^2)\left[1+\dfrac{\tau}{\tau_{in}}(A-B)\right]} \tag{5.45}$$

$$M(\Omega_R)\equiv\frac{C\dfrac{dD}{d\Omega_R}-D\dfrac{dC}{d\Omega_R}}{\tau[C^2+D^2]} \tag{5.46}$$

A detailed derivation is given in Appendix B. From the physical point of view, Eq.(5.38) should be satisfied for ensuring stability. Therefore, we may assert that the strict stability condition is

Strict Stability Condition

$$1 + \frac{\tau}{\tau_{in}} (A - B) > 0 \qquad (5.38)$$

and at the same time

$$1 + \frac{\alpha \frac{dL}{d\Omega_R} - 2 H(\Omega_R)}{\omega_0 [\tau_{in} - \tau M(\Omega_R)] + H(\Omega_R)} > 0 \qquad (5.47)$$

However, in most phase of short external cavity configuration, condition Eq.(5.38) is met unless R'_m is very close to R_2. In this case, we can simply use Eq.(5.44) as the measure of dynamical stability. In Figure 5.3, Eq.(5.44) is plotted when $R'_m = 0.2$. At short external cavity length, the system is quite stable for all the phase values. When d = 100 μm, the figure shows that the system becomes unstable around $\Omega\tau \approx 1.92\,\pi$. Figure 5.3 qualitatively shows that Eq.(5.44), i.e., the stability condition, is heavily dominated by the $dL/d\Omega_R$ term if we compare it with Figure 4.1. This implies that a frequency change effect caused by gain change (due to the external cavity) is dominant for determining the dynamical characteristics of the external cavity laser. An S-shaped peak and valley in the stability condition curve becomes sharper as R'_m becomes closer to R_2. As a result, Eq.(5.44) predicts that the system becomes abruptly unstable as the phase changes from $\Omega\tau = 2\pi^+$ to $\Omega\tau = 2\pi^-$, which is very unrealistic. However, in this specific example, we should also consider the condition Eq.(5.38), which will show the system is unstable around

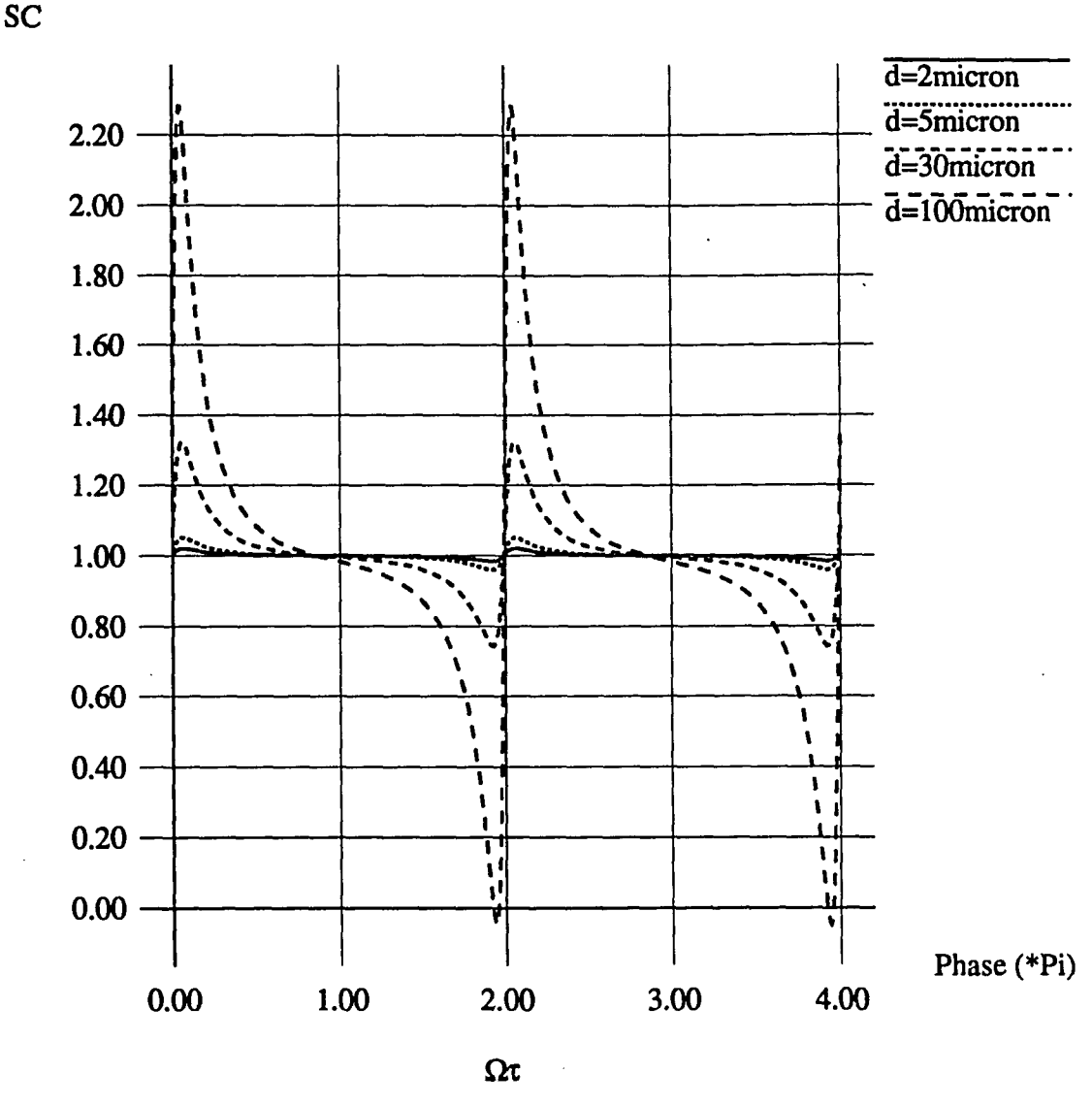

Figure 5.3. Plot of stability condition, where the negative value denotes the dynamically unstable region

$\Omega\tau = 2\pi$, if R'_m is close to R_2. This condition can easily be met in the short external cavity laser diode.

Numerical Simulations of Rate Equations

The rate equations (5.20) - (5.22) are solved numerically by using the Runge-Kutta algorithm. The physical parameters used in the calculation are summarized in Table 5.1. Typical simulation results are shown in Figures 5.4-5.6. Those plots are photon density, carrier density and angular lasing frequency of the laser diode coupled to a 3 μm long external cavity. The effective external reflectivity R'_m is chosen as 0.2, and relative current density $J_R = 1.02$. When the photon density S_R surpasses the steady state value, the carrier density N_R and frequency Ω_R have a negative slope with respect to time. As shown in Eq.(5.22) the derivative of Ω_R is proportional to the derivative of N_R. Therefore, the time evolution of angular frequency shows the same form as that of carrier density. The optical frequency is varying (laser chirping effect) according to the change in optical power. Therefore, the spectral line is broadened under current modulation (AM), since the intensity modulation is always accompanied by a frequency modulation. Marcuse et al. [96] showed approximate analytical solutions and numerical simulation results of rate equations. However, they used only two equations, considering S and N. Our solution can give the transient solutions for S, N, and Ω, so it may be used in investigating the suitable current pulse shape for reducing the laser chirp effect.

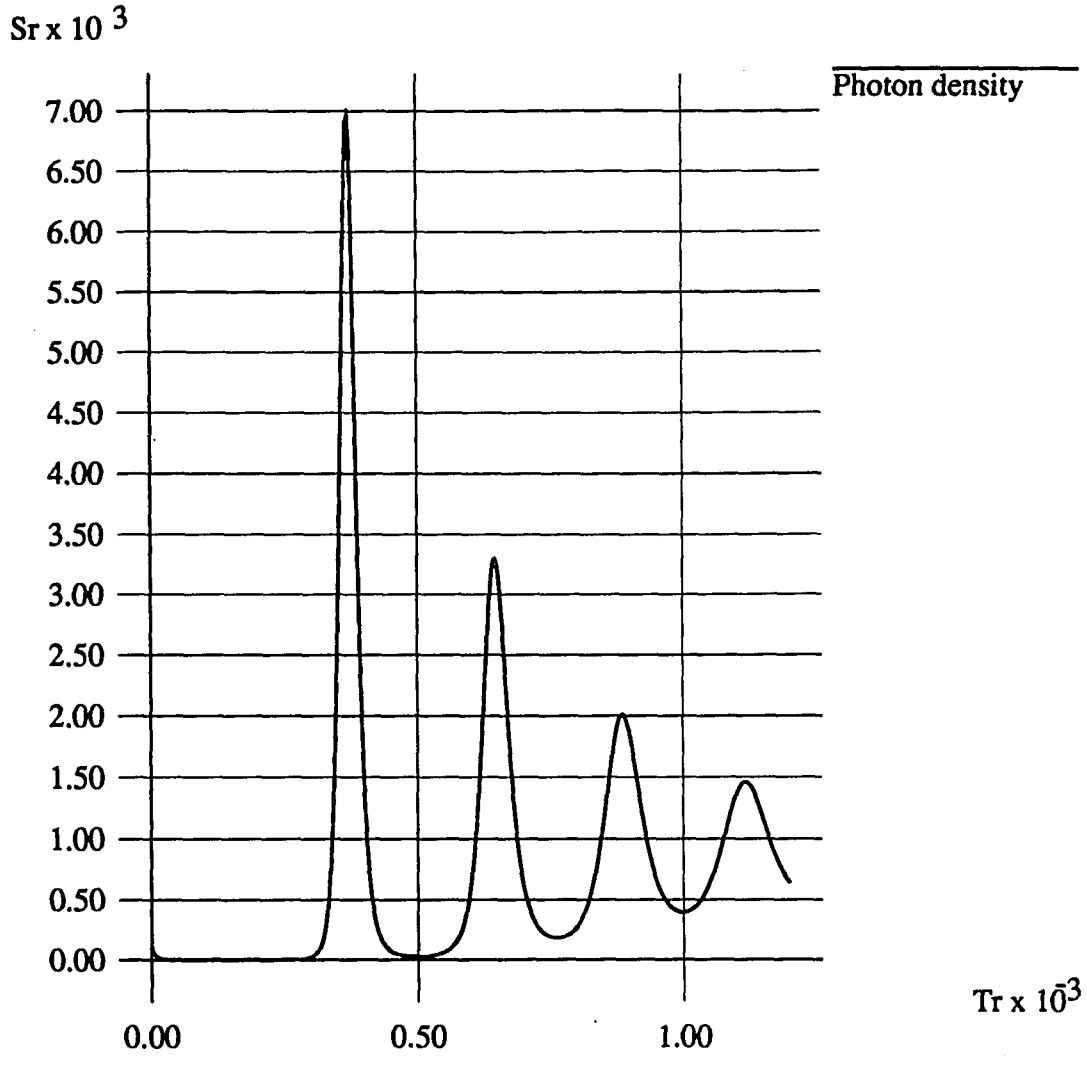

Figure 5.4. Simulation of photon density at $\lambda = 0.78$ μm, $R_1 = R_2 = 0.32$ $R'_m = 0.2$, d = 3 μm, and J = 1.02

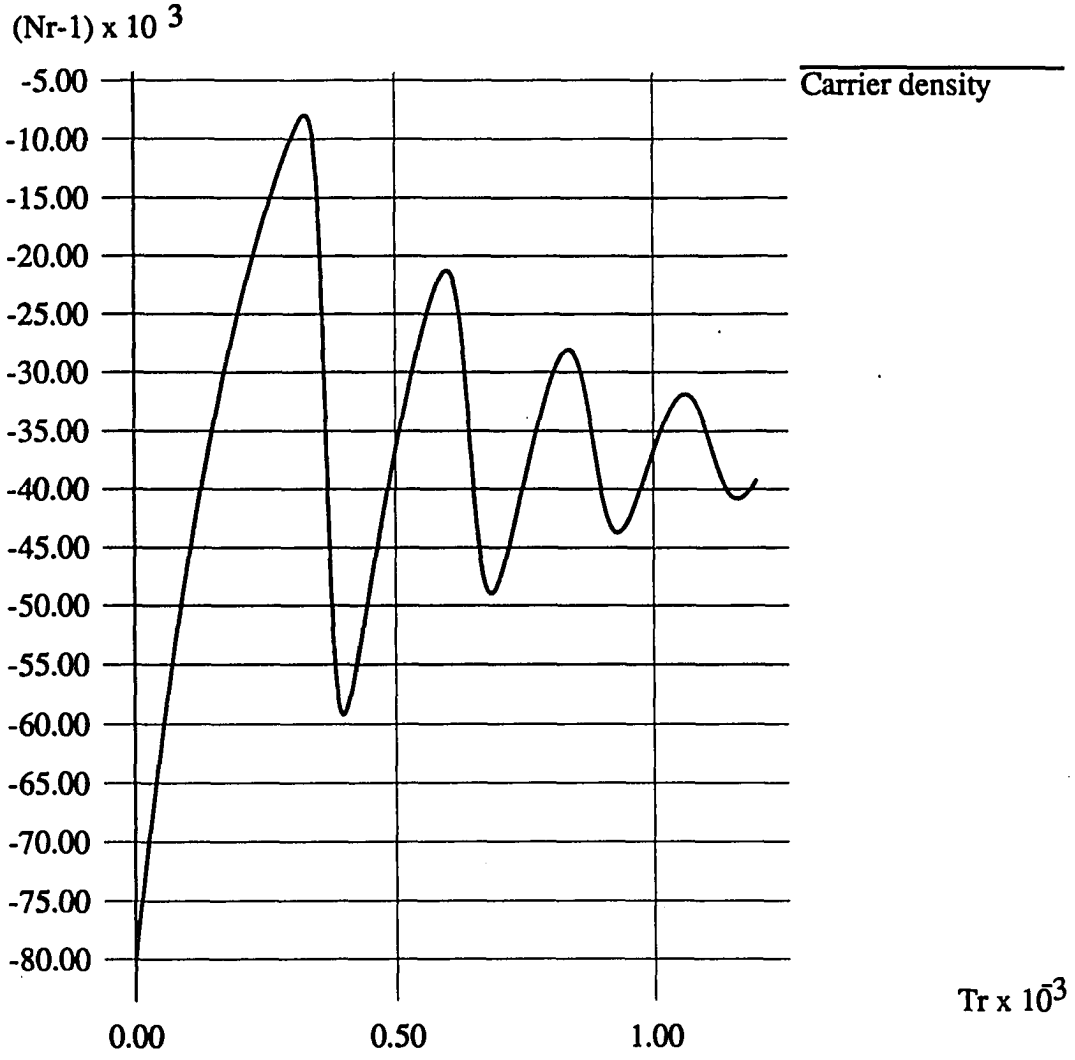

Figure 5.5. Simulation of carrier density at $\lambda = 0.78\ \mu m$, $R_1 = R_2 = 0.32$ $R'_m = 0.2$, $d = 3\ \mu m$, and $J = 1.02$

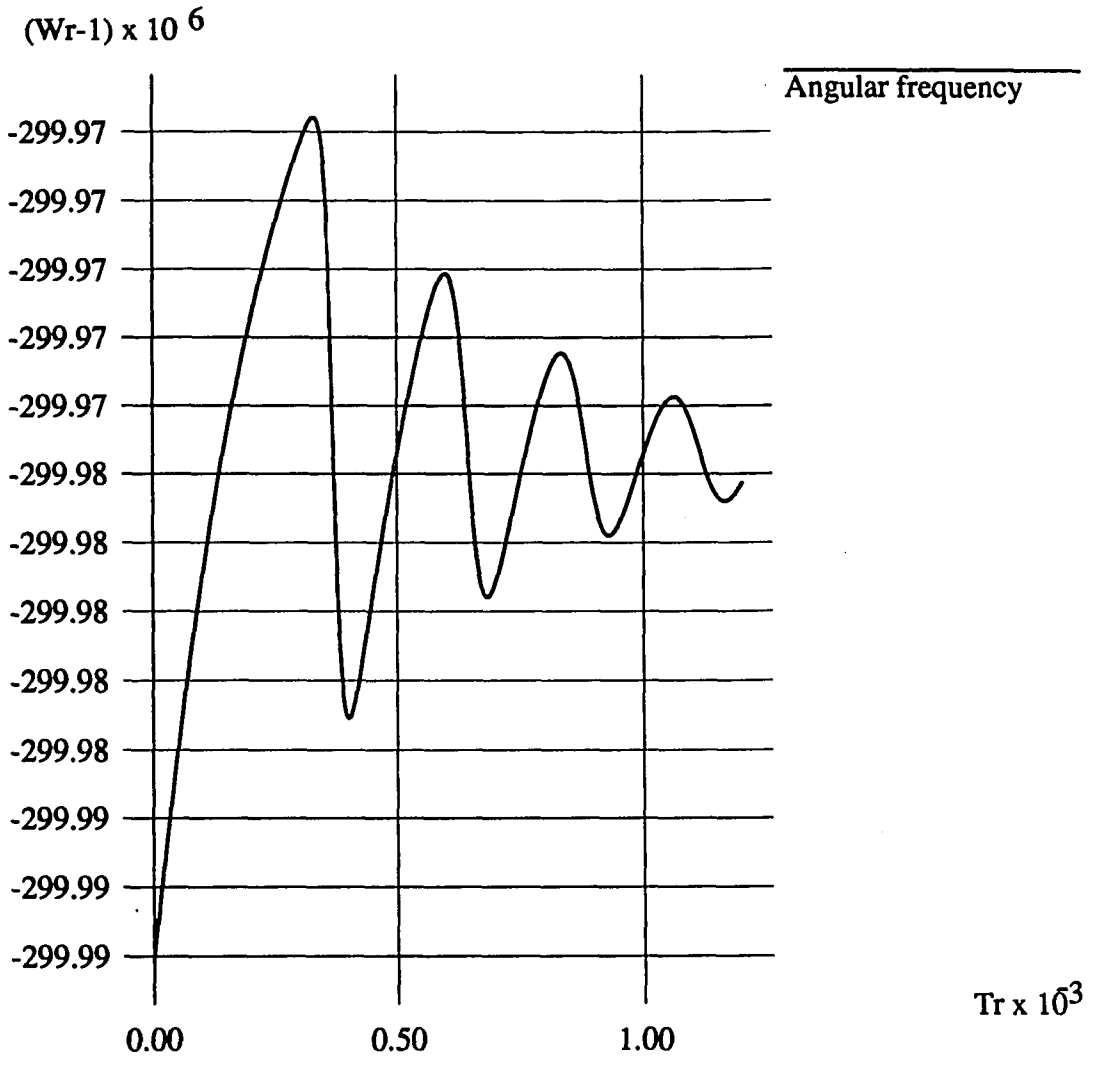

Figure 5.6. Simulation of lasing angular frequency at $\lambda = 0.78$ μm, $R_1 = R_2 = 0.32$ $R'_m = 0.2$, $d = 3$ μm, and $J = 1.02$

In Figures 5.7-5.9, we show the simulation result where the biasing current density is abruptly changed from 1.2 to 1.3. The parameters used in the calculation are d = 93.79 μm and R'_m = 0.3. The photon density is increased and settled down after damped relaxation oscillation, while the carrier density and angular frequency do not make noticeable changes after ringing.

In Figure 5.10, we plot the photon density as a function of time, for the case of d = 7.79 μm, R'_m = 0.3, and J_R = 1.25. The expected stationary conditions should be S_{RS}≈0.0005 and N_{RS}≈1.19. We use S_{Ri}=0.0001 and N_{Ri}=1.2 as the initial conditions. Physically, this example may be thought of as a simulation of the abrupt change experienced by the external cavity length (only few tenths of a μm), since the photon density is a very strong function of external cavity length, especially for the short cavity case as shown in Figure 4.18. As expected, the photon density will suffer the damped relaxation oscillation. If we calculate the ringing frequency using Eq.(5.34) - (5.36), we get f_r^{-1} ≈ 103, which is approximately half of the actual ringing period shown in Figure 5.10. The error in analytical estimation using Eq.(5.34) is mainly due to the linearized small signal approximation. As shown in Figure 5.10, the magnitude of relaxation oscillation is three times bigger than the steady state value. Therefore, the small signal approximation used to derive Eq.(5.34) does not hold in this case. However, the simple estimation is still useful since the estimation error is not significant, and it can show us the tendency of change in relaxation frequency as some parameters change. When the amplitude of relaxation oscillation is small, the approximate analytic estimation shows good agreement with the numerically calculated values.

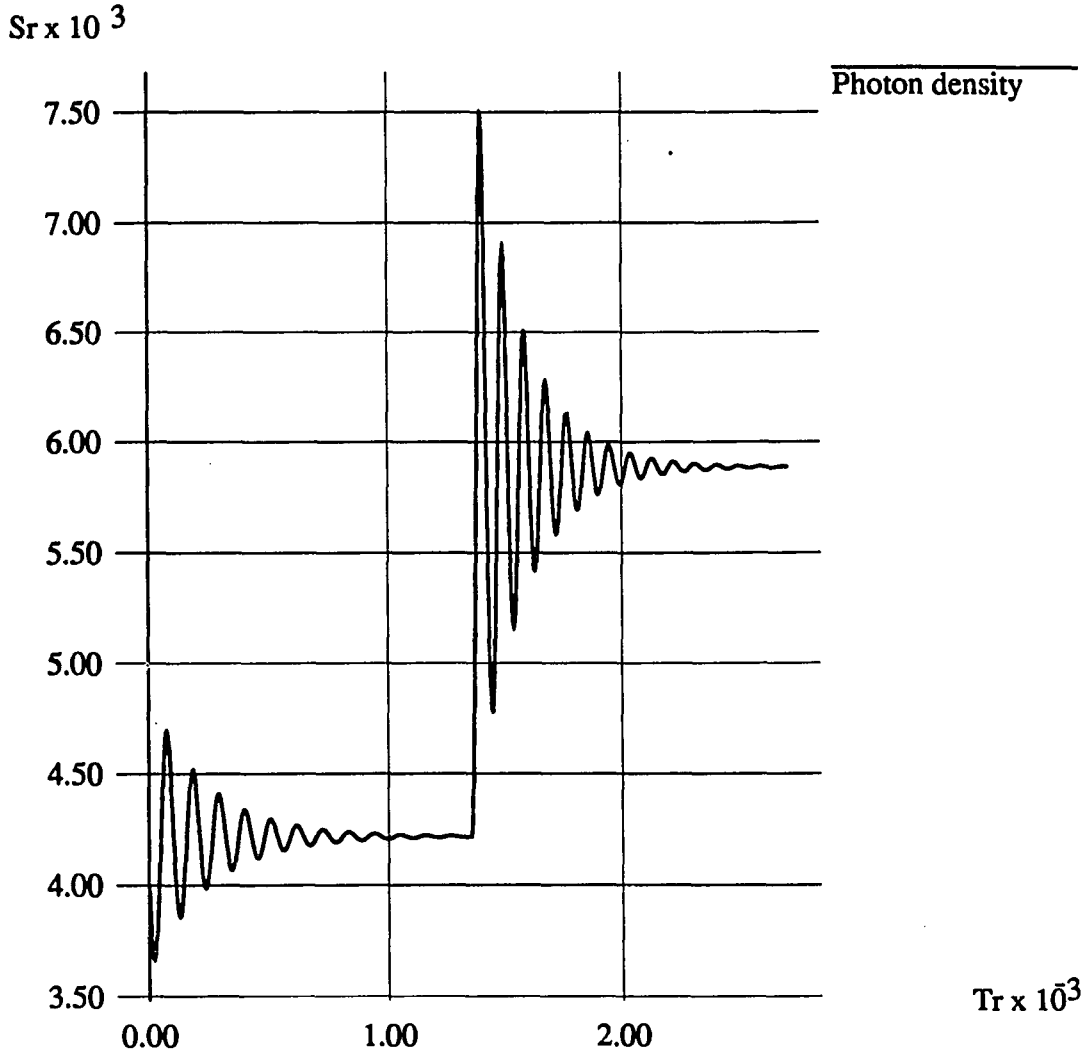

Figure 5.7. Simulation of photon density when J is abruptly changed from 1.2 to 1.3, at $\lambda = 0.78\ \mu m$, $R_1 = R_2 = 0.32$, $R'_m = 0.3$, and $d = 93.79\ \mu m$

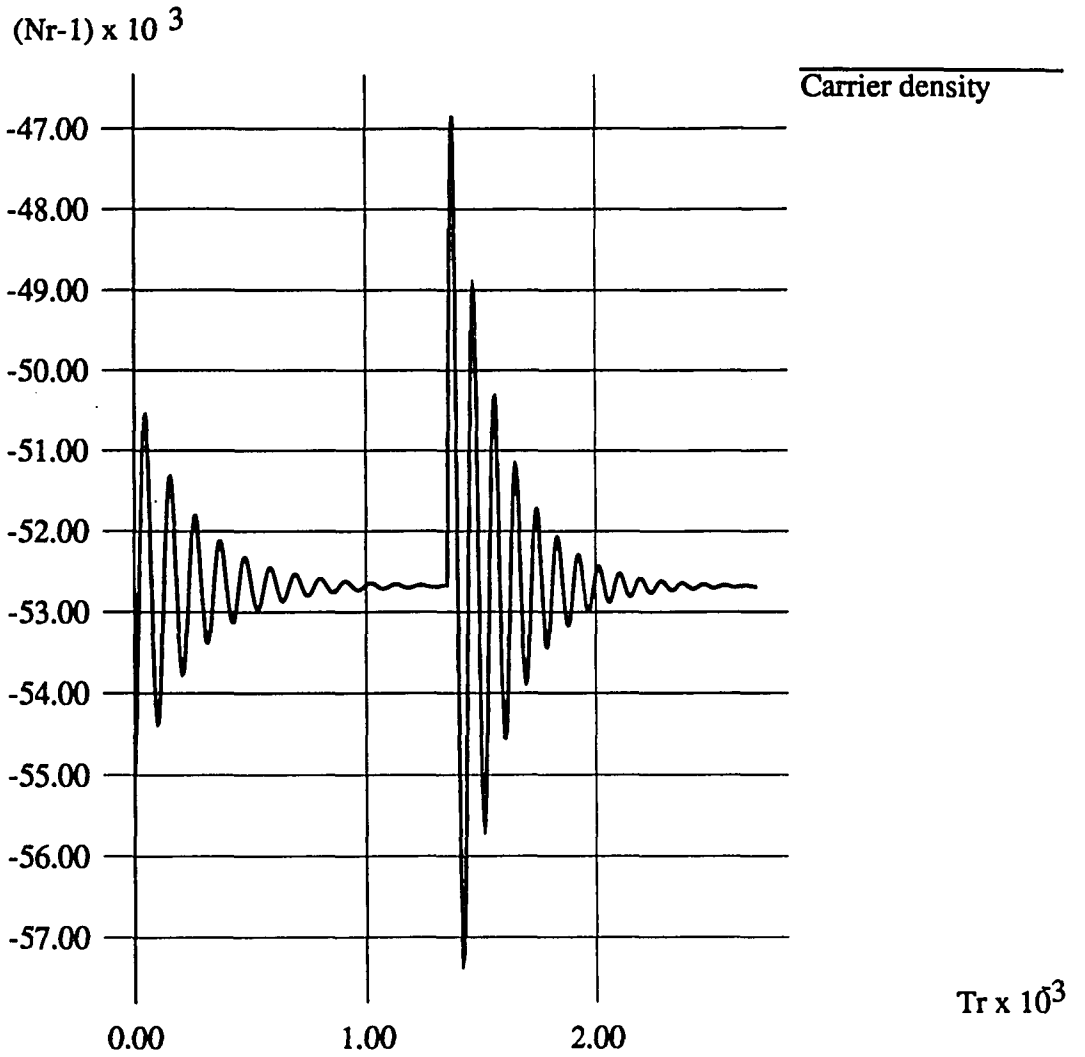

Figure 5.8. Simulation of carrier density when J is abruptly changed from 1.2 to 1.3, at $\lambda = 0.78\ \mu m$, $R_1 = R_2 = 0.32$, $R'_m = 0.3$, and $d = 93.79\ \mu m$

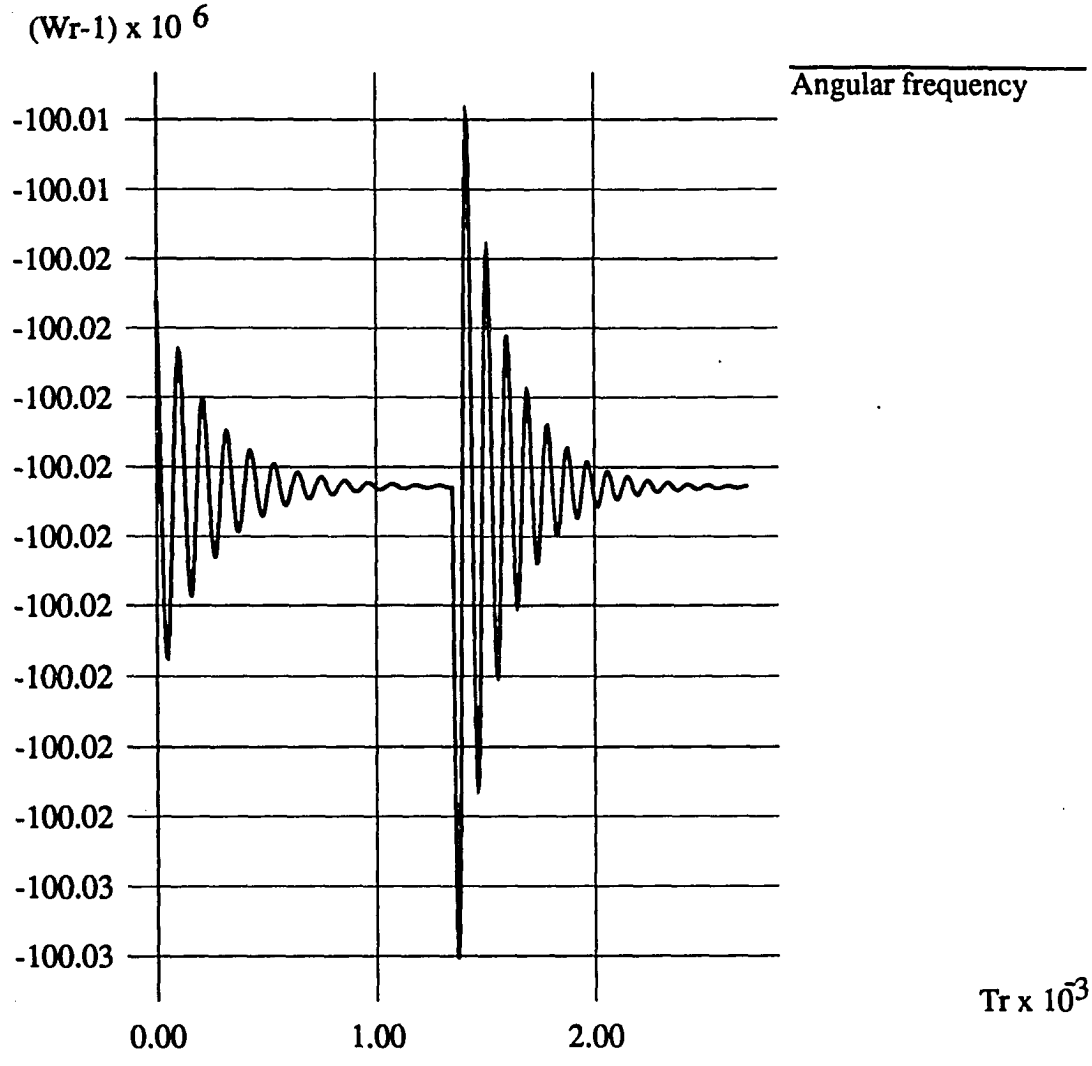

Figure 5.9. Simulation of lasing angular frequency when J is abruptly changed from 1.2 to 1.3, at $\lambda = 0.78\ \mu m$, $R_1 = R_2 = 0.32$, $R'_m = 0.3$, and $d = 93.79\ \mu m$

Figure 5.11 shows the time evolution of photon density with the same initial conditions and same physical parameters, except the external cavity length d = 7.985 μm. Since there is a big difference between the initial conditions and final stationary solutions, it will suffer a quite huge transient change. However, this is unrealistic of course, since it is impossible to change external cavity length abruptly (much faster than the photon lifetime). Nevertheless, we can draw some conclusions: first, relaxation oscillation frequency becomes higher as the average photon density increases, so it will be much nicer to maintain the operating external cavity length in phase so that the laser output maintains peak value in Figure 4.18. The next point which we want to emphasize is that even the small change in external cavity length will introduce not only a significant change in steady state characteristics as discussed in chapter 4, but also large change in transient effect to the laser diode parameters. The effect caused by current modulation will be discussed in the next chapter, using the simulation program whose validity is proven in this section.

Chaos in the External Cavity Laser Diode

Brief review of chaotic system

In the 19th century, H. Poincaré already discovered that certain mechanical systems whose time evolution is governed by Hamilton's equations could display chaotic motion. In 1963, Lorenz [97] found that even a simple set of three coupled, first order, nonlinear differential equations can lead to completely chaotic trajectories.

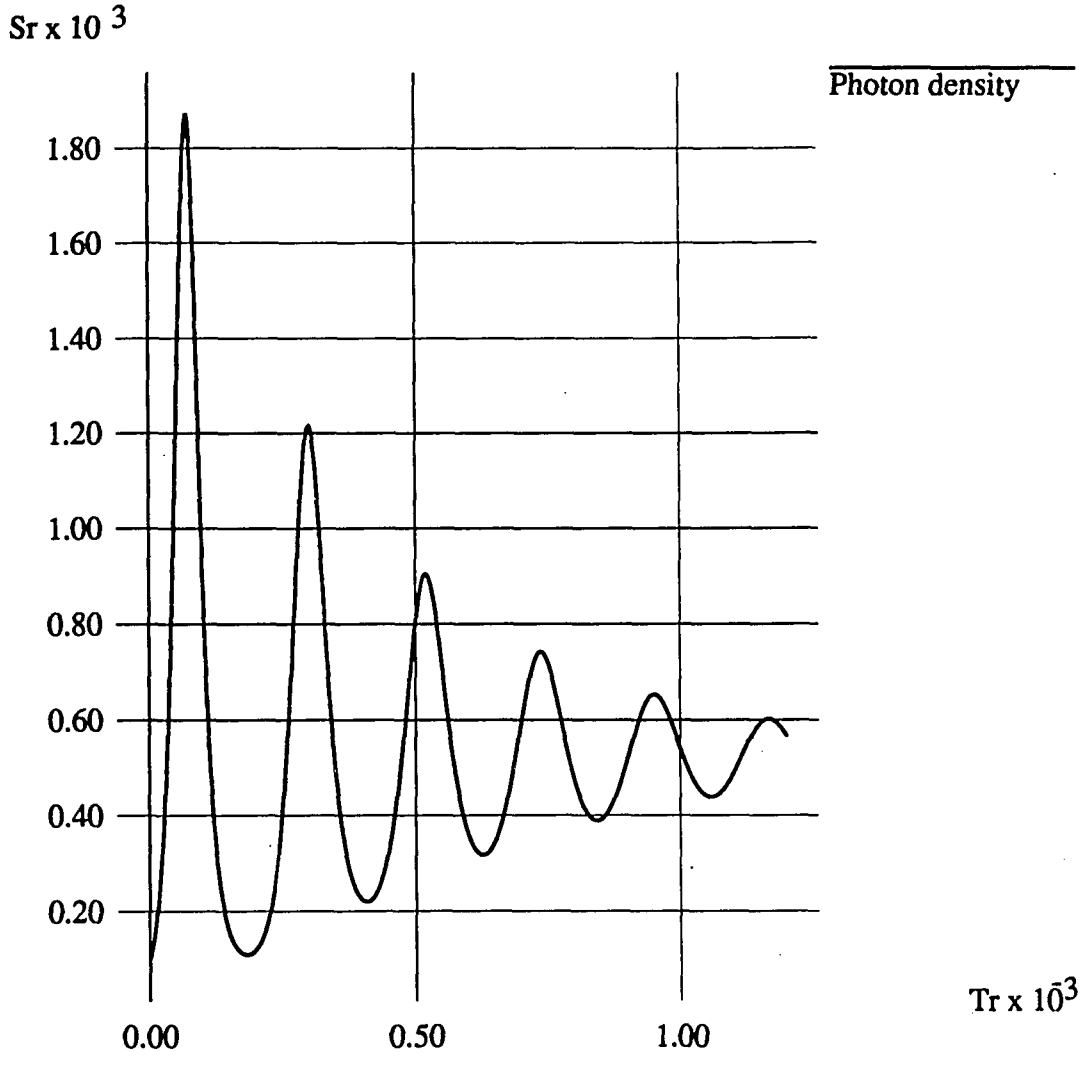

Figure 5.10. Simulation of photon density at $\lambda = 0.78$ μm, $R_1 = R_2 = 0.32$, $R'_m = 0.3$, $J_R = 1.25$, and $d = 7.79$ μm

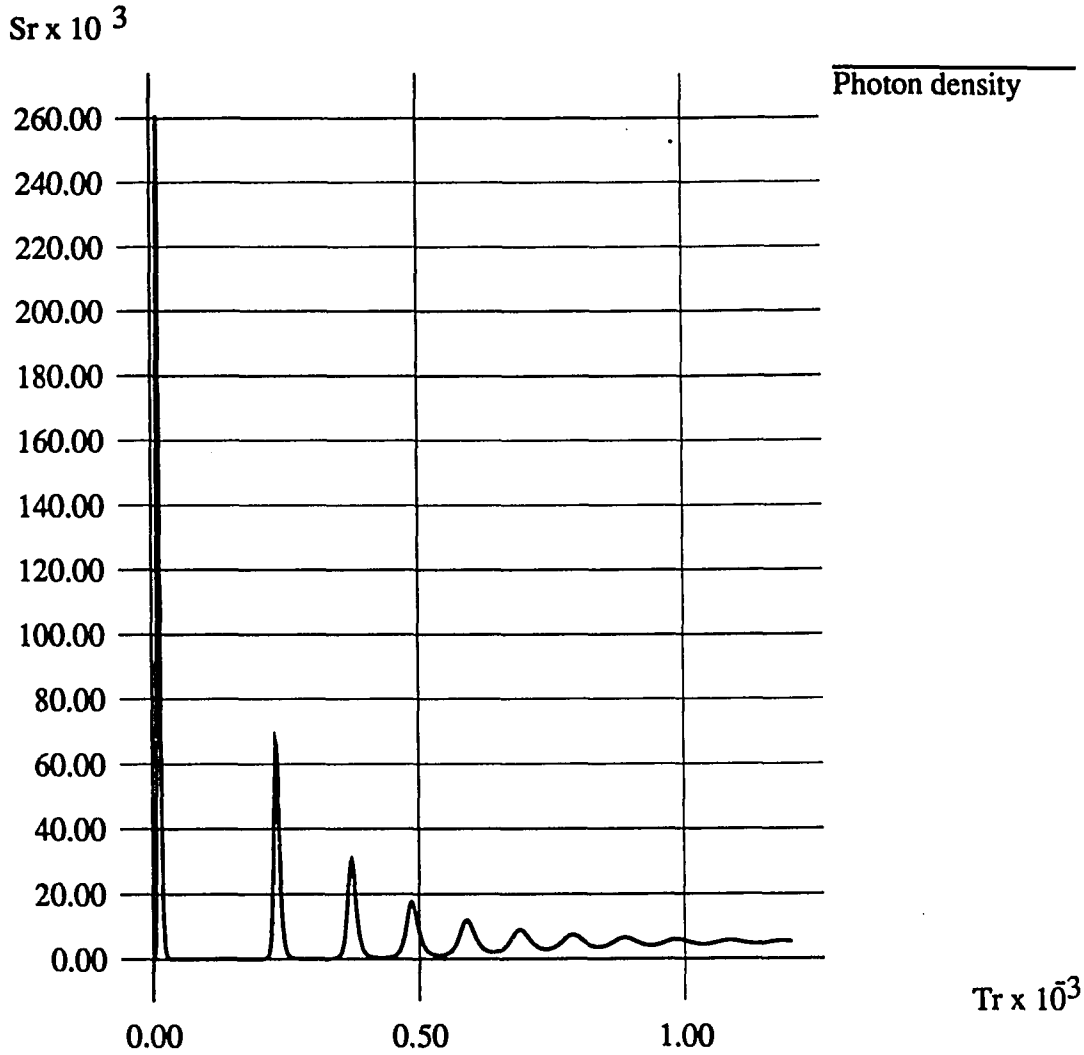

Figure 5.11. Simulation of photon density at $\lambda = 0.78\ \mu m$, $R_1 = R_2 = 0.32$, $R'_m = 0.3$, $J_R = 1.25$, and $d = 7.985\ \mu m$

In modern usage, deterministic chaos denotes the irregular or unpredictable motion that is generated by nonlinear systems whose dynamical laws uniquely determine the time evolution of a state of the system either in terms of differential or difference equations. Now, we must distinguish between random and chaotic motions. In random motion, we really do not know the input forces or we only know some statistical measures of the parameters. But the chaotic problems do not have any random or unpredictable inputs or parameters. In that sense, they are called deterministic chaos. The unpredictability comes from the property of the physical or mathematical systems, the time history of which has a very sensitive dependence on initial conditions. In recent years, it has been proven that this phenomenon is abundant in nature and in many branches of science (e.g., fluids mechanics, chemical reactions, plasma, and biological models etc.) and a lot of literatures deal with the general and broad theory about deterministic chaos [98-101]. The chaos in optical science was briefly reviewed in [102]. We will only consider the dissipative systems (e.g. , a forced pendulum with friction) [101]. Another branch of the chaotic system is the conservative systems (e.g., planetary motion, which is governed by Hamilton's equations).

There are three particularly important routes to chaos which are observed as some external parameter is changed and as the time evolution of the system changes from regular to chaotic. The most recent route to chaos is the period-doubling route. In the period-doubling phenomenon, one starts with a system with a fundamental periodic motion. Then as some experimental parameter is varied, the system undergoes successive period-doubling (or pitchfork) bifurcations. This process will accumulate at a critical value of the parameter,

after which the motion becomes chaotic. This phenomenon has been observed in a number of physical systems, especially in laser systems [82, 103 - 105].

A second route to chaos is called the intermittency route to chaos. Intermittency means that a signal which behaves regularly in time becomes interrupted by statiscally distributed periods of irregular motion (intermittent bursts). The rate of these bursts increases with the variation of an external parameter and the time evolution eventually becomes completely chaotic. This route to chaos provides a universal mechanism for 1/f-noise in nonlinear systems. A tangent bifurcation will lead to this type of route to chaos [101].

A third route is called the quasi - periodic route to chaos, or sometimes called the Ruelle - Takens - Newhouse route, after names of researchers who discovered this route. In 1944, Landau considered that chaos could be viewed as the result of an infinite sequence of Hopf bifurcations. However, Ruelle and Takens [106] and Newhouse [107] showed that after only two instabilities in the third step, the trajectory becomes attracted to a bounded region of phase space in which initially close trajectories (limit cycle solutions) separate exponentially such that the motion becomes chaotic. These particular regions of phase space are called strange attractors. [98,99]

<u>Coherence collapse and chaotic behavior in the long external cavity laser diode</u>

Several experimental and theoretical investigations [16,28,29,61,82,86-92] have dealt with irregular chaotic behavior in the external cavity laser diode. The external cavity considered is always much longer than the length of the laser diode and usually shorter than the coherence length of the solitary laser.

Typical external cavity lengths vary from a few millimeters to several meters. Many efforts were made to investigate the situation with moderate amounts of optical feedback (0.1 - 10 % output power coupled back into the laser), since low-frequency self-pulsations [16], and dramatic line broadening up to 25 GHz [29] were reported experimentally.

The theoretical work by Mørk et al.[28] shows that, at least well above threshold, the fluctuating instability in light intensity is caused from the nonlinear dynamics themselves, and the spontaneous recombination noise does not cause that instability. These can be thought of as strong indications in favor of deterministic chaos. However, not all experimentally observed phenomena are well understood so far. Another approach to investigating the coherence collapse phenomena is to study the relative intensity noise (RIN) [87], the spectral properties, and the coherence times [86,89] of the external cavity laser, to directly see the abrupt increase in noise figure as some parameter is varying.

The coherence collapse feedback regime is bounded by regimes of single mode narrow linewidth operation at both very high and very low feedback levels [30]. The coherence collapse at high feedback levels, which at low bias currents manifests itself as low-frequency intensity fluctuation due to the bistable stationary solutions [28], is demonstrated as following a period-doubling route to chaos [61]. In Tromborg and Mørk[61], they found the limit cycle solutions of rate equations using their injection locking model, which is valid only for the long external cavity configuration. And using the Poincaré mapping technique, they showed that the limit cycle solutions undergo a period-doubling bifurcation numerically. The transition to coherence collapse

at low feedback levels was studied by the same researchers [92]. Undamping of the relaxation oscillations will give rise to a self-sustained periodic limit cycle solution, and will initialize the route to chaos. And it is argued that this sequence follows the quasi-periodic route to chaos.

The coherence collapse in a long external cavity with moderate feedback level has tended to be recognized as a chaotic phenomenon recently, even though the efforts to clearly distinguish the deterministic chaos from the noise driven instabilities are still one of the active research areas. In Cohen and Lenstra [88], the authors argue that coherence collapse is dynamically stable for all values of linewidth enhancement factor α, (except α=0), which means that if a laser operates in the coherence collapsed state, it will stay there forever, and the presence of small fluctuations will not alter this situation.

Is the short external cavity laser always stable?

It has been shown that external cavity lasers exhibit a good stability without any coherence collapse in computer simulation, if the external cavity is shorter than about 5 mm [91]. And there have been no experimental reports for observing coherence collapse in the short external cavity configuration. In the work cited in the previous section [92], it is shown analytically that for a short external cavity, there may be no transition to coherence collapse at low feedback level. However, those works mentioned above have used the weak coupling approximation, which may not be justified for the ultra short external cavity configuration.

According to our simplified linearized model in Eq.(5.32), we can not expect the Hopf bifurcation to occur since the coefficient of the first derivative

term, i.e. $2a_d$, is always positive. This means it is highly possible that our model does not have limit cycle solutions. Furthermore, our model equations which are used in our numerical simulation Eqs.(5.20) - (5.22) assumed a slow-varying amplitude and a short external cavity length approximation. So, they differ from the original model equations derived in Chapter 3 in that Eqs. (5.20) - (5.22) do not have a complete 3 - degrees of freedom, since the derivatives of N_R and Ω_R are proportional each other (refer to Appendix B for the detailed calculation of eigenvalues of the Jacobian matrix). Only the system, whose degrees of freedom are greater than three has the possibility of having a chaotic or strange attractor for the autonomous system [99]. Therefore, with the model equations used in this chapter, we can not expect to ever find any chaotic solutions.

However, we show that the fixed stationary solution for the short external cavity laser becomes dynamically unstable in certain external cavity phases as shown in Figure 5.3. Those instabilities may be found even in a very short external cavity laser, but the range of external phase that shows those instabilities is so small (almost a pinpoint of $\Omega\tau \approx 2\pi$ and $R'_m = R_2$) that in a practical sense it might not be observed easily. In order to rigorously investigate dynamical stability and the possibility of chaos, we should solve our model equations derived in Chapter 3 directly without further approximation, which is difficult since inherently the equations do not allow simple numerical techniques to solve them. Those works remaine to be studied further. Another interesting point is that even though some chaotic behavior can exist, the frequency range of those chaotic signals may be far beyond the capability of the detecting system. The roundtrip time of the short

external cavity is only of the order of psec, so the intensity fluctuating noise or the oscillation due to Hopf bifurcation will easily have a several tens or several hundreds GHz frequency spectrum. This may be an explanation why the coherence collapse phenomena were not observed experimentally, if they ever did exist.

In this chapter, we discussed the chaos of an autonomous system (i.e. constant bias current). In the next chapter we will consider in detail the case of current modulation, which has more practical importance.

CHAPTER 6. ROUTE TO CHAOS IN THE CURRENT - MODULATED EXTERNAL CAVITY LASER DIODE

In this chapter, we study the chaotic behaviors in the current-modulated external cavity laser diode based on the numerical solutions of rate equations Eqs.(5.20) - (5.22). The chaotic behavior in nonautonomous laser systems has been investigated by several authors. And it was found that detuned laser systems have period-doubling bifurcations for injected light signals [103]. Modulation of the laser excitation rate or the modulation of the cavity losses was shown to result in chaotic behavior [108]. The period-doubling route to chaos in a directly modulated solitary laser diode has been reported [104] and analyzed [105,109]. Since this chaotic behavior may limit the data transmission rate in a high-speed optical communication system, this study on the chaos has practical importance. Therefore, the effects of spontaneous emission [104,105] and gain saturation [110] on the chaotic behavior in the current-modulated laser diode are also studied. On the same token, the effect of external feedback on the chaotic behavior is worth being investigated.

Mechanism for Period Doubling Bifurcation

We will introduce the concept of period - doubling bifurcation in this section by studying the logistic map

$$x_{n+1} = f_r(x_n) \equiv r \cdot x_n \cdot (1 - x_n) \tag{6.1}$$

shown in Figure 6.1. Even though we study the logistic map, the chaotic behavior is not tied to the special form of the logistic map. Feigenbaum [111] has shown that this route to chaos occurs in all first - order difference equations $x_{n+1} = f(x_n)$ in which $f(x_n)$ has (after a proper rescaling of x_n) only a single maximum in the unit interval $0 \leq x_n \leq 1$.

First, we investigate the stability of the fixed points of $f_r(x)$ and $f_r^2(x) = f_r[f_r(x)]$ as a function of r. Figure 6.2 shows that $f_r(x)$ has, for r<1, only one stable fixed point at zero, which becomes unstable for 1<r<3 in favor of $x^* = 1 - 1/r$. Generally, a point x^* is called a fixed point of a map f(x) if

$$x^* = f(x^*) \tag{6.2}$$

i.e., the fixed points are the intersections of f(x) with the bisector. A fixed point is locally stable if all points x_0 in the vicinity of x^* are attracted to it. The analytical criterion for local stability is easily shown as

$$\left| \frac{d}{dx^*} f(x^*) \right| < 1 \tag{6.3}$$

For $r>3=r_1$, we have $| f_r'(x^*) | = | 2 - r | > 1$, i.e., x^* also becomes unstable according to criterion Eq.(6.3). Figure 6.3 shows $f_r(x)$ together with $f_r^2(x)$ for $r>r_1$. For $r>r_1$, the old fixed point x^* in f^2 become unstable, and two new stable fixed points x_1, x_2 are created by a pitchfork bifurcation as shown in Figure 6.3 (b). This pair x_1, x_2 of stable fixed points of f^2 is called an attractor

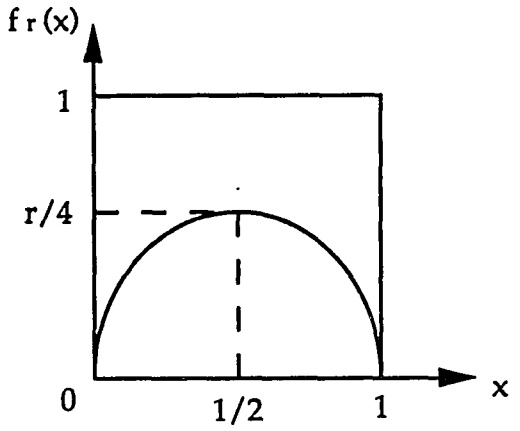

Figure 6.1. The quadratic map $f_r(x)$ on the unit interval

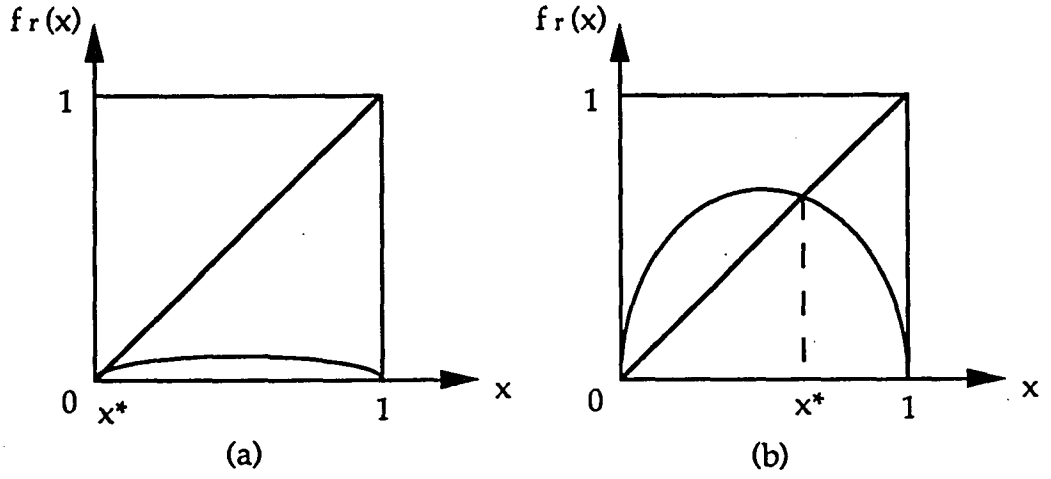

Figure 6.2. The fixed points of f_r for

(a) $r < 1$ and (b) $1 < r < 3$

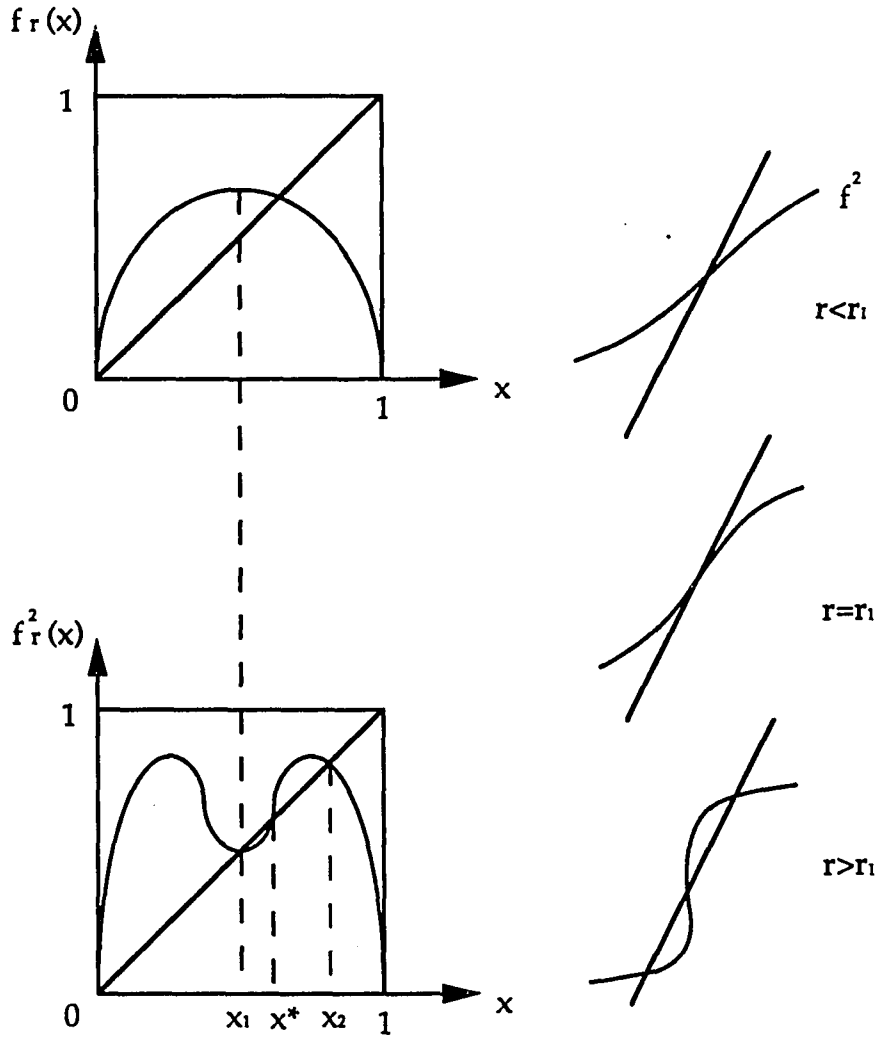

Figure 6.3. (a) f(x) and f [f(x)] for $r>r_1$

(b) Generation of two new stable fixed points in f [f] via a pitchfork bifurcation

of f(x) of period-two, because any sequence of iterates which starts in [0,1] becomes attracted by x_1 , x_2 in an oscillating fashion.

If we keep increasing r beyond a certain value r_2 , the fixed points of f^2 also become unstable. After this instability, the fourth iterate $f^4 = f^2 \bullet f^2$ displays two more pitchfork bifurcations which lead to an attractor of period four. These examples show the period-doubling bifurcation. For $r \geq r_\infty$, with a certain value r_∞ at which chaos starts, periodic and chaotic regions are densely interwoven, and one can find a sensitive dependence on the parameter values.

Numerical Simulation

In Figures 6.4 - 6.7 we show the simulated waveform of relative photon density S_r. After S_r reaches steady state (at $T_r = 1700$), sinusoidal current is superimposed on the bias current to make the total current

$$J_R = J_{R0} [1 + m \cdot \sin (\omega_m T_R)] \qquad (6.4)$$

where m is the modulation index and ω_m is the modulation angular frequency. This current modulation term is substituted into Eq. (5.21). And the set of rate equations (5.20) - (5.22) are solved numerically by the same algorithm discussed in Chapter 5. The parameters we use in calculation are: d = 7.6μm, $R_2 = 0.32$, $R'_m = 0.318$, and $J_{R0} = 1.5$. The modulation frequency is chosen as $\omega_m = 1.052\ \omega_{rx}$, where ω_{rx} is a relaxation oscillation frequency defined in Eq.(5.34). If we actually calculate this frequency, we get $f_m = 8.06$ GHz.

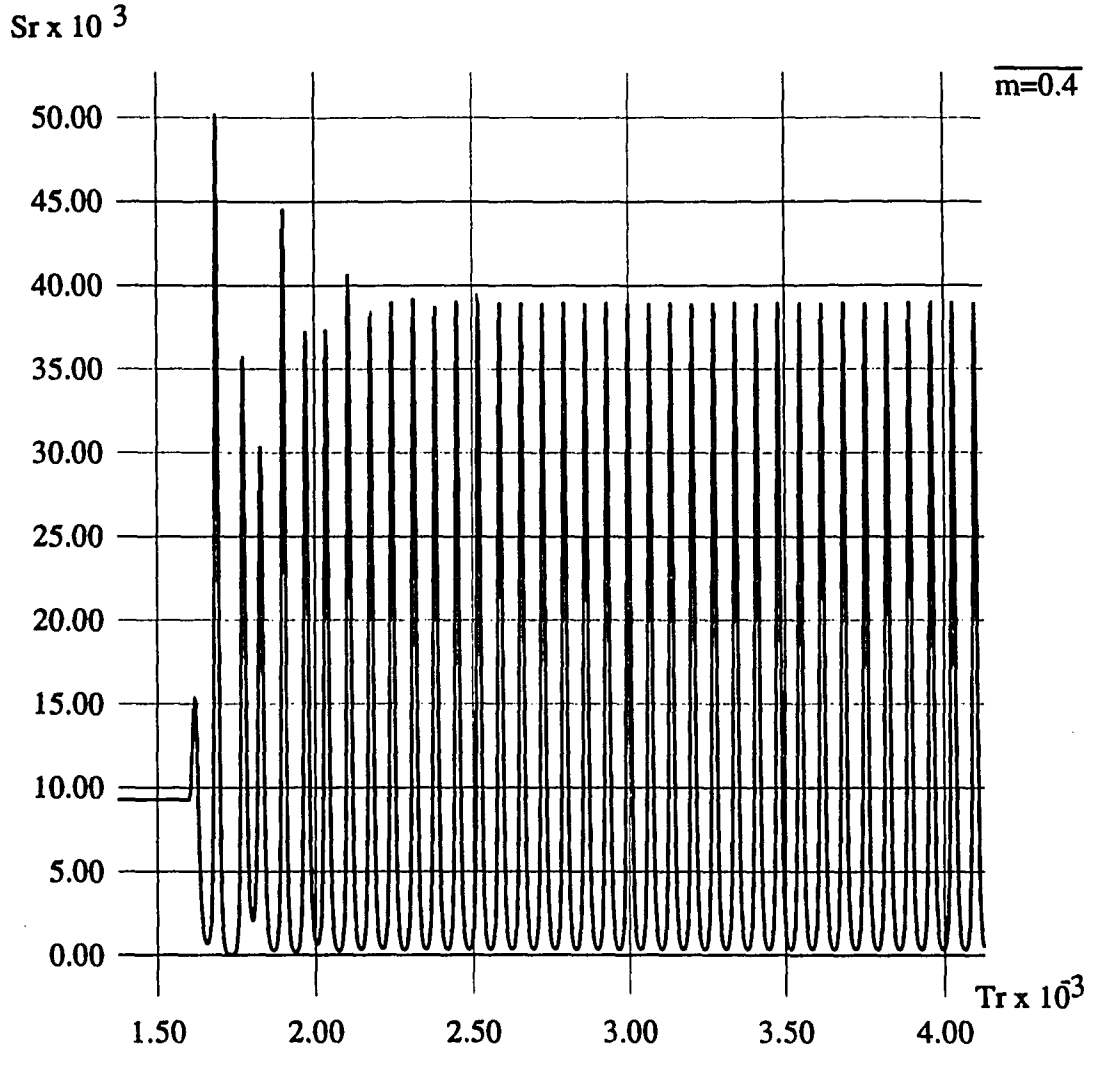

Figure 6.4. Simulation of photon density showimg 1 - T waveform, at d = 7.6 μm, R'_m = 0.318, J_{R0} = 1.5, and m = 0.4

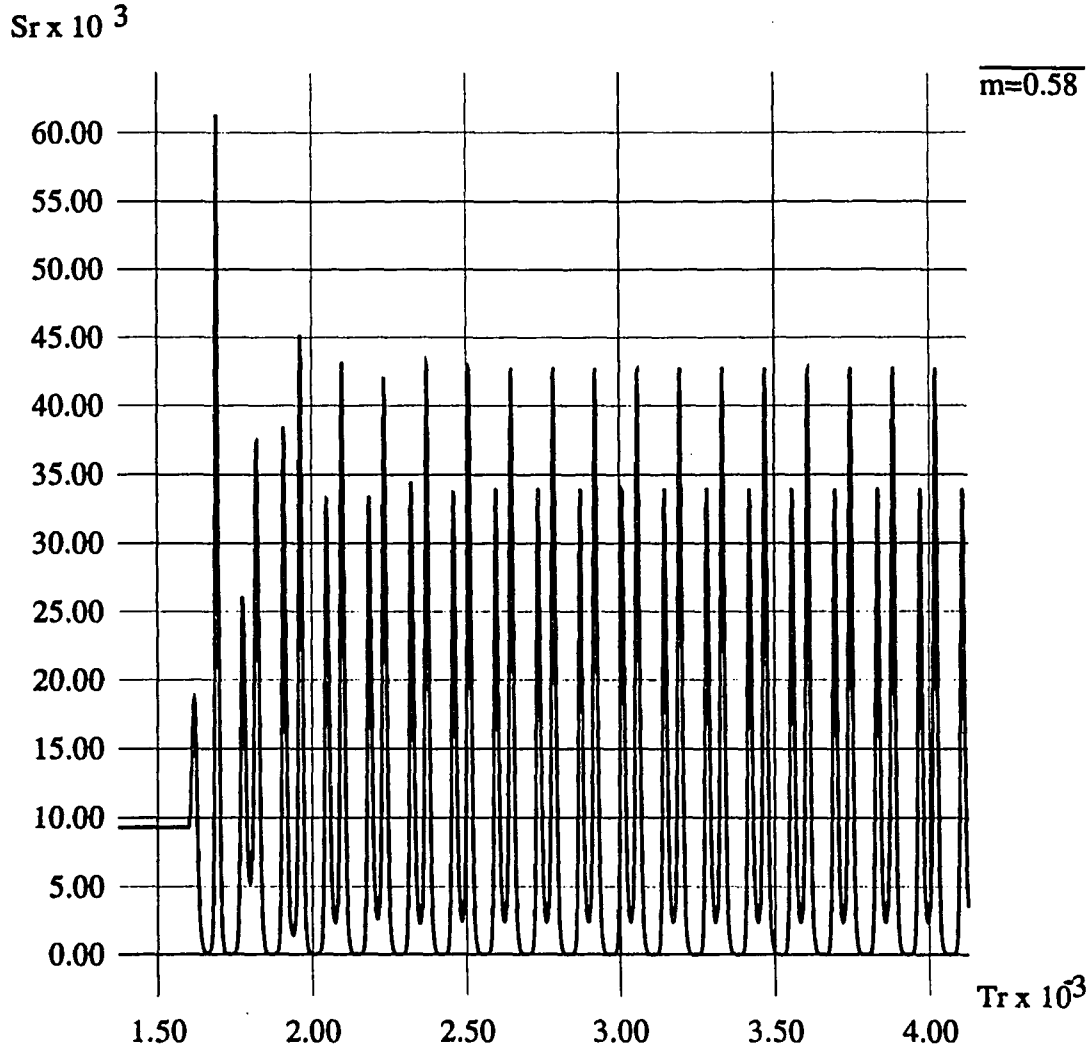

Figure 6.5. Simulation of photon density showimg 2 - T waveform, at d = 7.6 μm, R'_m = 0.318, J_{R0} = 1.5, and m = 0.58

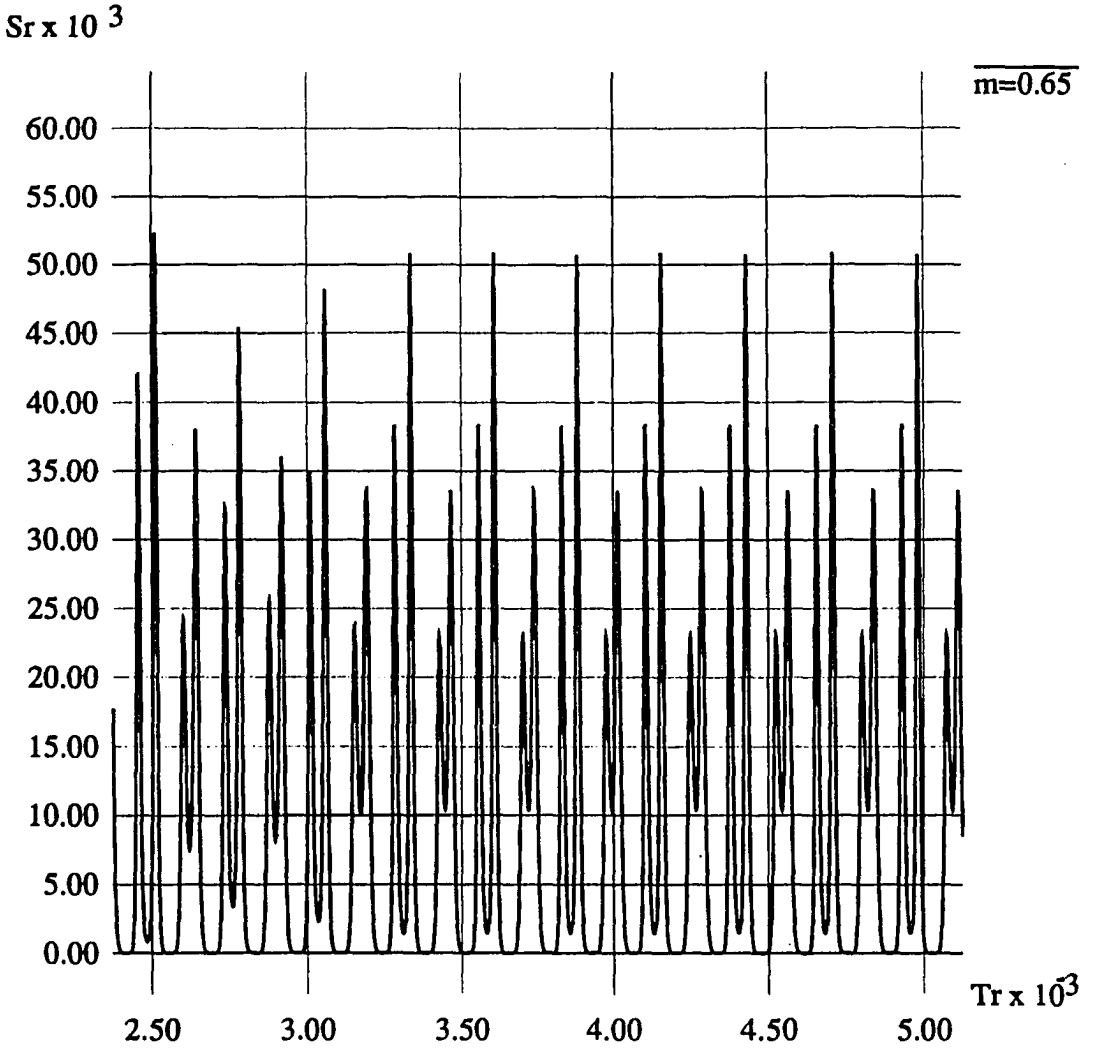

Figure 6.6. Simulation of photon density showimg 4 - T waveform, at d = 7.6 μm, $\bar{R}'_m$ = 0.318, J_{R0} = 1.5, and m = 0.65

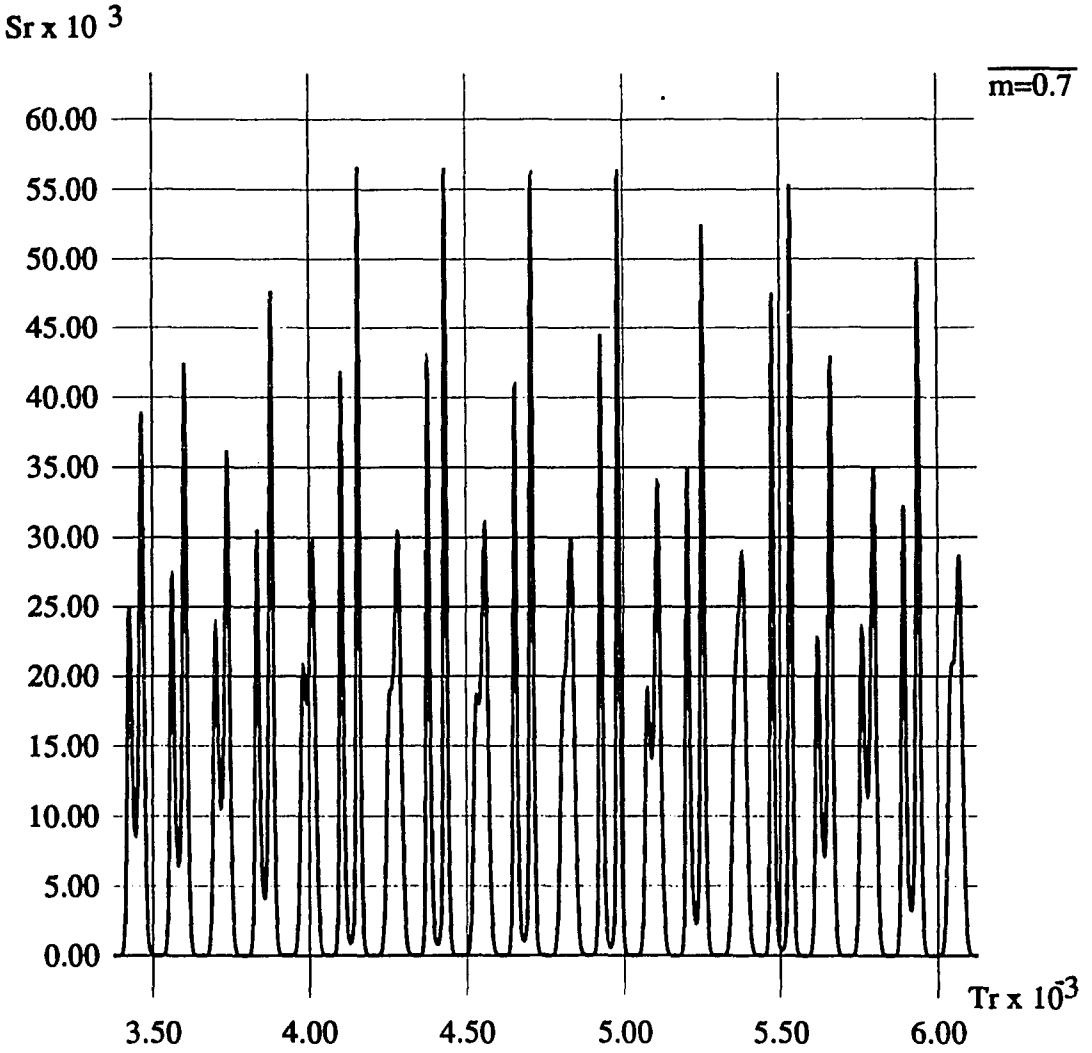

Figure 6.7. Simulation of photon density showimg chaos, at d = 7.6 μm, R'_m = 0.318, J_{R0} = 1.5, and m = 0.7

When the current modulation index m is 0.4 as in Figure 6.4, after some transient waveform, the waveform maintains the fundamental frequency ω_m. It will be suggestive to mention that modified relative threshold current density due to the external cavity in this case is $J_{Rth} = N_{RS} = 0.946$ (refer to Eq.(5.21)). At $\omega_m T_R = 1.5\pi$, current density J_R is 0.9, which is below the threshold value. But since the modulation frequency is high, the photon density never drops to zero. When the modulation index increases to 0.58 in Figure 6.5, the photon- density waveform shows period-doubling (subharmonic) bifurcation, which is called a 2-T waveform. With a further increase of m, we have a 4-T waveform at m=0.65 as shown in Figure 6.6, and finally a chaotic waveform at m=0.7 as shown in Figure 6.7.

We show the bifurcation diagram of this case in Figure 6.8. The sampled peak photon density is plotted as a function of modulation index m. We have the first 2-T bifurcation around m = 0.5. We can see clearly up to 8-T bifurcation, after which the bifurcation is hardly distinguishable. We have a chaos band around $0.68 < m < 0.73$; then we have a short window, and then the second chaos band again. This bifurcation diagram has a form similar to that of the solitary laser diode which was reported in the literature [104]. These bifurcations and chaotic effects also depend on the modulation frequency. At very low frequency such phenomena may not occur. And they may easily take place around the relaxation oscillation frequency. Therefore, it is worthwhile to study the influence of the change in the modulation frequency on the bifurcation phenomena. But in this work, we mainly focus our attention on the effect of the modulation index m on the bifurcation.

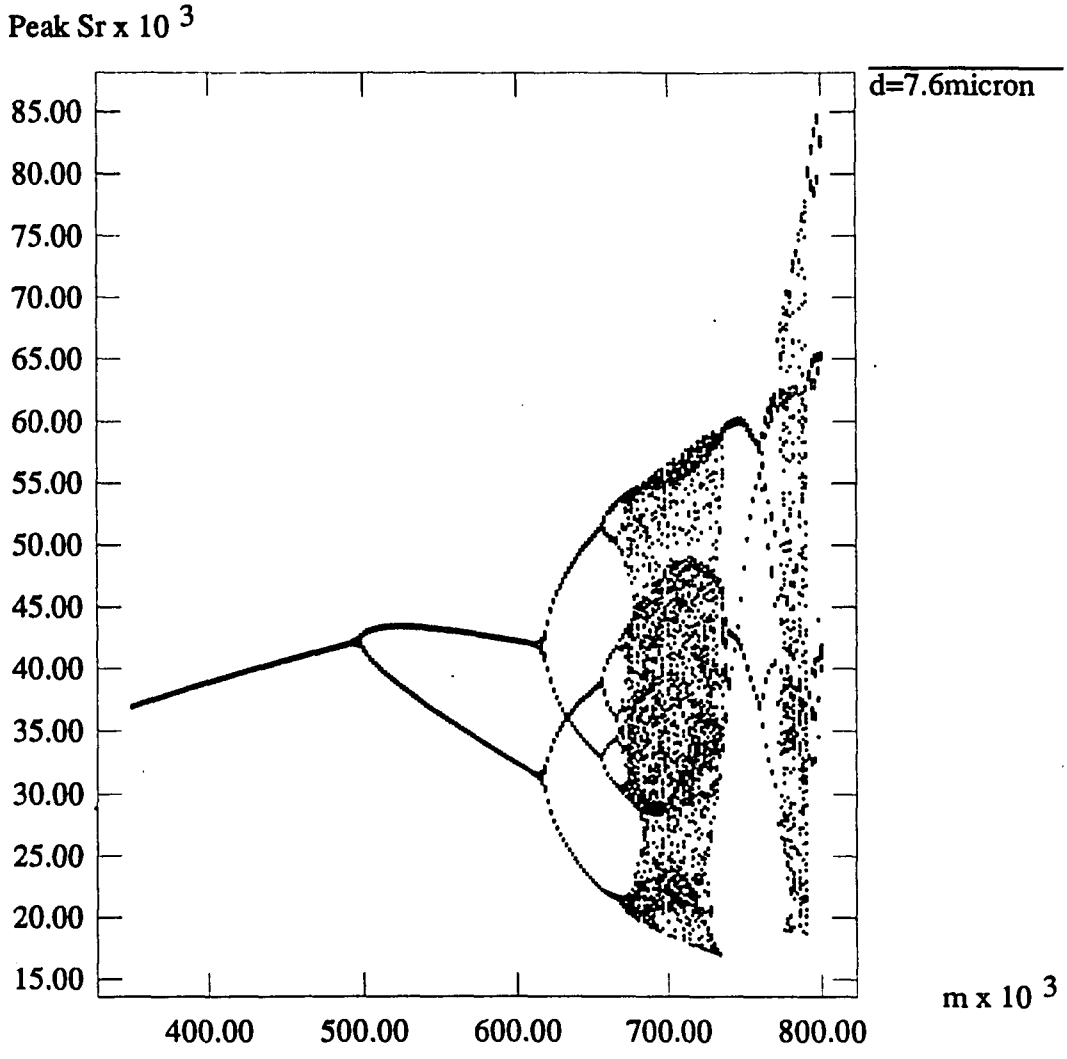

Figure 6.8. Bifurcation diagram at d = 7.6 μm, J_{R0} = 1.5, f_m = 1.052 f_{rx}, and R'_m = 0.318

Now, we change the external cavity length d to 7.79 μm, which is close to an out of phase condition ($\Omega\tau = 2\pi$). We use the same parameters as before: $R_2 = 0.32$, $R'_m = 0.318$, and $J_{R0} = 1.5$. The modulation frequency is chosen such that $\omega_m = 0.742\ \omega_{rx}$. In this situation, ω_{rx} is a different value from that of the previous example, and we get the actual modulation frequency $f_m = 3.85$ GHz. The modified relative threshold current density is $J_{Rth} = N_{RS} = 1.189$. A bifurcation diagram is shown in Figure 6.9 for this case. We find that the shape of this diagram is very peculiar. We have the first sub-harmonic generation around m=0.25. Around m=0.3, suddenly, the photon density shows a 3-T waveform. According to [104], at the modulation frequency, which is smaller than the relaxation oscillation frequency, the bifurcation diagram shows a shape which is a very typical form of the period-doubling route to chaos. Here, we have a sudden jump from a 2-T to a 3-T waveform, and a very strange chaotic band around 0.45<m<0.5. The corresponding 2-T, 3-T and chaotic waveforms are shown in Figures 6.10 - 6.12, at m=0.27, 0.3, and 0.4 respectively. As clearly shown in Figure 6.11, this 3-T waveform is an actual stable solution, which is totally different from the spurious 3-T window due to the hysteresis in the solitary laser [104].

In Figure 6.13, we expand the bifurcation diagram of Figure 6.9 around m=0.295 to investigate in detail. We can not find any explicit period-doubling route from a 2-T to a chaos before the diagram reaches a 3-T window at m=0.2973. A completed period-doubling cascade is known to be an infinite sequence of local bifurcation, each of which is a continuous bifurcation [118]. This continuity is evident in the logistic map bifurcation diagram. Therefore, the period- doubling cascade is referred to as a continuous transition to chaos.

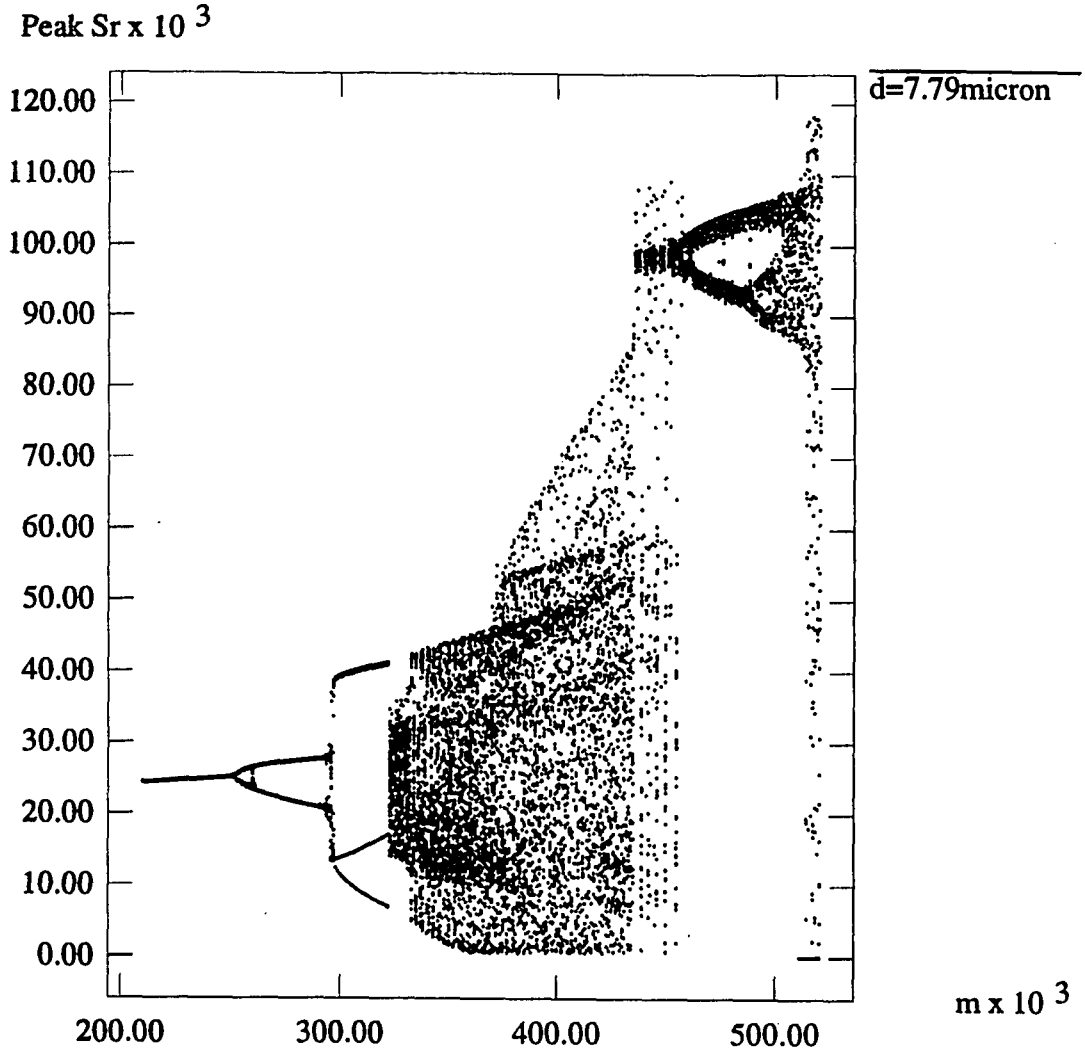

Figure 6.9. Bifurcation diagram at d = 7.79 μm, J_{R0} = 1.5, f_m = 0.742 f_{rx}, and R'_m = 0.318

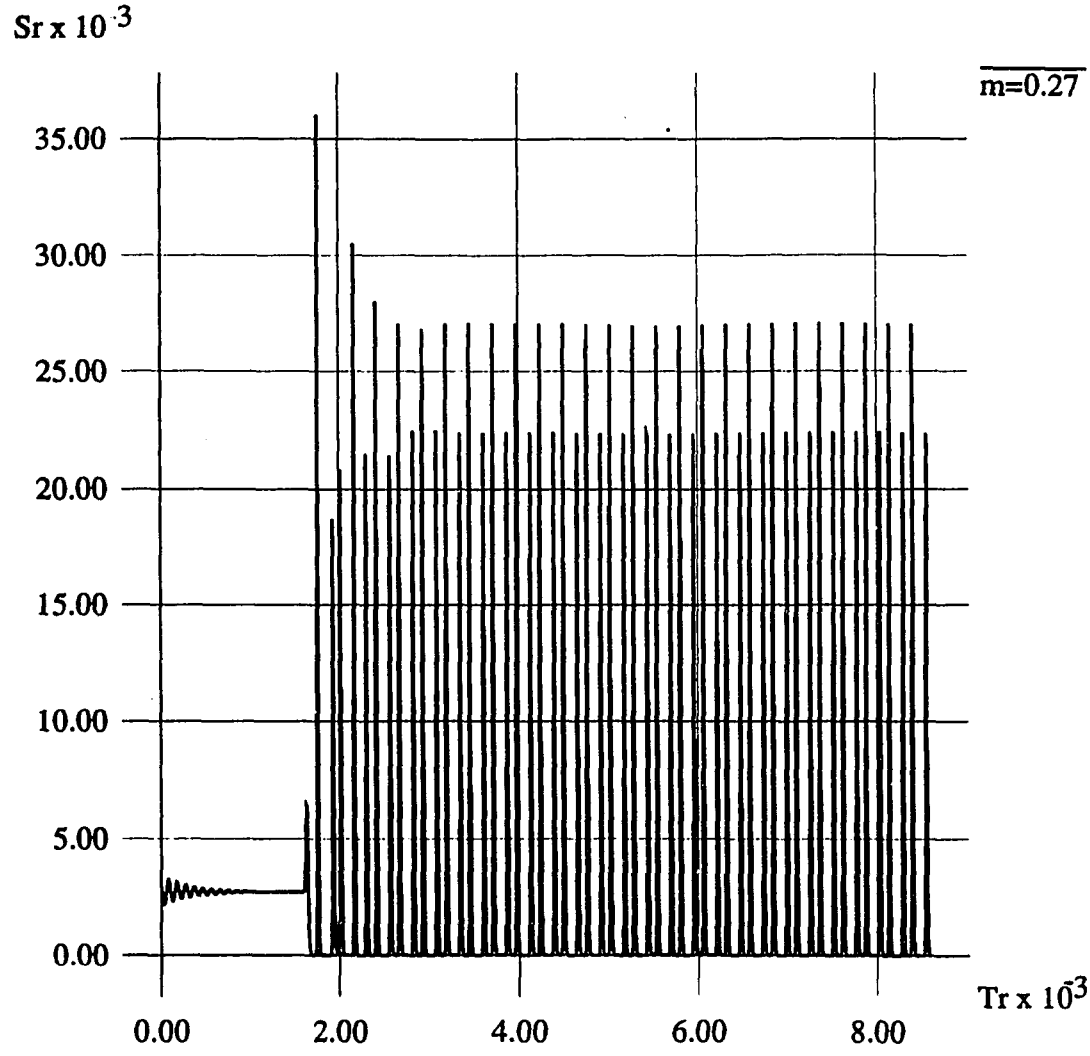

Figure 6.10. Simulation of photon density showing 2 - T waveform, at d = 7.79 μm, R'_m = 0.318, J_{R0} = 1.5, and m = 0.27

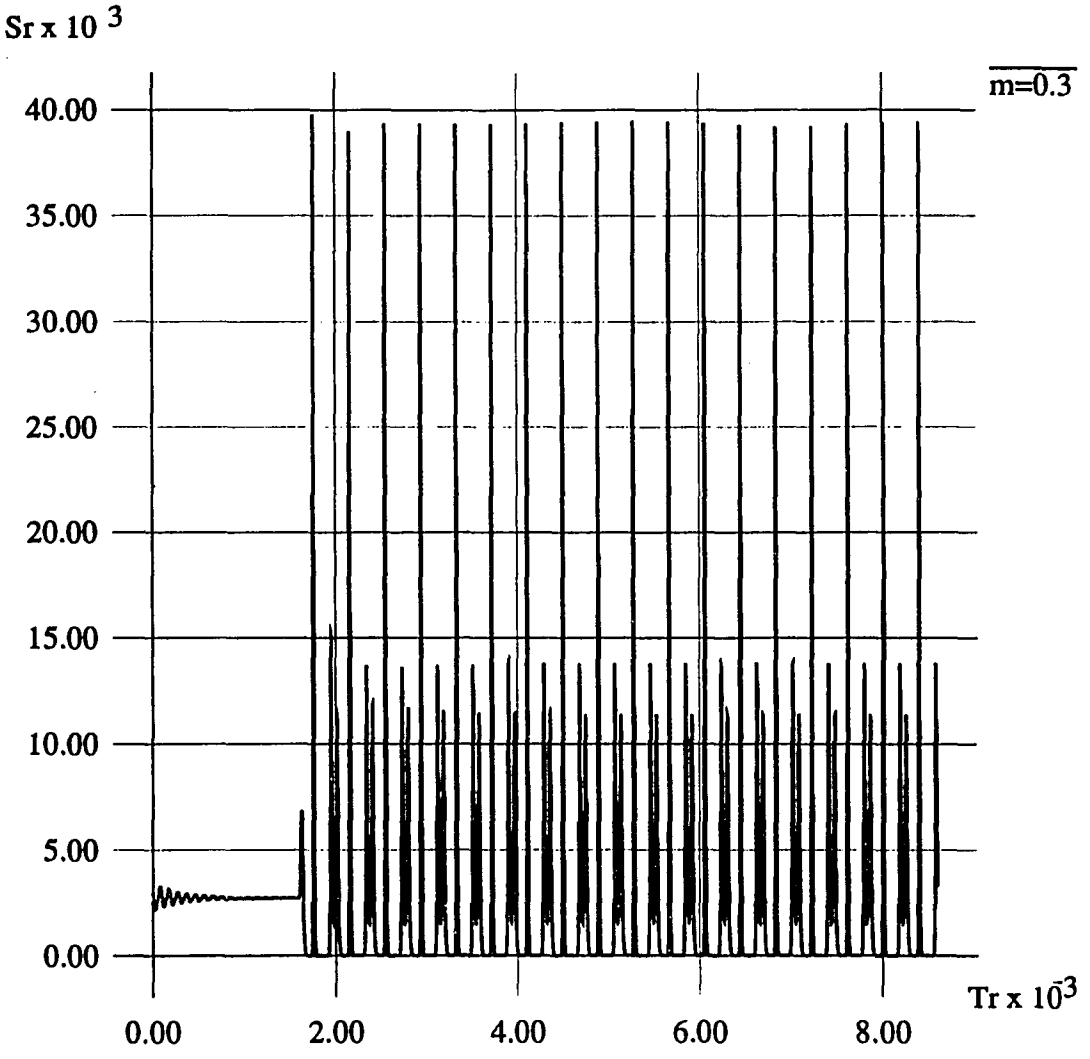

Figure 6.11. Simulation of photon density showing 3 - T waveform, at d = 7.79 μm, R'_m = 0.318, J_{R0} = 1.5, and m = 0.3

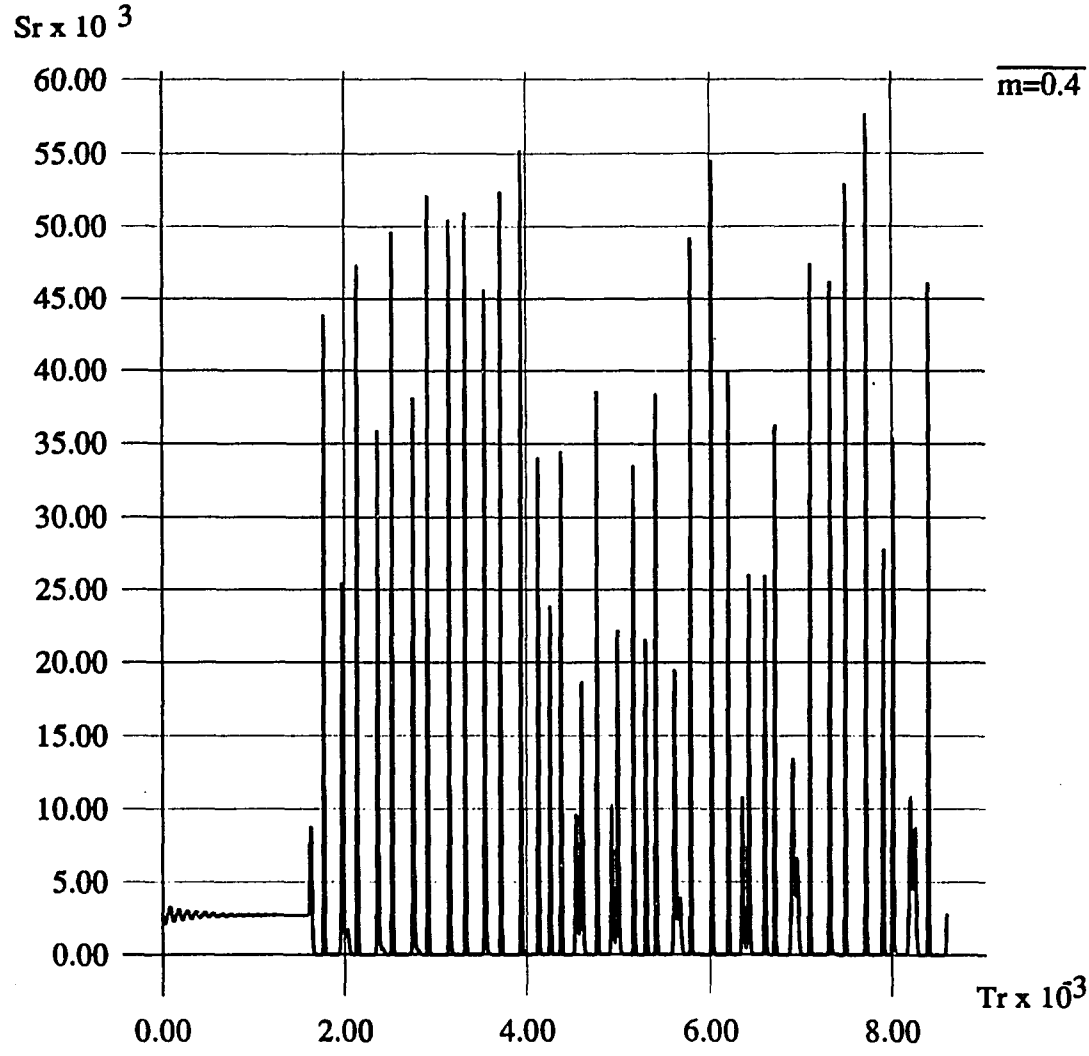

Figure 6.12. Simulation of photon density showing chaos, at d = 7.79 μm, R'_m = 0.318, J_{R0} = 1.5, and m = 0.4

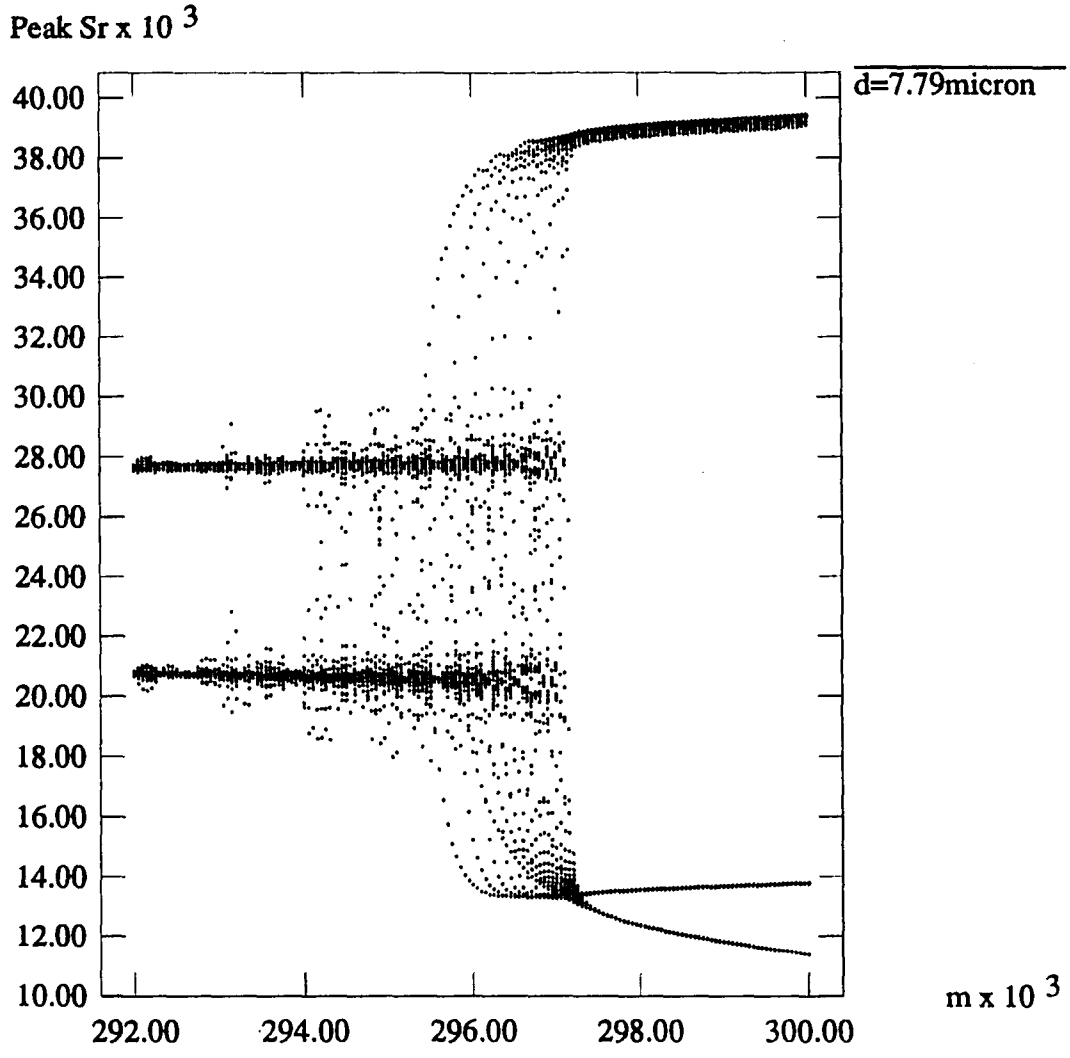

Figure 6.13. Expanded plot of bifurcation diagram of Fig. 6.9 around m = 0.295

In that sense, the route to chaos in the bifurcation diagram shown in Figure 6.9 can not be told as the perio-doubling bifurcation route.

In Figures 6.14 and 6.15, we show the bifurcation diagram for the weak coupling level. $R'_m = 0.005$, and $R_2 = 0.32$, for both figures. The parameters used in calculation of Figure 6.14 are $d = 7.6\ \mu m$, $J_{R0} = 1.5$, $\omega_m = 0.967\ \omega_{rx}$, which is 6.43 GHz, and the modified relative threshold current density $J_{Rth} = N_{Rs} = 0.990$. For Figure 6.15, $d = 7.79\ \mu m$, $J_{R0} = 1.5$, $\omega_m = 0.931\ \omega_{rx}$, which is 6.05 GHz, and $J_{Rth} = N_{Rs} = 1.012$. Surprisingly, in these examples, the bifurcation diagram for the in-phase configuration ($\Omega\tau = \pi$), i.e., Figure 6.14, shows more strange shape than that for the out-of-phase configuration in Figure 6.15. It has a sudden jump in peak photon density amplitude and folding structure, but does not have a 3-T window.

The small signal analysis which is discussed in Chapter 5 can not be applied to analyze this bifurcation phenomenon, since the modulation index is large. The large - signal analysis was introduced for analysis of solitary laser diode [119,120], and for explaining the first subharmonic generation of the modulated solitary laser diode [121]. By solving rate equations with perturbation methods [109], the period doubling bifurcations up to the 4-T bifurcation were accounted for under large - signal modulation.

In this work, the further analytical study about this route to chaos is not included. However, to see the qualitative characteristics of chaotic behavior, we show the return maps of peak photon density in Figures 6.16-6.20. We plot the peak photon density $S_R(n)$ vs. $S_R(n+1)$, where $S_R(n)$ represents the n-th peak photon-density. These return maps are similar to the Poincaré return map [118], but different from Poincaré return map since the actual time

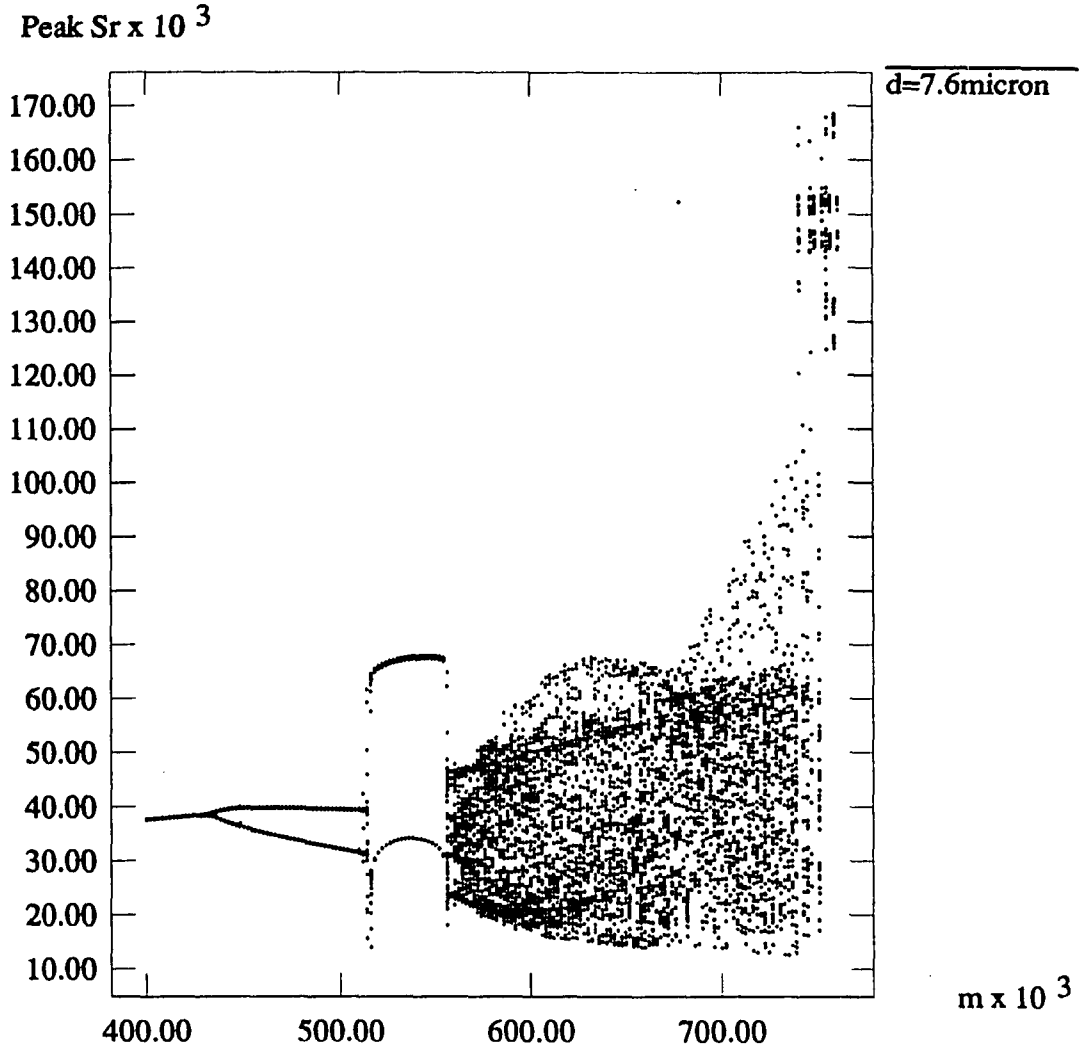

Figure 6.14. Bifurcation diagram at d = 7.6 μm, J_{R0} = 1.5 , f_m = 0.967 f_{rx} , and R'_m = 0.005

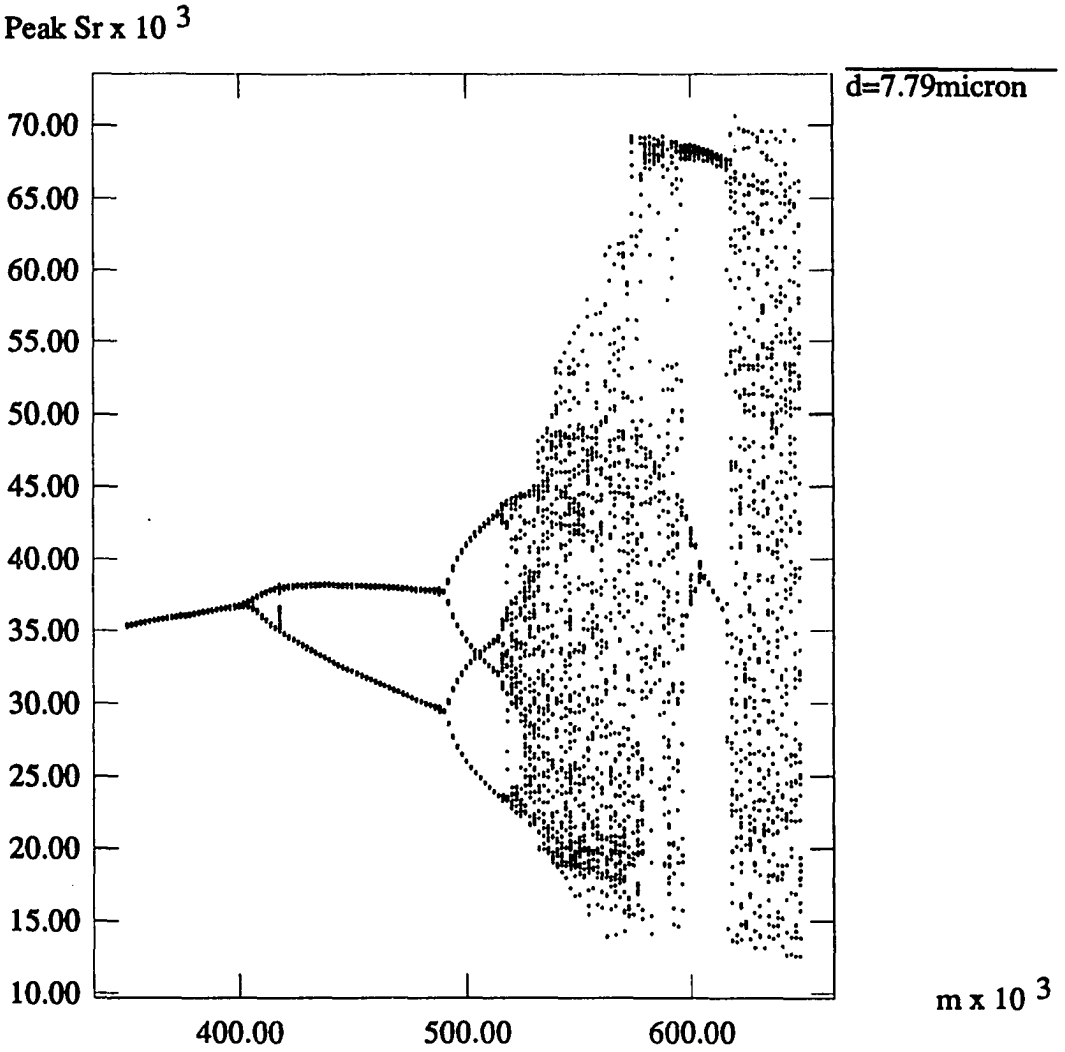

Figure 6.15. Bifurcation diagram at d = 7.6 μm, J_{R0} = 1.5 , f_m = 0.967 f_{rx} , and R'_m = 0.005

interval between the n-th sampling and the (n+1)-th sampling is not constant as shown in Figure 6.6.

Figure 6.16 shows the return map for the in-phase configuration whose bifurcation diagram is plotted in Figure 6.8. The modulation index m is 0.695. This return map basically is similar to the logistic map except a strong folding structure. It can be classified as a unimodal one-dimensional map [118], since it is defined on a finite interval and has a single smooth maximum. The logistic map is also one of the example of a unimodal map.

Figures 6.17 and 6.18 are the return maps for the out-of-phase configuration plotted in Figure 6.9, when m=0.35, and m=0.335 respectively. At m=0.335, it again shows clearly a 3-T feature.

Figure 6.19 is another example for the in-phase case of Figure 6.16. It is plotted for m=0.57. For the in-phase configuration, the return maps maintain their unimodal characteristics for both weak coupling (Figure 6.19) and strong coupling (Figure 6.16).

Figure 6.20 shows the return map for the out-of phase case with weak coupling, $R'_m = 0.005$. The shape of the return map is not a typical type of unimodal map, since three quadratic structures are overlapped each other. These inner structures evolve as the external coupling increases, and we get a twisted return map of Figure 6.17 for $R'_m = 0.318$. This different feature from the unimodal characteristic in return map for the out-of phase configuration is thought to be one of the reasons to make an abrupt 3-T window as shown in Figure 6.9.

We assert that the route to chaos in a modulated external cavity laser diode is not limited to the period-doubling route, which has been believed as

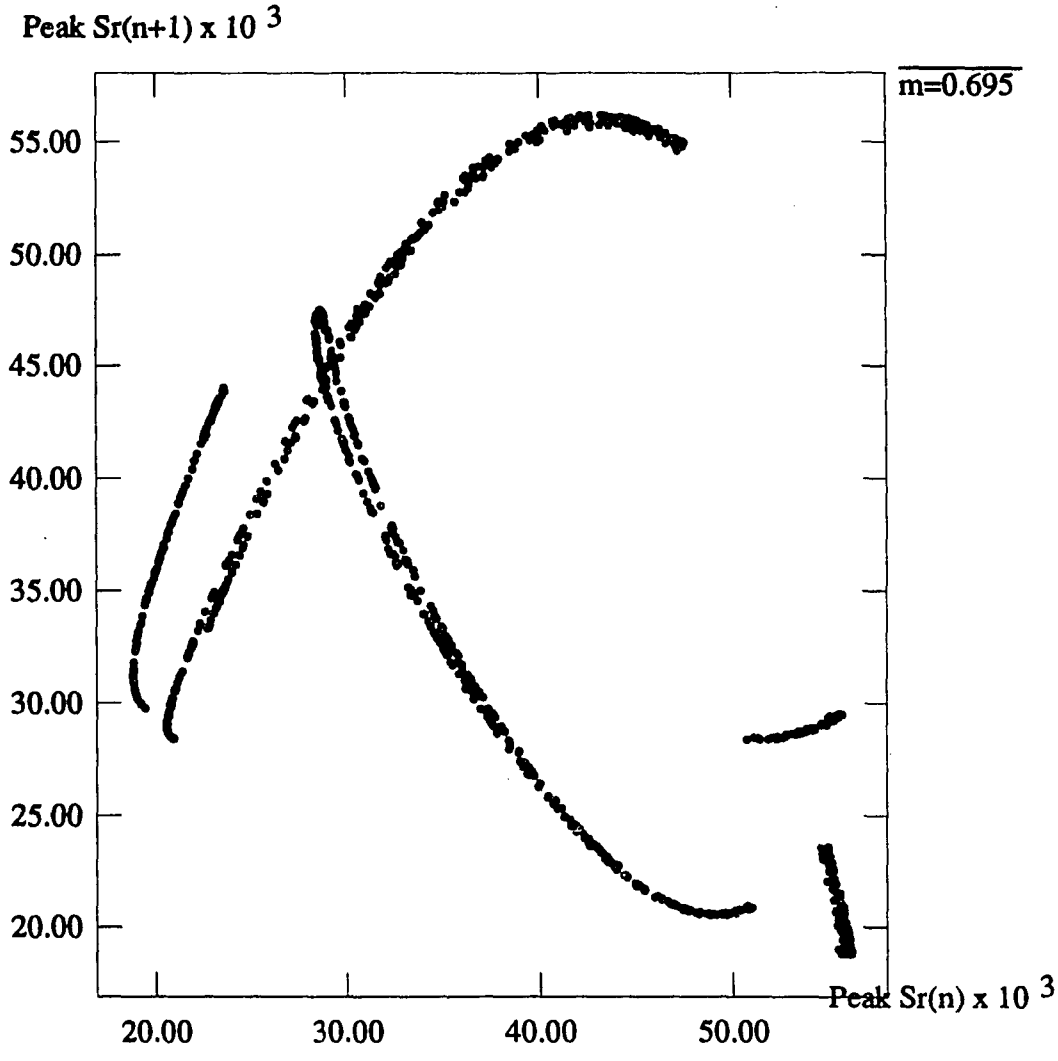

Figure 6.16. Return map corresponding to the condition in Fig. 6.8, with m = 0.695

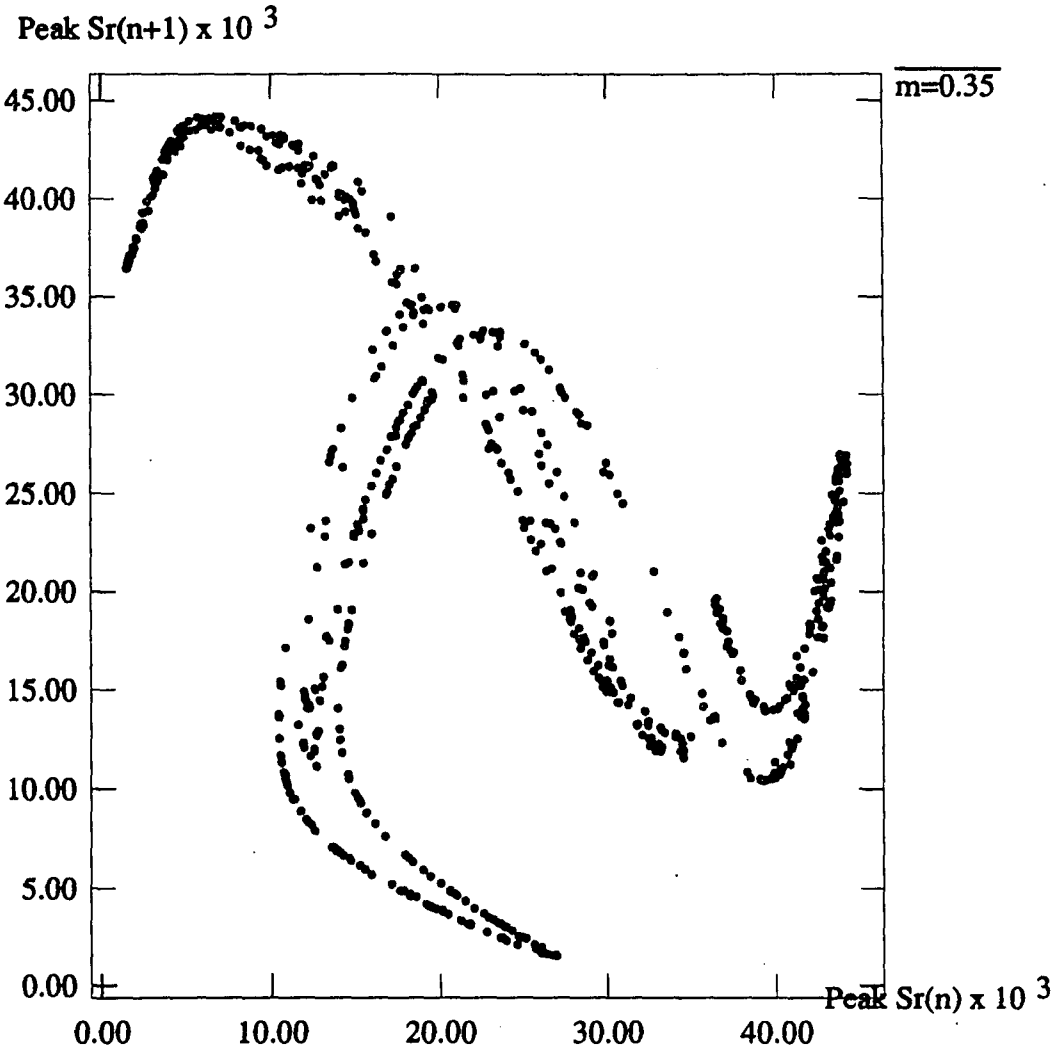

Figure 6.17. Return map corresponding to the condition in Fig. 6.9, with m = 0.35

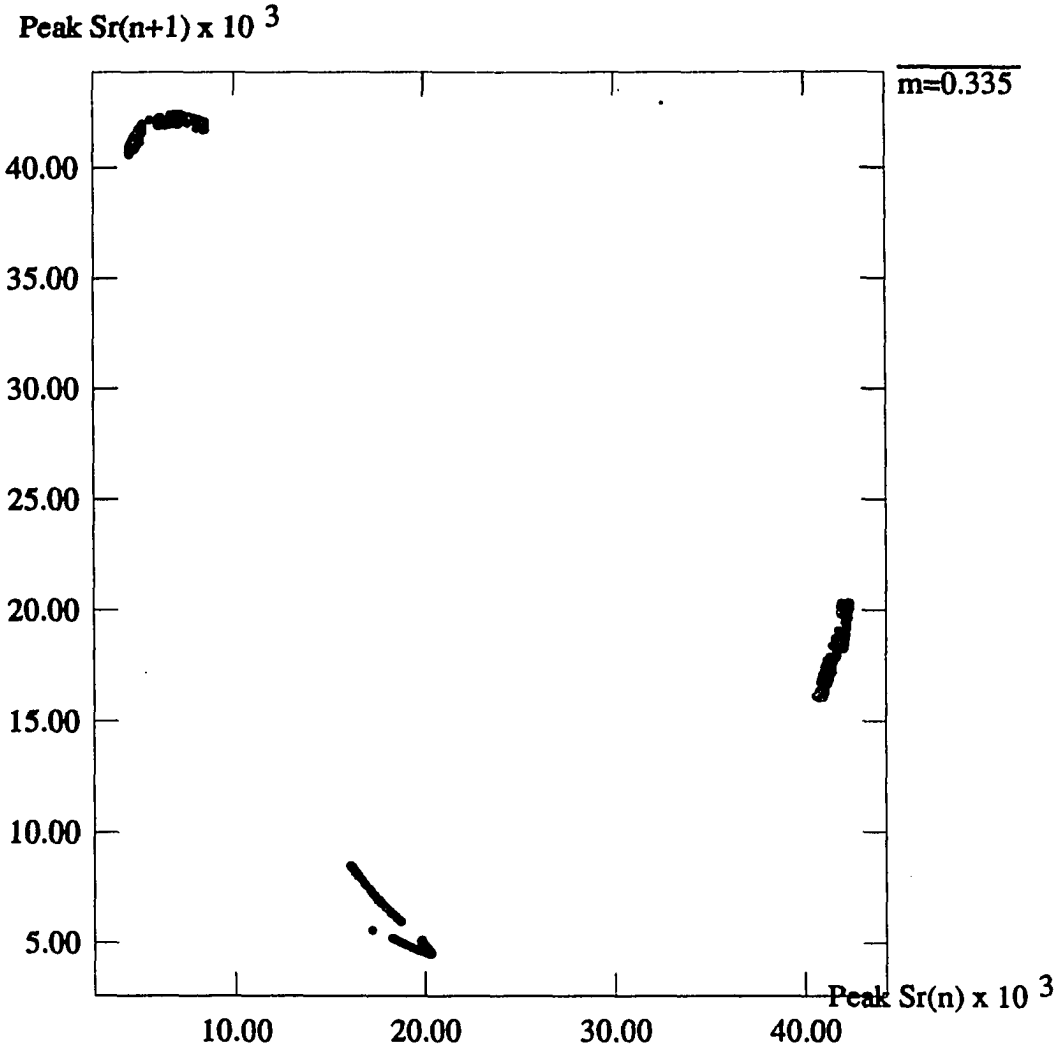

Figure 6.18. Return map corresponding to the condition in Fig. 6.9, with m = 0.335

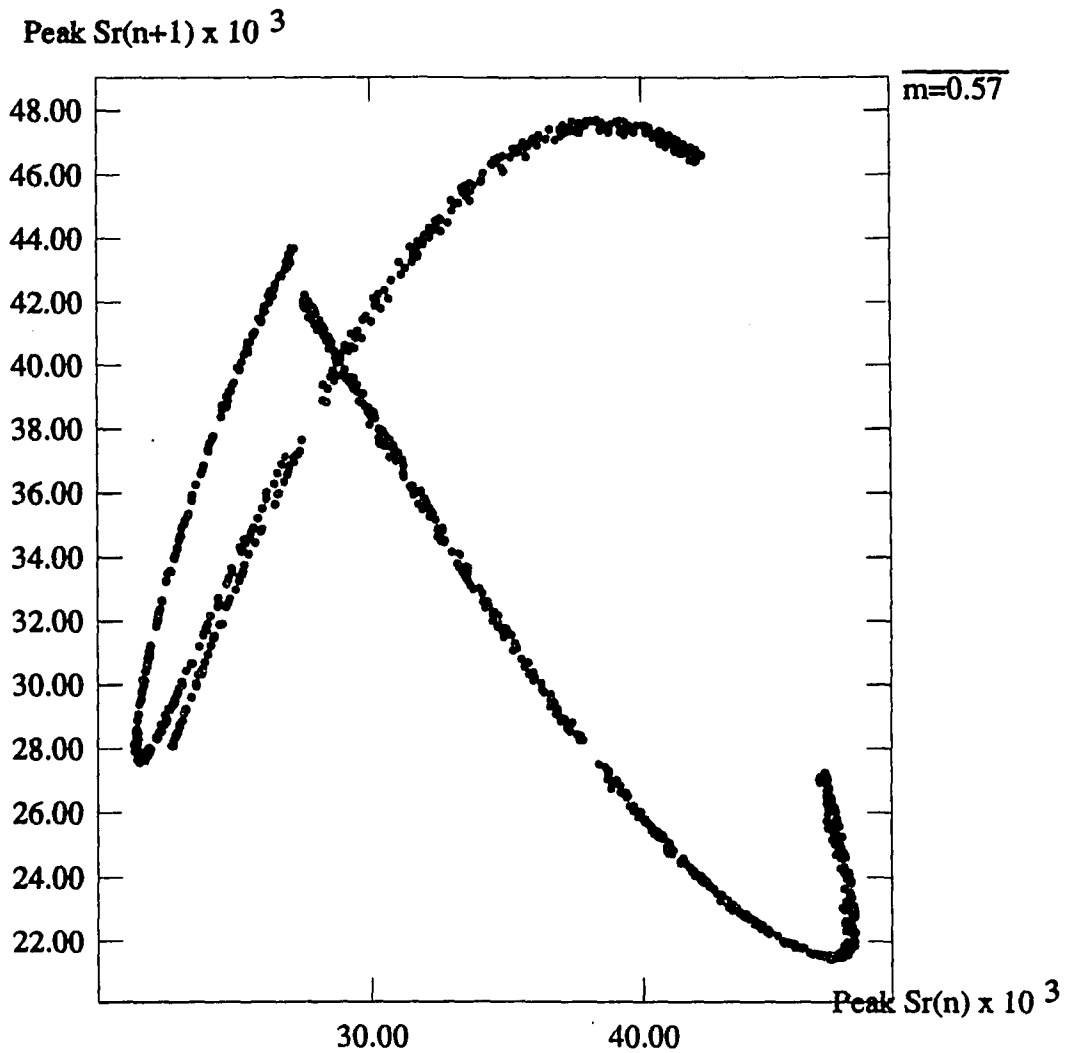

Figure 6.19. Return map corresponding to the condition in Fig. 6.14, with m = 0.57

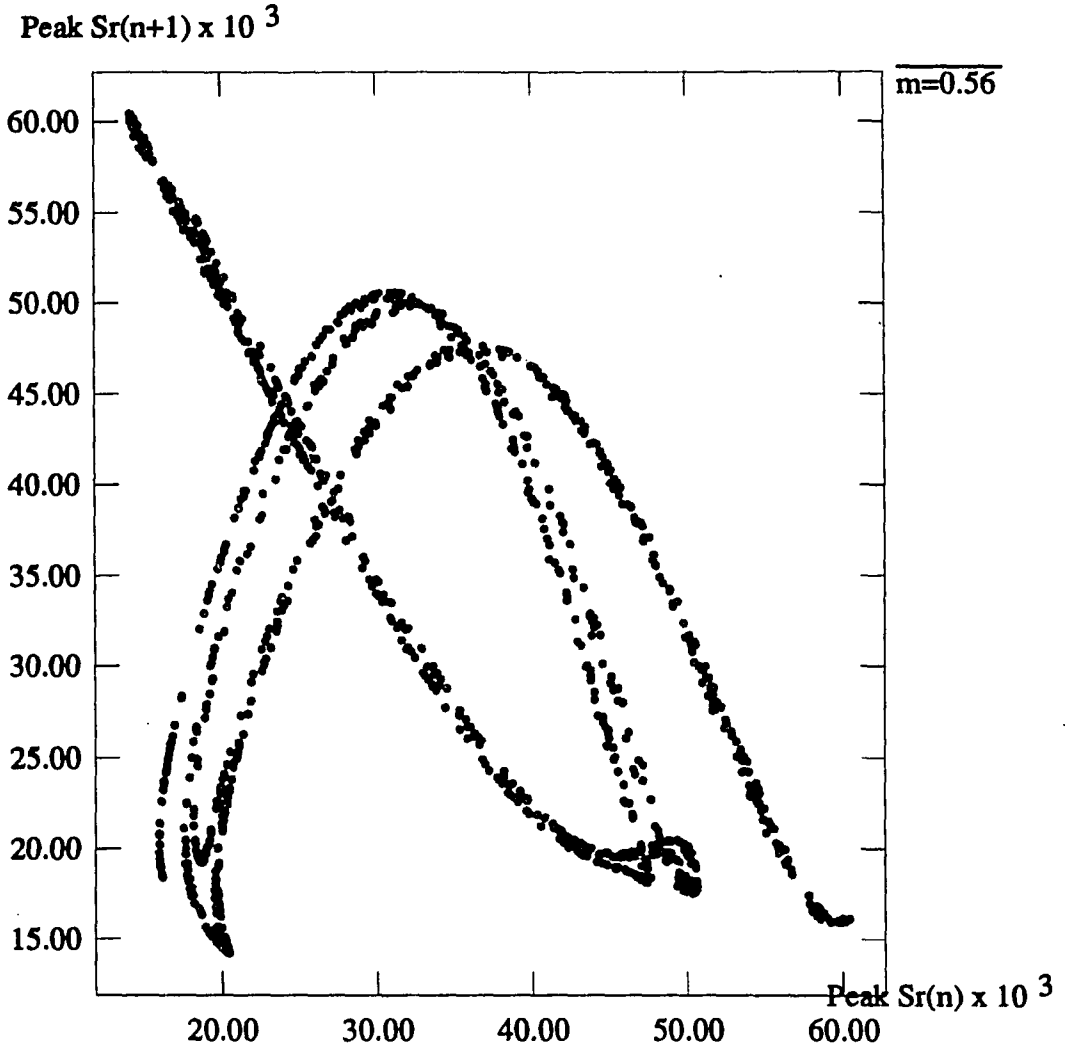

Figure 6.20. Return map corresponding to the condition in Fig. 6.15, with m = 0.56

the only route in modulated solitary laser diode, especially for the out-of-phase configuration. However, it will need further study to make it clear what specific kind of route to chaos is involved in this case exactly.

We should mention that if we add the spontaneous emission noise terms in our model, the chaotic behavior will be probably weakened, as supposed from the noise analysis of logistic map [101], and the solitary laser diode [104].

We may extract another useful conclusion from the analysis of this chapter. Again, it is better to maintain the operating distance close to the in-phase configuration. We can find that in the out-of-phase configuration, the modulated photon density will be bifurcated to a 2-T waveform at the lower modulation index than the in-phase configuration, which may limit the high frequency modulation capability of the laser diode.

CHAPTER 7. SOME APPLICATIONS OF THE SHORT EXTERNAL CAVITY LASER DIODE

Optical Disk Head

As one of the commercial applications, the ultrashort external-cavity laser diode can be used as the optical head for phase-change recording media [42, 112]. A long external cavity laser diode with two quarter - wave plates has been proposed as a detecting head for magnetooptic signals [113]. In particular, the external cavity optical head for phase-change media has performed with promise experimentally for providing high data transfer rate and short access time owing to its light weight [42].

The configuration of an optical disk head under consideration is shown in Figure 7.1. The phase-change recording medium is composed of two different parts, a high reflecting region with a power reflectivity R_m^h (or a field amplitude reflectivity ρ_m^h) and a low reflecting region with a power reflectivity of R_m^l (or ρ_m^l). Both the laser diode and a photodetector are attached to an air-bearing slider in a sealed, dust-free environment. As the optical disk rotates, an air-bearing scheme determines the flying height d (usually only a few micrometers) depending on the linear disk velocity. The output power detected by the photodetector located at the rear facet of the laser diode has either a value of P^h corresponding to R_m^h or P^l corresponding to R_m^l under the properly given bias current I_{bias}. The facet facing the medium was antireflection coated to reduce R_2, and a special ridged waveguide type laser diode is used to improve the performance of the optical head [42].

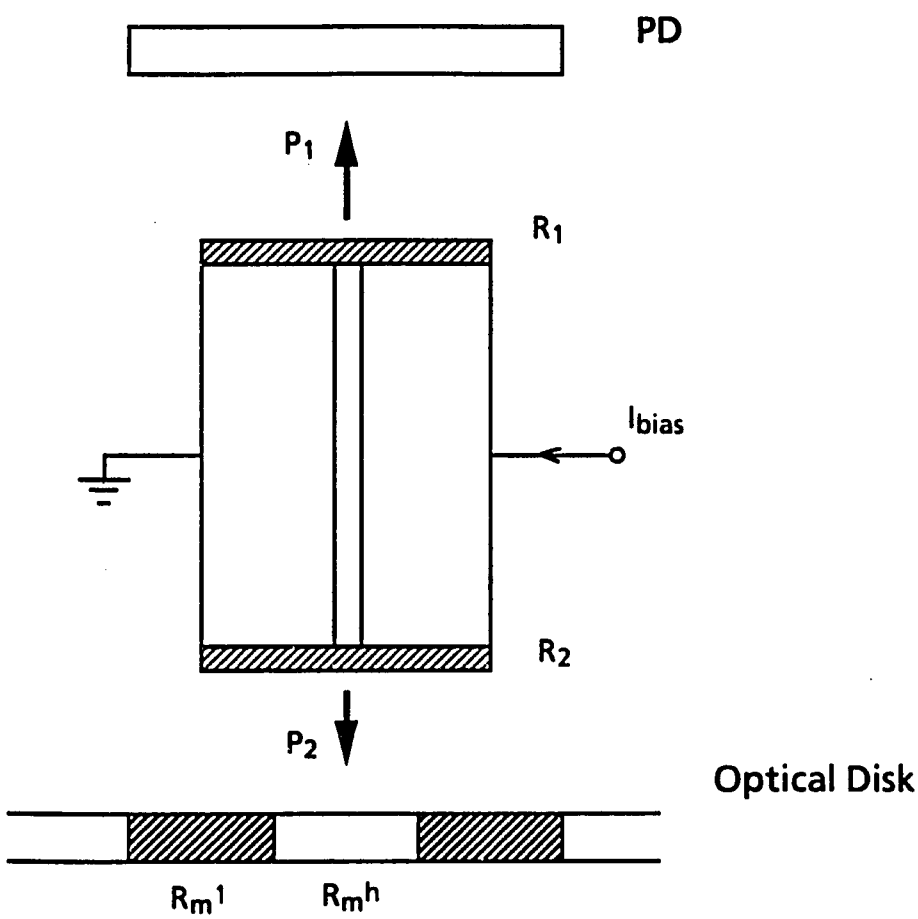

Figure 7.1. The optical disk head configuration

Some types of optical disk memory systems and optical video disk players are operated with constant angular velocity (CAV). In such cases, the linear velocity of rotating disk differs at different radii; this difference causes change in flying height d. When the disk rotates at 1200 r/min, the linear velocity at r = 50 mm is 6.3 m/sec and becomes 15.1 m/sec at r = 120 mm. According to [42], such a change in disk velocity corresponds to the change in flying height from 0.7 to 1.2 μm or from 2.5 to 4.2 μm depending on the type of air-bearing slider used. Even in a constant-linear-velocity (CLV) system, it is difficult to control the flying height precisely because it is difficult to assemble laser diode chip to the air bearing slider with high precision. However, as shown in Figure 4.17(c), the output power is not only a function of reflectivity of the external reflector but also a function of flying height d. The distance between two neighboring peaks or between two valleys is approximately $\lambda/2$. This suggests that the output power fluctuates badly as the flying height changes, as mentioned previously. For an example, Figure 7.2 shows the output power as a function of flying height. We use the open resonator model discussed in chapter 4, to calculate output power characteristics of this ultra short external cavity configuration. The solid line represents P^h corresponding to R_m^h = 0.35, and the dashed line represents P^l corresponding to $R_m^l = 0.04$. One of the laser facets is assumed to be antireflection coated to give $R_2 = 0.05$. The emitting area is assumed to be 1.2 μm X 1.2 μm [78, 112]. As shown in Figure 7.2, P^h is not always bigger than P^l, especially at large d (d > 1.5 μm) ; P^l is larger than P^h around the valleys. Also, P^h at the first valley (d ≈ 0.8 μm) is smaller than P^l at the first peak (d ≈ 0.6 μm). Consequently, in this case if the

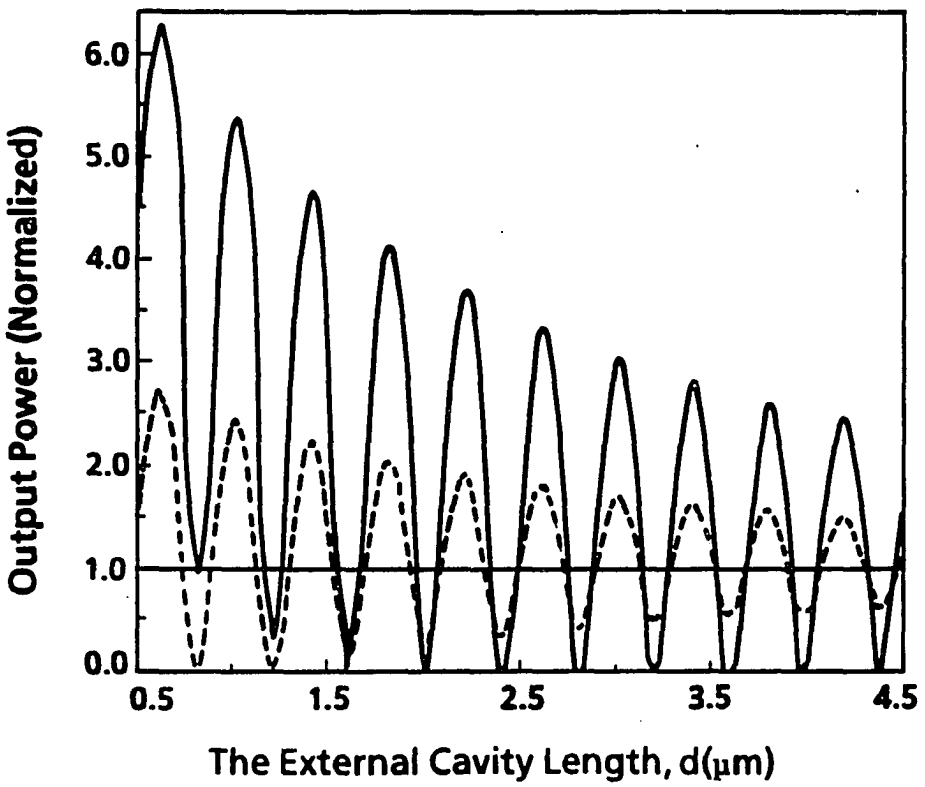

Figure 7.2. Variation of output power with flying height d for the case $2a = 2b = 1.2\ \mu m$, $R_1 = 0.32$, $R_2 = 0.05$, and $\lambda = 0.78\ \mu m$, where the solid line represent the plot of P^h corresponding to $R_m{}^h = 0.35$, while the dashed line represents that of P^l corresponding to $R_m{}^l = 0.04$

flying height changes about 0.2 μm, it is impossible to read the data recorded in the optical disk because the detected data are reversed.

It is, therefore, desirable to know under what condition P^h becomes always greater than P^l (i.e., $P^h > P^l$) within the given range of flying height. Such a desired condition is derived in the following subsection for two cases.

Case A: With coupling coefficient $c_n = r^n$ (r is constant)

Let us start from the simplest case of constant r. Often r=1 is used. We assume here that c_n=1. Then from Eq.(4.44) the effective field-amplitude reflectivity ρ_e can be written into the following form:

$$\rho_e = \frac{\rho_2 + \rho_m \exp(j\psi)}{1 + \rho_2 \rho_m \exp(j\psi)} \tag{7.1}$$

and the effective power power reflectivity can be written as

$$R_e = \frac{R_2 + R_m + 2\rho_2 \rho_m \cos\psi}{1 + R_2 R_m + 2\rho_2 \rho_m \cos\psi} \tag{7.2}$$

in which $\psi = 4\pi d/\lambda$ as defined in Eq. (4.45). The field amplitude reflectivities ρ_2 and ρ_m are assumed to be real quantities as usual.

It should be noted that R_e is a periodic function of the external cavity length d and the plot of R_e versus d has relative maxima (referred to as peaks) and relative minima (referred to as valleys). The values of the maxima or minima do not vary with d. In other words, the value of R_e at each peak is same throughout the whole range of flying height under consideration.

For convenience of discussion, we define $R_{ev}{}^{h}$ and $R_{ep}{}^{l}$ as the value of R_e at the valley for the case of high reflective medium with $\rho_m = \rho_m{}^{h}$ and as that at the peak for the case of low reflective medium with $\rho_m = \rho_m{}^{l}$, respectively. Because $dP_1/dR_e > 0$, the necessary condition for $P^h > P^l$ can be expressed as

$$R_{ev}{}^{h} > R_{ep}{}^{l} \tag{7.3}$$

For the configuration being considered, ρ_m is a negative quantity and R_e takes its relative minima when $\cos\psi = -1$ and $+1$, respectively. Consequently it can be shown that the requirement Eq.(7.3) can be met if the following condition that is to be imposed on the reflectivity is satisfied:

$$R_m{}^{h} > R_{co}{}^{h}(\rho_2, \rho_m{}^{l}) \tag{7.4}$$

where

$$R_{co}{}^{h} = \left(\frac{Q - \rho_m{}^{l}}{1 - Q\,\rho_m{}^{l}} \right)^2 \tag{7.5}$$

in which

$$Q \equiv \frac{2\,\rho_2}{1 + R_2}\,, \quad \text{and} \quad \rho_m{}^{l} < 0\,. \tag{7.6}$$

The variation of R_{co}^{h}, given by Eq.(7.5), with R_2 for different values of R_m^{l}, is shown in Figure 7.3. We observe that the values of R_{co}^{h} increases monotonically with R_2 for the case of a fixed R_m^{l}, and it also increases with R_m^{l} for the case of a fixed R_2. This implies that the range of R_m^{h}, over which the requirement Eq.(7.3) can be met, is broadened by reducing either R_2, R_m^{l}, or both. It should be pointed out that a constant r may be used to determined approximately the effective power reflectivity R_e in the case of a long external cavity, but it is not adequate for studying the case of an ultrashort external cavity configuration such as in the optical disk head.

Case B: Variable complex coupling coefficient

The complex coupling coefficient c_n for the n-th reflection, given by Eq.(4.46), can be expressed in the following form:

$$c_n = \exp(-\alpha \cdot d \cdot n) \tag{7.7}$$

where the complex loss factor α is defined as

$$\alpha \equiv \alpha'' + j\,\alpha' \tag{7.8}$$

Expressing the coupling coefficient in the complex form as given by Eq.(7.7) is equivalent to considering the configuration in which the external cavity resonator is regarded as lossy resonator.

In this case, the ρ_e is given as

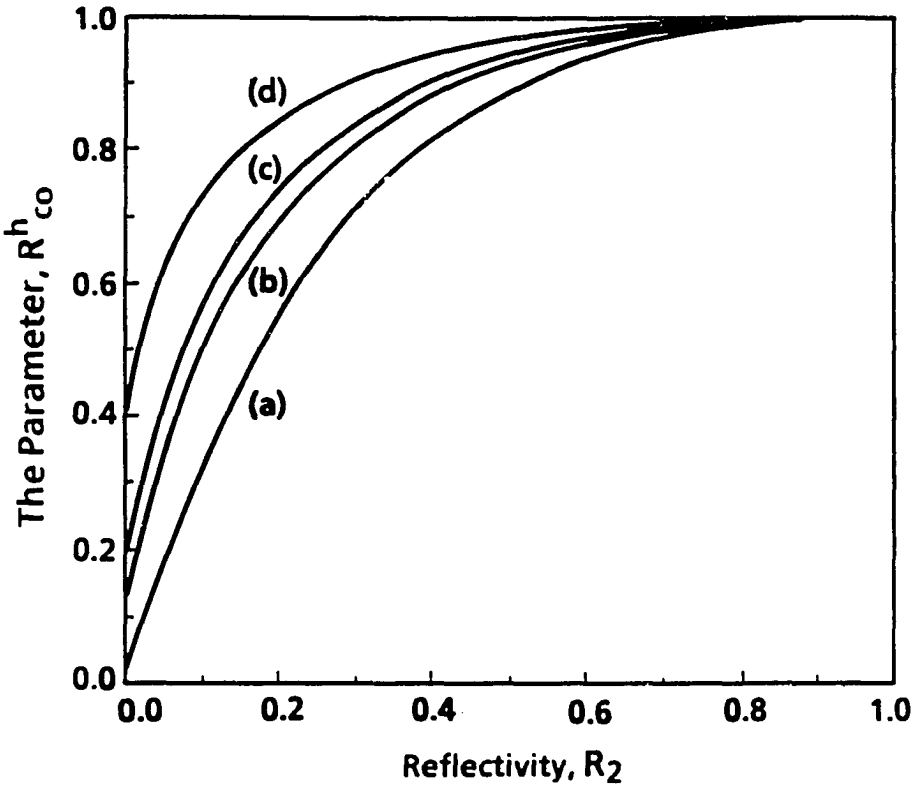

Figure 7.3. Variation of R_{co}^h with the reflectivity R_2 in the case of c_n = 1.0 for different values of R_m^l ; (a) R_m^l = 0, (b) R_m^l = 0.05, (c) R_m^l = 0.1, and (d) R_m^l = 0.3

$$\rho_e = \frac{\rho_2 + \rho_m \exp(-\alpha d)\exp(j\psi)}{1 + \rho_2 \rho_m \exp(-\alpha d)\exp(j\psi)} \tag{7.9}$$

and R_e is given by

$$R_e = \frac{R_2 + R_m \exp(-2\alpha'' d) + 2\rho_2 \rho_m \exp(-\alpha'' d)\cos(\psi - \alpha' d)}{1 + R_2 R_m \exp(-2\alpha'' d) + 2\rho_2 \rho_m \exp(-\alpha'' d)\cos(\psi - \alpha' d)} \tag{7.10}$$

Note that as α' and α'' approach to 0, Eq.(7.9) and (7.10) reduce to Eq.(7.1) and (7.2), respectively, as expected. From Eq.(4.46) and (7.7) we obtain

$$\alpha' = \frac{\Delta_n}{n\,d} \tag{7.11}$$

$$\alpha'' = \frac{\delta_n}{n\,d} \tag{7.12}$$

Because a circular beam spot is preferred to achieve high performance [78] for the optical disk head application, we consider, for simplicity's sake, the case where the emitting area of a laser diode has a square shape, that is , a = b. In this case, α'' and α' can be expressed as

$$\alpha' = 2\lambda N_a(n)\Delta_n / a^2 \tag{7.13}$$

$$\alpha'' = 2\lambda N_a(n)\delta_n / a^2 \tag{7.14}$$

It should be noted that the plot of R_e versus d, given by Eq.(7.10), has relative maxima and minima as in the previous case A. However, any two adjacent peaks or valleys do not have the same value of R_e, which is in contrast to the case A.

Following the procedure used in case A, we can derive the necessary condition for $P^h > P^l$, which is expressible as

$$R_m{}^h > R_c{}^h \tag{7.15}$$

where

$$R_c{}^h \equiv \left\{ \frac{Q - \rho_m{}^l \exp(-\alpha'' d_s)}{1 - Q\,\rho_m{}^l \exp(-\alpha'' d_s)} \right\} \exp(2\alpha'' d_l) \tag{7.16}$$

in which d_s represents the shortest distance at which $R_e{}^l$ has one of its relative maxima while d_l represents the longest distance at which $R_e{}^h$ has one of its relative minima within the range of d. Here $R_e{}^l$ denotes the value of R_e for the case of a low reflective medium with $\rho_m = \rho_m{}^l$; $R_e{}^h$ denotes that for the case of the high reflective medium $\rho_m = \rho_m{}^h$. These distances d_s and d_l must satisfy the following equations:

$$[\,\psi(d_s) - \alpha' d_s\,] = (2m_1 + 1)\,\pi \tag{7.17}$$

$$[\,\psi(d_l) - \alpha' d_l\,] = 2m_2\,\pi \tag{7.18}$$

where m_1 and m_2 are integers.

As an illustration, we consider a specific example where 2a = 2b = 1.2 μm, λ = 0.78 μm, and the corresponding Fresnel zone number becomes

$$N_a(n) = N_b(n) = \frac{a^2}{2\,n\,d\,\lambda} = \frac{0.231}{n\,d} \tag{7.19}$$

where the flying height d is given in micrometers. The variation of parameters α' and α" with N is calculated and illustrated in Figure 7.4. We observe that α' increases with N monotonically while α" increases with N initially then gradually decreases after it reaches a maximum.

In the optical disk head, since the flying height d is usually less than a few micrometers, we can determine the range of interest for N to be $0.05 < N < 0.5$. In this range, α" varies little and maintains almost a constant value of 0.015, whereas α' varies considerably, as shown ib Figure 7.4, even though α' also approaches a constant value as N approaches infinity. Fortunately the phase - modification effect by the presence of Δ_n of the coupling coefficient does not change the shape of plot of output power versus flying height very much except for a little transitional shift as shown in Figure 4.17(c). Therefore, in deriving the necessary condition for $P^h > P^l$, we can neglect the effect of phase modification, i.e., by setting $\alpha' = 0$ or $\Delta_n = 0$.

To satisfy the necessary condition for $P^h > P^l$ within the flying height range of $0.5\ \mu m < d < 1.5\ \mu m$ with $2a = 2b = 1.2\ \mu m$ and $\lambda = 0.78\ \mu m$, we can use Figure 7.4 and Eq.(7.14) to determine $\alpha'' = 0.3313\ (1/\mu m)$ and set $\alpha' = 0$. Consequently, we obtain $d_s = 0.585\ \mu m$ and $d_l = 1.56\ \mu m$ from Eqs.(7.17) and (7.18), respectively. Using the above parameters, the variation of the parameter R_c^h with R_2, given by Eq.(7.16), is illustrated for the different

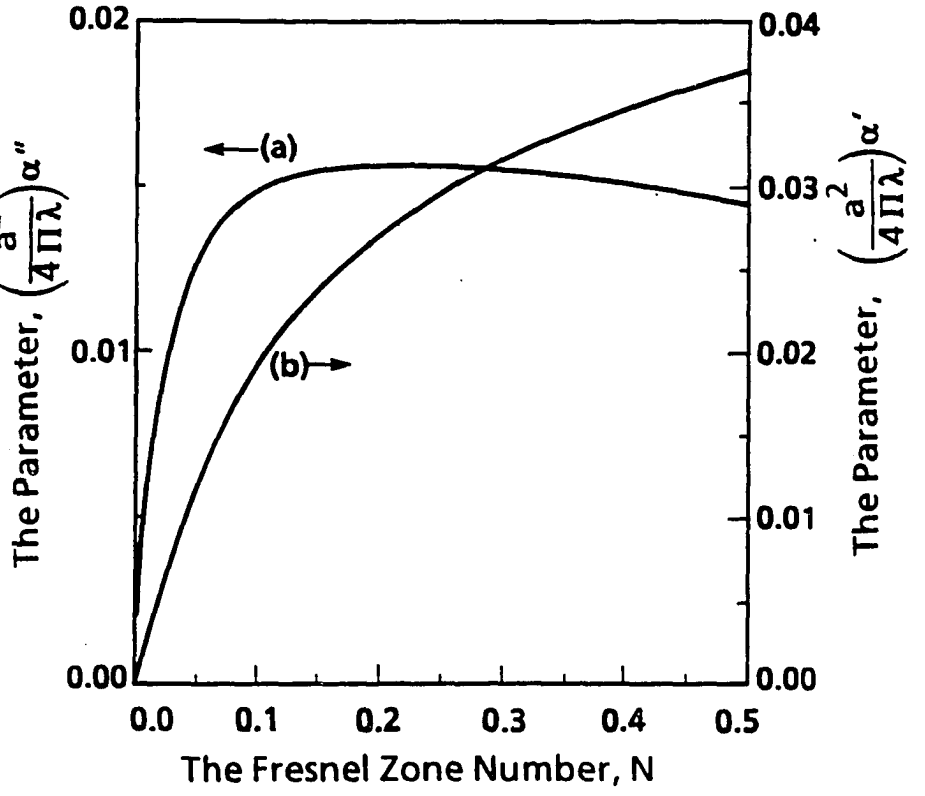

Figure 7.4. Variation of parameters $(a^2/4\pi\lambda)\,\alpha'$ and $(a^2/4\pi\lambda)\,\alpha''$ with Fresnel zone number N

values of R_m^l in Figure 7.5. This figure can be used as guide for the design of the optical disk head, which has a large tolerance in flying height. To check the validity of the criterion specified by Eq.(7.15), we choose the set of values of power reflectivities, $R_2 = 0.02$, $R_m^h = 0.6$, and $R_m^l = 0.04$, which satisfies the requirement Eq.(7.15). Keeping other parameters the same as those used in calculation of Figure 7.2, the plot of output power P_1 versus flying height d is calculated and illustrated in Figure 7.6. The result shown in Figure 7.6 clearly indicates that our prediction based on Eq.(7.15) has proven reasonable. Within the flying height range of $0.5\ \mu m < d < 1.5\ \mu m$, P^h is indeed greater than P^l. The comparison of Figures 7.2 and 7.6 also demonstrate the importance of the choice of values of R_2, R_m^h, and R_m^l in order to satisfy the condition $P^h > P^l$.

In summary, the necessary condition for which a short external - cavity laser diode can be used as the optical disk head is derived approximately. The optical disk head is one of the biggest area of commercial application of laser diodes. A single laser diode and reflecting surface of the optical disk can form an external cavity configuration. In order to make this optical disk head more practical, a large tolerance in flying height is preferred. By approximating our open resonator model derived in chapter 4 further to deal with the short lossy external cavity resonator, we have derived a criterion for this tolerance which we believe to be useful for the design of the optical disk head.

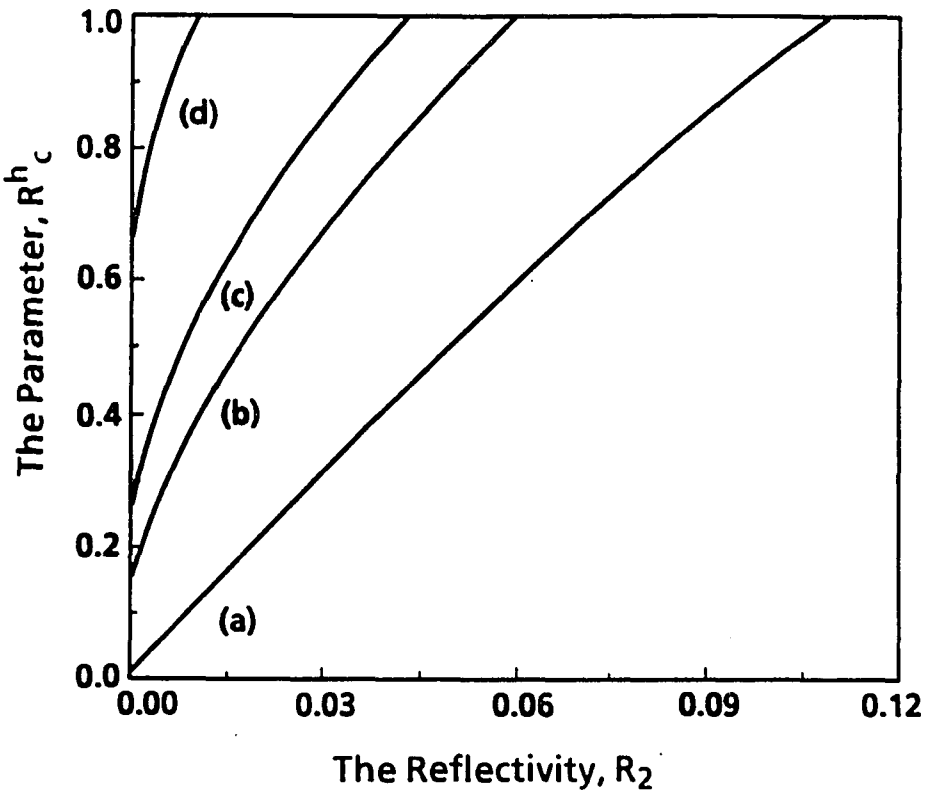

Figure 7.5. Variation of R_c^h with the reflectivity R_2 for different values of R_m^l in the case of 2a = 2b = 1.2 μm and λ = 0.78 μm $\alpha' = 0$, $\alpha'' = 0.3313\ \mu m^{-1}$, $d_s = 0.585\ \mu m$ and $d_l = 1.56\ \mu m$; (a) $R_m^l = 0$, (b) $R_m^l = 0.05$, (c) $R_m^l = 0.1$, and (d) $R_m^l = 0.3$

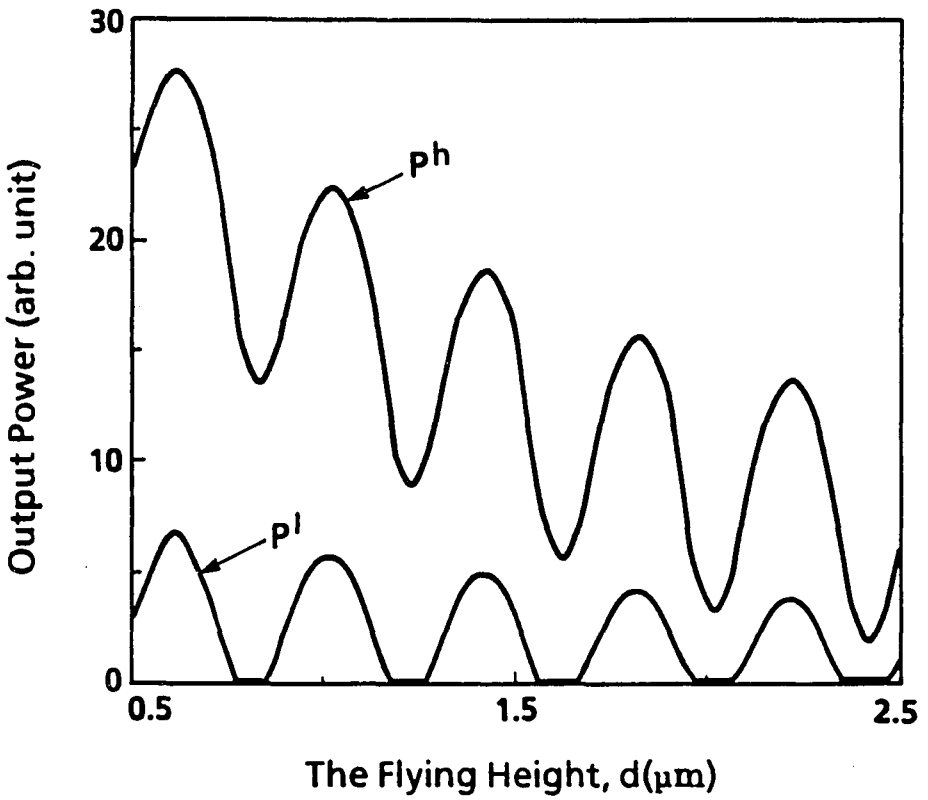

Figure 7.6. Variation of output power with the flying height d for the case $R_1 = 0.32$, $R_2 = 0.02$, $\lambda = 0.78$ μm, $2a = 2b = 1.2$ μm: The plot of P^h corresponds to $R_m{}^h = 0.6$, while that of P^l corresponds to $R_m{}^l = 0.04$

Laser Diode Sensor

Since the optical feedback from the external reflector strongly affects the laser diode properties, especially the light output power characteristic, the short external cavity configuration has been used to build various laser diode sensors [45,73]. In this section, we present measurements of the thermal distortion on the gold coated glass plate, produced by an modulated Ar laser beam. The results help to understand the liftoff effect in the photoinductive (PI) signal, which is the new dual-mode nondestructive evaluation (NDE) method, combining the thermal wave and eddy current methods [114 and references therein].

Figure 7.7 shows a schematic diagram of the experiment. A modulated Ar laser is focused on the 2.5 μm thick gold film through the 1 mm glass substrate to provide a thermal excitation, which is the same configuration as that used in the PI method. As usual, a decapsulated package (Mitsubishi ML4402 λ = 780 nm) of AlGaAs laser chip and Si photodiode is mounted on a temperature stabilized platform by means of a Peltier device. A laser diode is coupled to the opposite side of the gold film which forms the external cavity of the laser. As the gold film expands due to localized temperature perturbation, the coupling distance of the external cavity is changed which affects the output power level of the laser diode. The detected signal at the photodetector is fed to a lock-in amplifier to give a synchronized signal to the mechanical chopper which is used to modulate the Ar laser .

Since the output power shows the pseudo-periodic response to the external cavity length with a period of half a wavelength, the operating

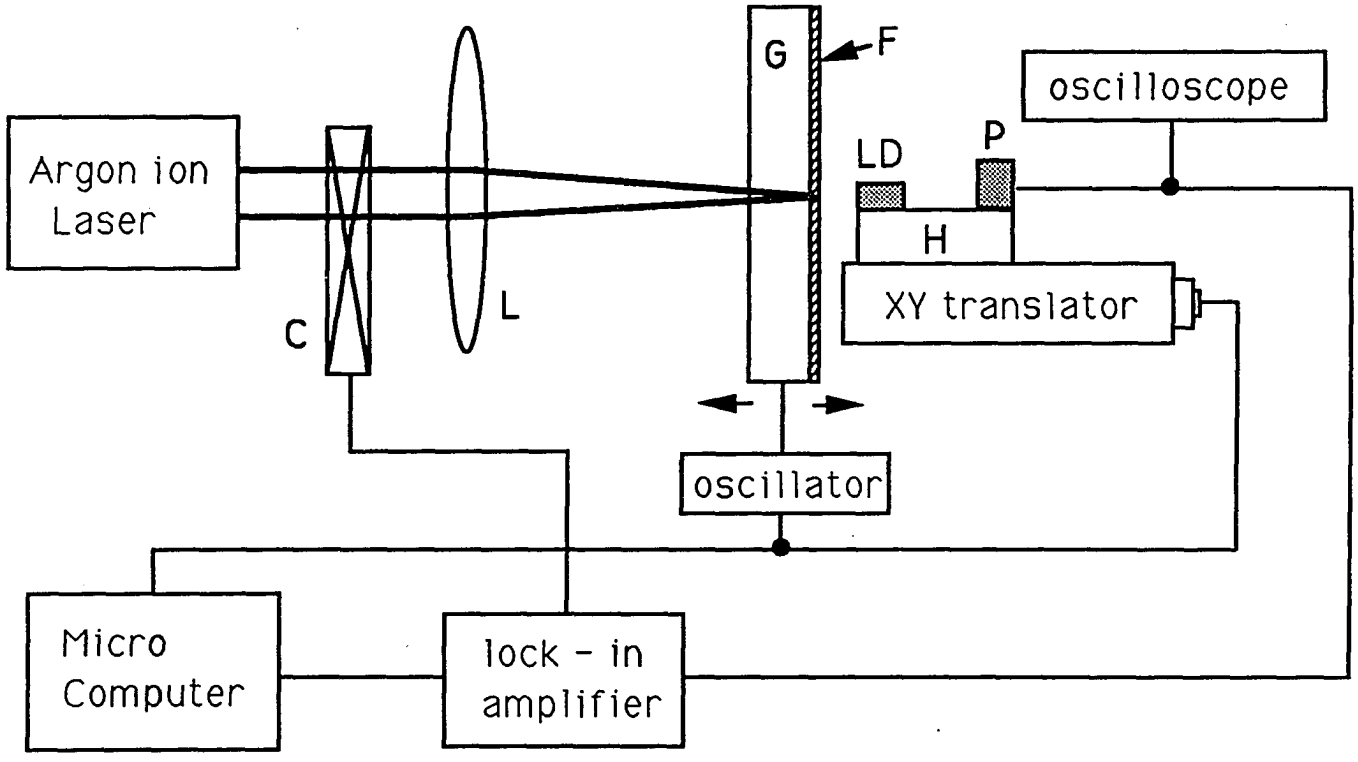

Figure 7.7. A schematic diagram of the experimental set-up, where C is a mechanical chopper, L is a lens, G is a glass substrate, F is a gold film, LD is a laser diode , P is a photo detector, and H is a temperature stabilized platform

distance (external cavity length without thermal excitation) should remain within several hundredth of a micron in order to give a linear small signal relationship. This can be done by introducing any kind of feedback to control either the operating distance or the wavelength, unless the thermal distortion height is larger than the quarter wavelength (0.19 μm) of the laser diode. At 20 Hz modulation, the thermal distortion height approaches this limit with 5W Ar laser power. In chapter 4, the asymmetry in the output response curve is discussed. Due to this phenomenon, the differential sensitivity $|\partial P/\partial d|$, which represents the ratio of the optical power change to the distortion height, can vary depending on the polarity of $\partial P/\partial d$. The sensitivity is greater at an upward slope than at a downward slope.

We devised a simple method to solve all these problems without any complicated feedback scheme. Extremely low frequency vibration is purposely introduced to the sample as shown in Figure 7.7. The amplitude is chosen to be small (about 2 μm) but large enough to cover the several periods of the response curve. During a preset window time a microcomputer finds a maximum value of the lock-in amplifier output, which is proportional to the distortion height that we want to measure. A result of a line scanning across the thermal spot is shown in Figure 7.8. As the modulation frequency increases, the thermal distortion height is shown in Figure 7.9. The error bars in the figure show the measurement obtained with the 1W Ar laser power, 0.1 Hz sample vibration, and a 13 second window time. The focal length of the lens L is 12 cm. The focused beam spot size is measured to be about 100 μm. The solid line in the figure is the best fit curve, which shows $f^{-0.814}$ dependence.

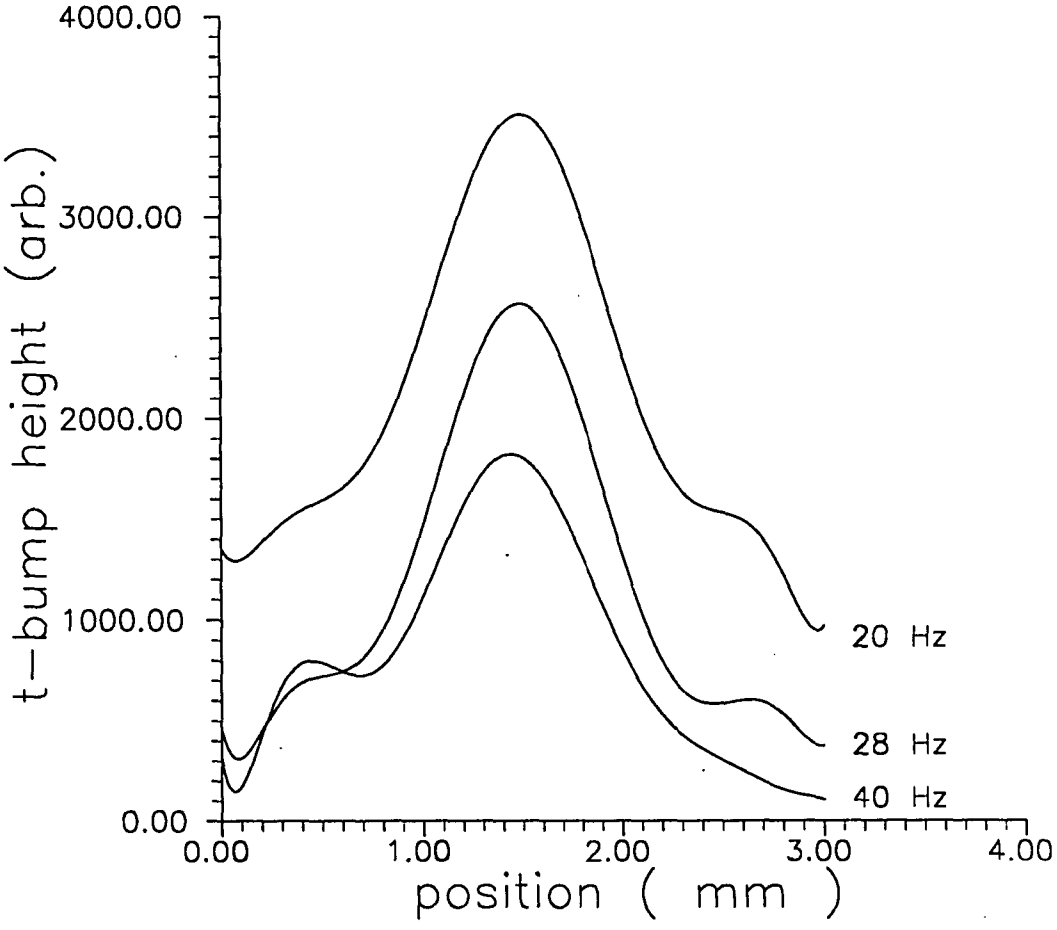

Figure 7.8. Results of a line scan across the thermal spot for various laser chopping frequency: The focal length of the lens is 12 cm, and the operating distance is about 50 μm

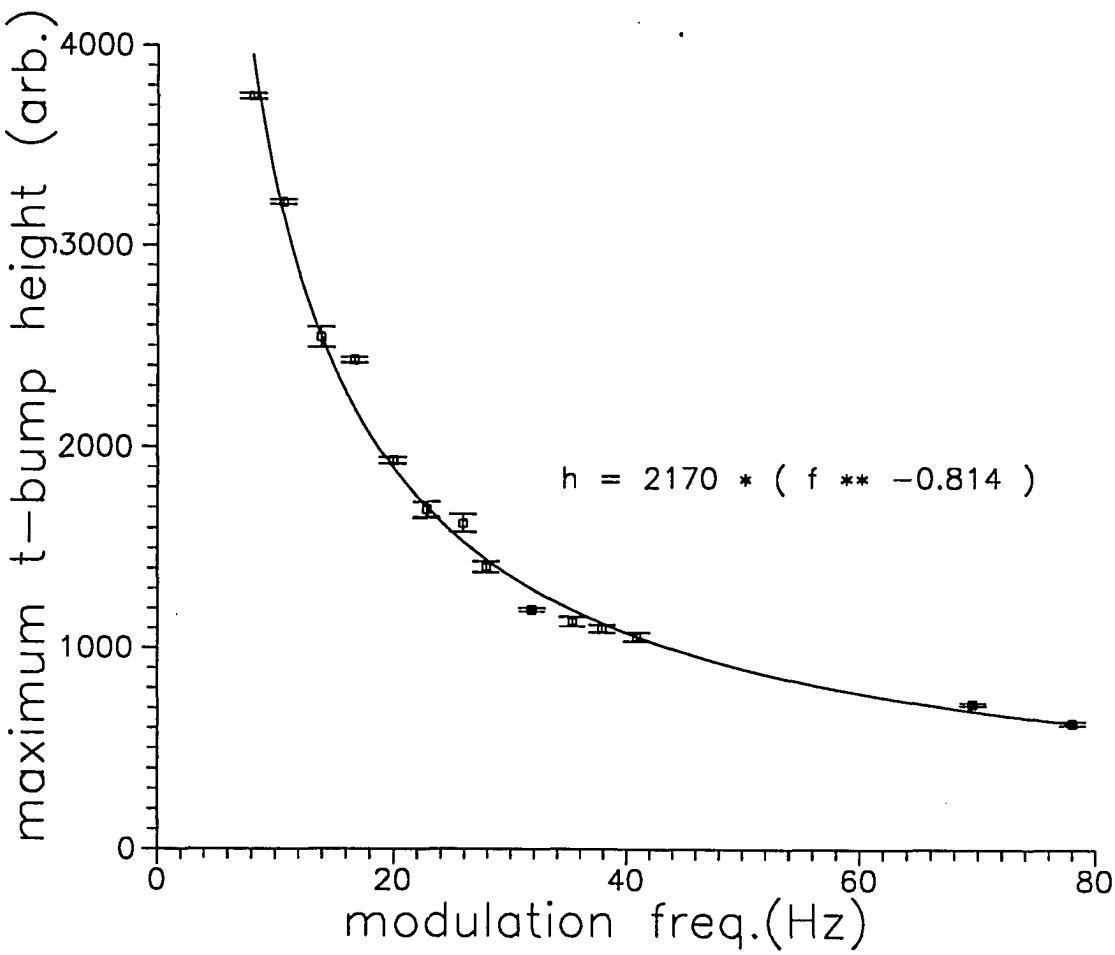

Figure 7.9. The dependence of thermal distortion height on the laser chopping frequency: The error bars represent the measured values, and the solid line is given by the best fit curve, where 1W Ar laser power, 0.1 Hz sample vibration, and a 13 second window time are used

Now, we will check the validity of our measurement results which are obtained using external cavity laser diode sensor. Comparing with the interferometric technique [115], the direct scan method can give an actual thermal distortion shape and direct reading of distortion height. The thermal diffusion length is defined as the distance over which the magnitude of a harmonic thermal wave decays exponentially to 1/e of its initial value, and it is given by [116]

$$L_{th} = (K / \pi f \rho C)^{0.5} \qquad (7.20)$$

where K is the thermal conductivity, ρ is mass density, and C is the specific heat. With the nominal values [117], L_{th} of gold and glass at 20 Hz can be calculated as 1.42 mm and 0.095 mm respectively. In our sample, Ar laser power is absorbed at the thin film layer of gold, but the heat diffusion process is controlled by both the gold layer and the glass substrate. Therefore, thermal spot size is expected to be some value between those two. Considering the beam divergence due to about 50 μm operating distance and 100 μm beam size, we may roughly estimate the effective distortion width as 0.8 mm from the result shown in Figure 7.8. The distortion height may be roughly calculated by [117]

$$h = \alpha_{th} \eta P / (2 \pi f \rho C A_{eff}) \qquad (7.21)$$

where α_{th} is the thermal expansion coefficient, P is the incident Ar laser power, η is the absorption efficiency, and A_{eff} is the effective heated area.

Using the nominal value of glass $\alpha_{th} = 10^{-5}$ and $A_{eff} = \pi (0.8) / 4$, $\eta = 0.5$, P = 5W, h becomes 0.2 μm, which agrees with the experiment as described earlier. A rigorous calculation of the surface displacement involves solving the Navier - Stokes equation [117], but frequency dependence may be qualitatively obtained from the simple relation described above for the two extreme cases. First, in the case where the laser spot size w is much greater than L_{th}, A_{eff} remains constant, so that thermal distortion height will have 1/f dependence. Second, in the opposite extreme of $w \ll L_{th}$, the thermal distortion height will be constant for the frequency change, since $A_{eff} \approx L_{th}^2$ is inversely proportional to the frequency. In our experiment w and L_{th} are comparable to each other, and the frequency dependence shown in Figure 7.9 is obtained.

Since the PI signal is more likely proportional to the surface integral of temperature change, rather than the volume integral, it shows different frequency characteristics from those of the thermal distortion height. Therefore, by comparing the frequency dependence of the PI signal and thermal distortion height, we hope to see the liftoff effect in the PI measurement. This is one application of the external laser diode sensor to measure small displacements directly.

CHAPTER 8. CONCLUSIONS

This work deals with the characteristics of external cavity laser diodes. Emphasis has been placed on the short external cavity configuration.

First, the general governing model equations which include the multiple reflection effect have been derived. The multiple reflection effect is handled with an effective reflectivity operator. Here, we take two different approaches to investigate the stationary solutions of model equations.

In the ultra short external cavity configuration, where external cavity length d is less than 20 μm, we show that the coupling coefficient c_n, representing the fractional amount of the coupled field into the laser diode at the n-th reflection, becomes a complex function of the external cavity length and the near field beam size of the laser diode. The coupling coefficient consists of an amplitude-reduction factor and a phase-modification factor. The diffraction loss is responsible for producing the complex coupling coefficient, which is derived through the open resonator theory. We observe experimentally the asymmetry in optical power versus external cavity length characteristic in the short external cavity configuration, and show that this phenomenon can be explained only by introducing a complex coupling coefficient, which proves the validity of our open resonator model. Applying this model, we have derived a criterion for which a short external cavity laser diode configuration can be used as the optical disk head practically, which we believe to be useful for the design of the optical disk head. The asymmetry has practical importance in laser diode sensor application, since the slope of the characteristic curve will determine the sensitivity of the sensor. In this analysis we have assumed a fixed lasing wavelength, which may be justified

since the amount of actual wavelength shift in the ultra short cavity configuration is very small.

When the external cavity length is longer than several 10 μm, the variation in coupling coefficient due to diffraction loss becomes negligible, and we may assume simply that $c_n = r^n$ (i.e., the external cavity resonator is regarded as a lossy resonator and constant loss per roundtrip is assumed). In this case, the normalized feedback operator Z(t) can be reduced to the closed form with slow varying and short cavity length approximation. The set of stationary solutions for the photon density, lasing frequency, and carrier density are studied. The graphical solution method is illustrated, and the single longitudinal mode condition has been derived. It has been shown that the single mode condition will be more likely met for the short external cavity laser and for the external reflectivity well below or beyond the facet reflectivity. In order to analyze rigorously the spectral characteristics of the short external cavity laser, it is recommended that a complex coupling coefficient, defined from open resonator theory, be used because the additional phase-modifying effect may affect the phase condition. Though the amount of the correction term is not significant, it may add some instability to the laser diode characteristics. This effect has been left for a future investigation.

Dynamical stabilities have been investigated for the stationary solutions obtained. External cavity operation changes the laser gain. Our analysis shows that lasing frequency change caused by this gain change effect has a dominant influence on the dynamical characteristics of the external cavity laser diode. As previously reported, shorter external cavity length tends to be more

stable than the longer one if every other parameter is kept the same. But, we show that even in case of the very short external cavity, dynamical instability may happen when the external reflectivity becomes close to the facet reflectivity, and simultaneously, feedback phase enters an out-of phase condition. The three coupled differential model equations are solved numerically by using the Runge - Kutta algorithm to give the time evolution of laser parameters. In order to do this easily, the model equations are transformed and normalized. Numerical simulation results agree well with the analytic solution in the simple case, which proves the validation of the simulation program. Also, with some approximation, they are solved analytically by linearized small signal expansion to give a simple expression for the relaxation oscillation frequency. It is shown that the relaxation oscillation characteristic is very different from that of the solitary laser diode and changes severely as feedback phase varies. We can not expect to find the strange attractor for the autonomous (d.c. bias current) system with our model due to the inherent characteristics of the approximations we made. In order to investigate rigorously dynamical stability and the possibility of chaos, we should solve our general model equations directly without further approximation, which may be a subject of future work.

The chaotic behavior in the current modulated external cavity laser diode is investigated for the first time, mainly based on the numerical solutions of model equations. We have found that the route to chaos in this nonautonomous system may not be limited to the period-doubling route, which had been believed to be the only route in the modulated solitary laser diode so far, by showing that there is a route to reach a chaotic band followed

by a 3-T window. Further study will be needed to investigate this chaotic behavior analytically and experimentally, and to make it clear what specific kind of route to chaos is involved in this case.

In general, we have drawn a conclusion that it is better to operate the external cavity laser at the operating distance close to the in-phase configuration (constructive interference position), since it will not only give better stationary properties such as higher optical output power at the same injection current level, but also will offer more stable dynamical characteristics for both autonomous and nonautonomous cases. In addition, it is the least sensitive operating position with respect to any parameter change.

Finally, we have shown the experimental results to measure the thermally expanded distribution of metal coated glass substrate as one of the application examples of the short external cavity laser diode. In performing this experiment, the asymmetry in the P - d curve should be considered and treated in a proper manner in order to obtain good results.

BIBLIOGRAPHY

[1] A. Einstein. "Die quanten theorie der strahlung." *Phys. Leit.* 18 (1917): 121.

[2] A.L. Schawlow, and C.H. Townes. "Infrared and optical masers." *Physical Review* 112 (1958): 1940 - 1949.

[3] T.H. Maiman. "Optical and microwave-optical experiments in ruby." *Physical Review Lett.* 4 (1960): 564 - 566.

[4] P.P. Sorokin, and M.J. Stevenson. "Stimulated infrared emission from trivalent uranium." *Physical Review Lett.* 5 (1960): 557 - 559.

[5] R.N. Hall, G.E. Fenner, J.D. Kingsley, T.J. Soltys, and R.O. Carlson. "Coherent light emission from GaAs junctions." *Physical Review Lett.* 9 (1962): 366 - 368.

[6] R. Lang, and K. Kobayashi. "External optical feedback effects on semiconductor injection laser properties." *IEEE J. Quantum Electron.* QE-16 (1980): 347 - 355.

[7] K.R. Preston, K.C. Woollard, and K.H. Cameron. "External cavity controlled single longitudinal mode laser transmitter module." *Electron.Lett.* 17 (1981): 931 - 932.

[8] K. Kikuchi, and T. Okoshi. "Simple formula giving spectrum - narrowing ratio of semiconductor laser output obtained by optical feedback." *Electon. Lett.* 18 (1982): 10 - 12.

[9] R. Wyatt, and W.J. Devlin. "10 kHz linewidth 1.5 μm InGaAsP external cavity laser with 55 nm tuning range." *Electron. Lett.* 19 (1983): 110 - 112.

[10] E. Patzak, H. Olesen, A. Sugimura, S. Saito, and T. Mukai. "Spectral linewidth reduction in semiconductor lasers by an external cavity with weak optical feedback." *Electron. Lett.* 19 (1983): 938 - 940.

[11] A.R. Chraplyvy, K.Y. Liou, R.W. Tkach, G. Eisenstein, Y.K. Jhee, T.L. Koch, P.J. Anthony, and U.K. Chakrabarti. "Simple narrow - linewidth 1.5 μm InGaAsP DFB external - cavity laser." *Electron. Lett.* 22 (1986): 88 - 89.

[12] G. Wenke, E. Patzak, and P. Meissner. "Reliable laboratory transmitter with submegahertz linewidth." *Electron. Lett.* 22 (1986): 206-207.

[13] R. Wyatt. "Spectral linewidth of external cavity semiconductor lasers with strong frequency-selective feedback." *Electron. Lett.* 21 (1985): 658 - 659.

[14] R.W. Tkach, and A.R. Chraplyvy. "Linewidth broadening and mode splitting due to weak feedback in single - frequency 1.5 μm lasers." *Electron. Lett.* 21 (1985): 1081 - 1083.

[15] N.K. Dutta, N.A. Olsson, and K.-Y. Liou. "Effect of external optical feedback on spectral properties of external cavity semiconductor lasers." *Electron. Lett.* 20 (1984): 588 - 589.

[16] M. Fujiwara, K. Kubota, and R. Lang. "Low - frequency intensity fluctuation in laser diodes with external optical feedback." *Appl. Phys. Lett.* 38 (1981): 217 - 220.

[17] Y.C. Chen. "Phase noise characteristics of single mode semiconductor lasers with optical feedback." *Appl. Phys. Lett.* 44 (1984): 10 -12.

[18] L.A. Coldren, and T.L. Koch. "External - cavity laser design." *J. Lightwave Technol.* LT-2 (1984): 1045 - 1051.

[19] O. Yamamoto, H. Hayashi, N. Miyauchi, S. Maei, H. Kawanishi, T. Morimoto, S. Yamamoto, S. Yano, and T. Hijikata. "Stable single longitudinal mode operation in visible (AlGa)As semiconductor lasers coupled with a short external cavity." *J.Appl.Phys.* 61 (1987) : 870 - 874.

[20] H. Kawanishi, H. Hayashi, O. Yamamoto, N. Miyauchi, S. Maei, S. Yamamoto, and T. Hijikata. "Stable single longitudinal mode operation over wide temperature range on semiconductor lasers with a short external cavity." *Japan. J. Appl. Phys.* 26 (1987): L590 - L592.

[21] T. Fujita, J. Ohya, K. Matsuda, M. Ishino, M. Sato, and H. Serizawa. "Narrow spectral linewidth characteristics of monolithic integrated - passive - cavity InGaAsP/InP semiconductor lasers." *Electron. Lett.* 21 (1985): 374 - 376.

[22] S. Murata, S. Yamazaki, I. Mito, and K. Kobayashi. "Spectral characteristics for 1.3 μm monolithic external cavity DFB lasers." *Electron. Lett.* 22 (1986): 1197 - 1198.

[23] N.K. Dutta, T. Cella, A.B. Piccirilli, and R.L. Brown. "Integrated external cavity laser." *Appl. Phys. Lett.* 49 (1986): 1227 - 1229.

[24] T.P. Lee, S.G. Menocal, S. Sakano, V. Valster, and S. Tsuji. "Linewidth and FM characteristics of a distributed feedback laser monolithically integrated with a tunable external cavity." *Electron. Lett.* 23 (1987): 153 - 154.

[25] N.A. Olsson, and W.T. Tsang. "Transient effects in external cavity semiconductor lasers." *IEEE J. Quantum Electron.* QE-19 (1983): 1479 - 1481.

[26] H. Temkin, N.A. Olsson, J.H. Abeles, R.A. Logan, and M.B. Panish. "Reflection noise in index - guided InGaAsP lasers." *IEEE J. Quantum Electron.* QE-22 (1986): 286 - 293.

[27] C.H. Henry, and R.F. Kazarinov. "Instability of semiconductor lasers due to optical feedback from distant reflectors." *IEEE J. Quantum Electron.* QE-22 (1986): 294 - 301.

[28] J. Mørk, B. Tromborg, and P.L. Christiansen. "Bistability and low - frequency fluctuations in semiconductor lasers with optical feedback : a theoretical analysis."*IEEE J. Quantum Electron.* 24 (1988): 123 - 133.

[29] F. Favre, and D. Le Guen. "Spectral properties of a semiconductor laser coupled to a single mode fiber resonator."*IEEE J. Quantum Electron.* QE-21 (1985): 1937 -1946.

[30] R.W. Tkach, and A.R. Chraplyvy. "Regimes of feedback effects in 1.5 μm distributed feedback lasers." *J. Lightwave Technol.* LT-4 (1986): 1655 - 1661.

[31] C. Voumard, R. Salathé, and H. Weber. "Resonance amplifier model describing diode lasers coupled to short external resonators." *Appl. Phys.* 12 (1977): 369 - 378.

[32] R.P. Salathé. "Diode lasers coupled to external resonators." *Appl. Phys.* 20 (1979) :1 - 18.

[33] T. Kanada, and K. Nawata. "Injection laser characteristics due to reflected optical power." *IEEE J. Quantum Electron.* QE-15 (1979): 559 - 565.

[34] R.A. Suris, and A.A. Tager. "Coherence and spectral properties of radiation emitted by a semiconductorlaser with an external reflector." *Soviet J. Quantum Electron.* 14 (1984): 21 - 26.

[35] P. Spano, S. Piazzolla, and M. Tamburrini. "Theory of noise in semiconductor lasers in the presence of optical feedback."*IEEE J. Quantum Electron.* QE-20 (1984): 350 - 357.

[36] C.H. Henry. "Theory of the linewidth of semiconductor lasers." *IEEE J. Quantum Electron.* QE-18 (1982): 259 - 264.

[37] C.H. Henry. "Phase noise in semiconductor lasers." *J. Lightwave Technol.* LT-4 (1986): 298 - 311.

[38] G.P. Agrawal. "Line narrowing in a single - mode injection laser due to external optical feedback."*IEEE J. Quantum Electron.* QE-20 (1984): 468-471.

[39] G.A. Acket, D. Lenstra, A.J. Den Boef, and B.H. Verbeek. "The influence of feedback intensity on longitudinal mode properties and optical noise in index - guided semiconductor lasers."*IEEE J. Quantum Electron.* QE-20 (1984): 1163 - 1169.

[40] N. Schunk, and K. Petermann. "Minimum bit rate of DPSK trnsmission for semiconductor laser with a long external cavity and strong linewidth reduction." *J. Lightwave Technol.* LT-5 (1987): 1309 - 1314.

[41] N. Schunk, and K. Petermann. "Numerical analysis of the feedback regimes for a single - mode semiconductor laser with external feedback." *IEEE J. Quantum Electron.* 24 (1988): 1242 - 1247.

[42] H. Ukita, Y. Katagiri, and S. Fujimori. "Supersmall flying optical head for phase change recording media." *Appl. Opt.* 28 (1989): 4360 - 4365.

[43] H. Ukita, Y. Sugiyama, H. Nakada, and Y. Katagiri. "Read/write performance and reliability of a flying optical head using a monolithically integrated LD - PD." *Appl. Opt.* 30 (1990): 3770 - 3776.

[44] R. Chung, R. Weber, and D.C. Jiles. "A Terfenol based mognetostrictive diode laser magnetometer." in *Proceedings of the 5th Joint MMM - Intermag Conference in Pittsburgh, Pensylvania June 1991,* to be published in *IEEE Trans. Magn.*

[45] R. Chung, J.-Y. Kim, R. Weber, J. Doherty, and J. Lamont. "Pocket - sized magnetometer with digital processing capabilities." in *Proceedings of the 29th annual EPRC meeting in Ames, Iowa May 1992,* ed. J. W. Lamont (Ames, Electric Power Research Center), 7-14.

[46] L.J. Bonnell, and D.T. Cassidy. "Allignment tolerances of short - external - cavity InGaAsP diode lasers for use as tunable single - mode sources." *Appl. Opt.* 28 (1989): 4622 - 4628.

[47] B.F. Ventrudo, and D.T. Cassidy. "Operating characteristics of a tunable diode laser absorption spectrometer using short - external - cavity and DFB laser diodes." *Appl. Opt.* 29 (1990): 5007 - 5013.

[48] J.H. Osmundsen and N. Gade. "Influence of optical feedback on laser frequency spectrum and threshold conditions." *IEEE J. Quantum Electron.* QE-19 (1983): 465 - 469.

[49] J.P. Van Der Ziel, and R.M. Mikulyak. "Single - mode operation of 1.3 μm InGaAsP/InP buried crescent lasers using a short external optical cavity." *IEEE J. Quantum Electron.* QE-20 (1984): 223 - 229.

[50] H. Sato and J. Ohya. "Theory of spectral linewidth of external cavity semiconductor lasers." *IEEE J. Quantum Electron.* QE-22 (1986): 1060 - 1063.

[51] J. Wang, H. Zhang, Q. Wu, and B. Zhou. "Single mode characteristics of short external cavity semiconductor lasers." *IEEE J. Quantum Electron.* QE-23 (1987): 1005 - 1009.

[52] R.-Q. Hui, and S.-P. Tao. "Improved rate equations for external cavity semiconductor lasers." *IEEE J. Quantum Electron.* 25 (1989): 1580 - 1584.

[53] J.-Y. Kim, and H.C. Hsieh. "An open - resonator model for the analysis of a short external - cavity laser diode and its application to the optical disk head." *J. Lightwave Technol.* LT-10 (1992): 439 - 447.

[54] J.-Y. Kim, and H.C. Hsieh. "Asymmetry in the optical output power characteristics of a short - external cavity laser diode." *IEEE Photon. Technol. Lett.* 4 (1992): 537 - 539.

[55] K. Petermann. *Laser diode modulation and noise.* Boston: Kluwer Academic Publishers, 1988.

[56] M. Lax, and W.H. Louisell. "Quantum noise IX : Quantum Fokker - Planck solution for laser noise." *IEEE J. Quantum Electron.* QE-3 (1967) : 47 - 58.

[57] M. Lax. "Quantum noise X : Density matrix treatment of field and population difference fluctuations." *Phys. Rev.* 157 (1967): 213 - 231.

[58] C.H. Henry. "Theory of spontaneous emission noise in open resonators and its application to lasers and optical amplifiers." *J. Lightwave Technol.* LT-4 (1986): 288 - 297.

[59] C.H. Henry. "Theory of the phase noise and power spectrum of a single mode injection laser." *IEEE J. Quantum Electron.* QE-19 (1983): 1391 - 1397.

[60] J.S. Cohen, R.R. Drenten, and B.H. Verbeek. "The effect of optical feedback on the relaxation oscillation in semiconductor lasers." *IEEE J. Quantum Electron.* 24 (1988): 1989 - 1995.

[61] B. Tromborg, and J. Mørk. "Nonlinear injection locking dynamics and the onset of coherence collapse in external cavity lasers." *IEEE J. Quantum Electron.* 26 (1990): 642 - 654.

[62] B. Tromborg, J.H. Osmundsen, and H. Olesen. "Stability analysis for a semiconductor laser in an external cavity." *IEEE J. Quantum Electron.* QE-20 (1984): 1023 - 1032.

[63] D.R. Hjelme, and A.R. Mickelson. "On the theory of external cavity operated single - mode semiconductor lasers." *IEEE J. Quantum Electron.* QE-23 (1987): 1000 - 1004.

[64] D.-S. Seo, J.-D. Park, J.G. McInerney, and M. Osinski. "Multiple feedback effects in asymmetric external cavity semiconductor lasers." *IEEE J. Quantum Electron.* 25 (1989): 2229 - 2238.

[65] H. Olesen, J.H. Osmundsen, and B. Tromborg. "Nonlinear dynamics and spectral behavior for an external cavity laser." *IEEE J. Quantum Electron.* QE-22 (1986): 762 - 773.

[66] L. Goldberg, H.F. Taylor, A. Dandridge, J.F. Weller, and R.O. Miles. "Spectral characteristics of semiconductor lasers with optical feedback." *IEEE J. Quantum Electron.* QE-18 (1982): 555 - 563.

[67] R.F. Kazarinov, and C.H. Henry. "The relation of line narrowing and chirp reduction resulting from the coupling of a semiconductor laser to a passive resonator." *IEEE J. Quantum Electron.* QE-23 (1987): 1401 - 1409.

[68] J.H. Osmundsen, B. Tromborg, and H. Olesen. "Experimental investigation of stability properties for a semiconductor laser with optical feedback." *Electron. Lett.* 19 (1983): 1068 - 1070.

[69] E. Patzak, A. Sugimura, S. Saito, T. Mukai, and H. Olesen. "Semiconductor laser linewidth in optical feedback configurations." *Electron. Lett.* 19 (1983): 1026 - 1027.

[70] R.S. Vodhanel, and J.-S. Ko. "Reflection induced frequency shifts in single - mode laser diodes coupled to optical fibers." *Electron. Lett.* 20 (1984): 973 - 974.

[71] J. O'Gorman, B.J. Hawdon, J. Hegarty, and D.H. Heffernan. "Feedback induced instabilities in external cavity injection lasers." *Electron. Lett.* 25 (1989): 114 - 115.

[72] E.G. Vicente de Vera, and E. Bernabéu. "External feedback effects on I/L characteristics of laser diode." *Electron. Lett.* 25 (1989): 976 - 978.

[73] R.O. Miles, A. Dandridge, A.B. Tveten, and T.G. Giallorenzi. "An external cavity diode laser sensor." *J. Lightwave Technol.* LT-1 (1983) : 81 - 92.

[74] C. Lin, C.A. Burrus, Jr., and L.A. Coldren. "Characteristics of single - longitudinal - mode selection in short - coupled cavity (SCC) injection lasers." *J. Lightwave Technol.* LT-2 (1984): 544 - 549.

[75] K. Kawano, T. Mukai, and O. Mitomi. "Optical output power fluctuation due to reflected lightwaves in laser diode modules." *J. Lightwave Technol.* LT-4 (1986): 1669 - 1677.

[76] L.A. Vainshtein. "Open resonators for lasers." *Soviet Phys. JETP.* 17 (1963): 709 - 719.

[77] A.G. Fox, and T. Li. "Resonant modes in a maser interferometer." *Bell Syst. Tech. J.* 40 (1961): 453 - 488.

[78] Y. Uenishi, Y. Isomura, R. Sawadt, H. Ukita, and T. Toshimad. "Beam converging laser diode by taper ridge waveguide." *Electron. Lett.* 24 (1988): 623 - 624.

[79] D. Ross. *Lasers, light amplifiers, and oscillators.* London/New York : Academic Press, 1969: 172 - 174.

[80] M. Ettenberg, H.S. Sommers, Jr., H. Kressel, and H.F. Lockwood. "Control of facet damage in GaAs laser diodes." *Appl. Phys. Lett.* 18 (1971): 571 - 573.

[81] F.C. Moon. *Chaotic vibrations : An introduction for applied scientists and engineers.* New York: John Wiley & Sons, 1987.

[82] T. Mukai, and K. Otsuka. "New route to optical chaos : successive - subharmonic - oscillation cascade in a semiconductor laser coupled to an external cavity." *Phys. Rev. Lett.* 55 (1985): 1711 - 1714.

[83] H. Sato, Y. Matsui, J. Ohya, and H. Serizawa. "Bistability and intensity noise of semiconductor lasers due to weak optical feedback." *J. Appl. Phys.* 63 (1988): 2200 - 2205.

[84] J. Mørk, P.L. Christiansen, and B. Tromborg. "Limits of stable operation of air - coated semiconductor lasers with strong optical feedback." *Electron. Lett.* 24 (1988): 1065 - 1066.

[85] K. Tatah, and E. Garmire. "Low-frequency intensity noise resonance in an external cavity GaAs laser for possible laser characterization." *IEEE J. Quantum Electron.* 25 (1989): 1800 - 1807.

[86] J.S. Cohen, and D. Lenstra. "Spectral properties of the coherence collapsed state of a semiconductor laser with delayed optical feedback." *IEEE J. Quantum Electron.* 25 (1989): 1143 - 1151.

[87] J. Wang, and K. Petermann. "Noise analysis of semiconductor lasers within the coherence collapse regime." *IEEE J. Quantum Electron.* 27 (1991): 3 - 9.

[88] J.S. Cohen, and D. Lenstra. "The critical amount of optical feedback for coherence collapse in semiconductor lasers." *IEEE J. Quantum Electron.* 27 (1991): 10 - 13.

[89] R. Müller, and P. Glas. "Bistability, regular self - pulsing, and chaos in lasers with external feedback." *J. Opt. Soc. Am. B.* 2 (1985): 184 - 192.

[90] J. Helms, N. Schunk, and K. Petermann. "Stable operation range for laser diodes with an integrated passive cavity in the presence of external optical feedback." *IEEE. Phot. Technol. Lett.* 1 (1989): 409 - 411.

[91] N. Schunk, and K. Petermann. "Stability analysis for laser diodes with short external cavities." *IEEE. Phot. Technol. Lett.* 1 (1989): 49 - 51.

[92] B. Tromborg, and J. Mørk. "Stability analysis and the route to chaos for laser diodes with optical feedback." *IEEE Phot. Technol. Lett.* 2 (1990) : 549 -552.

[93] C. Hayashi. *Nonlinear oscillations in physical systems.* New York: McGraw - Hill Book Company, 1964.

[94] J. Gibson. *Nonlinear automatic control.* New York: McGraw - Hill Book Company, 1963

[95] O.I. Elgerd. *Control systems theory.* New York: McGraw - Hill Book Company, 1967.

[96] D. Marcuse, and T.-P. Lee. "On approximate analytical solutions of rate equations for studying transient spectra of injection lasers." *IEEE J. Quantum Electron.* QE-19 (1983): 1397 - 1406.

[97] E.N. Lorentz. "Deterministic nonperiodic flow." *J. Atoms. Sci.* 20 (1963) : 130

[98] J.D. Farmer. "Chaotic attractors of an infinite - dimensional dynamical system." *Physica* 4D (1982): 366 - 393.

[99] T. Parker, and L. Chua. "Chaos : A tutorial for engineers." *Proceedings IEEE* 75 (1987): 982 - 1008.

[100] A. Mees, and C. Sparrow. "Some tools for analyzing chaos." *Proceedings IEEE* 75 (1987): 1058 - 1070.

[101] H.G. Schuster. *Deterministic chaos: an introduction: 2nd Ed.* Weinheim: VCH Verlagsgesellschaft mbH, 1988.

[102] P.W. Milonni, J.R. Ackerhalt, and M.-L. Shih, "Optical chaos." *Optics News* (March 1987): 34 - 37.

[103] K. Otsuka, and H. Kawaguchi. "Period - doubling bifurcations in detuned lasers with injected signals." *Phys. Rev. A.* 29 (1984): 2953 - 2956.

[104] C.-H. Lee, T.-H. Yoon, and S.-Y. Shin, "Period doubling and chaos in a directly modulated laser diode." *Appl. Phys. Lett.* 46 (1985): 95 - 97.

[105] Y. Hori, H. Serizawa, and H. Sato. "Chaos in a directly modulated semiconductor laser." *J. Opt. Soc. Am. B.* 5 (1988): 1128 - 1132.

[106] D. Ruelle, and F. Takens. "On the nature of turbulence." *Commun. Math. Phys.* 20 (1971): 167.

[107] S. Newhouse, D. Ruelle, and F. Takens. "Occurrence of strange axiom - A attractors near quasiperiodic floe on T^m , $m \geq 3$." *Commun. Math. Phys.* 64 (1978): 35

[108] J.R. Tredicce, N.B. Abraham, G.P. Puccioni, and F.T. Arecchi. "On chaos in lasers with modulated parameters : a comparative analysis." *Optics Commun.* 55 (1985): 131 - 134.

[109] T.-H. Yoon, C.-H. Lee, and S.-Y. Shin. "Perturbatiosn analysis of bistability and period doubling bifurcations in directly - modulated laser diodes." *IEEE J. Quantum Electron.* 25 (1989): 1993 - 2000.

[110] G.P. Agrawal. "Effect of gain nonlinearities on period doubling and chaos in directly modulated semiconductor lasers." *Appl. Phys. Lett.* 49 (1986): 1013 - 1015.

[111] M.J. Feigenbaum. "Quantitative universality for a class of nonlinear transformations." *J. Stat. Phys.* 19 (1978): 25.

[112] H. Ukita, Y. Katagiri, and Y. Uenishi. "Readout characteristics of micro - optical head in bi - stable mode." *Japan. J. Appl. Phys.* 26 suppl. 26-4 (1987): 111 - 116.

[113] N. Fukushima, K. Miura, and I. Sawaki. "Detection of magneto - optic signals using an external cavity laser diode." in *Tech. Dig. Top. Meet. on Opt. Data Storage,* 55 - 58. Washington DC: Optical Society of America

[114] M.S. Hughes, J.C. Moulder, M.W. Kubovich, and B.A. Auld. "Mapping eddy current probe fields using the photoinducive effect." in *Review of Progress in Quantitative NDE vol. 10A,* ed. D. O. Thompson, and D. E. Chimenti, 905 - 912. New York: Plenum, 1991.

[115] P.K. Kuo, M. Mundidasa. "Single beam interferometry of a thermal bump." in *Review of Progress in Quantitative NDE vol. 8A,* ed. D. O. Thompson, and D. E. Chimenti, 627 - 640. New York: Plenum, 1989.

[116] M.A. Olmstead, N.M. Amer, S. Kohn, D. Fournier, and C. Boccara. "Photothermal displacement spectroscopy : An optical probe for solids and surfaces." *Appl. Phys. A.* 32 (1983): 141 - 154.

[117] G.E. Myers. *Analytical methods in conduction heat transfer.* New York : McGraw - Hill Book Company, 1971.

[118] J.M.T. Thompson, and H.B. Stewart. *Nonlinear dynamics and chaos.* New York: John Wiley & Sons, 1986.

[119] W. Harth. "Large - signal direct modulation of injection lasers." *Electron. Lett.* 9 (1973): 532 - 533.

[120] C.-H. Lee, T.-H. Yoon, and S.-Y. Shin. "Large - signal modulation characteristics of a diode laser." *J. Korean Ins. Elect. Eng.* 23 (1986): 91 - 100.

[121] W. Harth, and D. Siemsen. "Subharmonic resonance in the direct modulation of injection lasers." *Arch. Elektron. Ubertragungstchn.* 28 (1974): 391 - 392.

ACKNOWLEDGEMENTS

I would like to express my sincere appreciation to Dr. Hsung-Cheng Hsieh for his inspiration, advice and guidance during the course of this work. Without his constant encouragement, I could not have completed this dissertation one way or another. Especially the last few months were extremely hard times for him. But he has never stopped helping me to finish this work. I owe my deepest gratitude to him.

I wish to express my gratitude to the entire Thermal Wave and Optics group at the Center for Nondestructive Evaluation at Iowa State University for providing me with a very pleasant and scientific atmosphere during the last three years. Special thanks go to Dr. Donald Thompson and Mr. John Moulder for providing me with generous funding during my graduate studies in ISU. Throughout this period I have had the honor and pleasure of working with Mr. Moulder, one of the best scientists I have ever met. I also appreciate all the valuable discussions I had with Dr. Michael Hughes, Dr. Norio Nakagawa and Mark Kubovich.

Also, I would like to extend my gratitude to my committee members Dr. William Lord, Dr. Robert Weber, Dr. Marshall Luban, and Dr. James Corones for their valuable comments and help which led to an improved dissertation. And I wish to extend a word of thanks to Dr. Rajbir Dahiya, who served as a substituting committee member in my Preliminary Examination.

Part of my graduate studies were supported by the Electrical Power Research Institute at ISU. During one year for performing the project, I am indebted a lot to Dr. John Lamont, Dr. Robert Weber, Dr. David Jiles, and Dr. John Doherty.

Special thanks to Russell W.-C. Chung, for all the time we had at ISU. I have learned enthusiasm from him. All the valuable discussions and his timely help are very much appreciated.

I would like to thank all my friends and family - my parents and brother - for their constant love, encouragement and support which make this dissertation possible.

Finally, I happily dedicate this dissertation to my wife Eun-Hai, and my son Hyun-Tai. I wish to express my utmost gratitude to Eun-Hai, for her love, cooperation, understanding , encouragement, unrecognized sacrifices, but most importantly for just 'being there'. This work could not have been started nor completed without my son's innocent smile and my wife's faithful love.

APPENDIX A. SINGLE MODE CONDITION AROUND OUT-OF PHASE POSITION

Here, we investigate the single mode condition Eq.(4.25) around $\Omega_s\tau = 2m\pi$ (out-of phase condition), since it is obvious that only around this region, single mode condition has a chance to fail as shown in Figure 4.11. Also, from Figure 4.10, we can narrow down the range of investigation to around $R'_m = R_2$. Let us assume

$$\Omega_s\tau = 2m\pi + \sigma, \quad |\sigma| << 1 \tag{A.1}$$

and

$$r\rho_m = -\rho_2\cdot(1+\delta), \quad |\delta| << 1 \tag{A.2}$$

or

$$R'_m = R_2(1+2\delta) \tag{A.3}$$

Then, the single mode condition (RHS of Eq.(4.25)) is approximately reduced to

$$\text{S.M.C.} = 1 - \frac{\tau}{\tau_{in}}\cdot\frac{1}{\delta}\left[\frac{1-R_2}{1+R_2} - \alpha\frac{\sigma}{\delta}\right] \tag{A.4}$$

which may be used as a rough estimating criterion.

When $R'_m < R_2$, i.e., $\delta < 0$, Eq.(A.4) shows that single mode condition is satisfied for $\sigma > 0$, i.e., $\Omega_s\tau > 2m\pi$, but for certain negative value of σ, it becomes dissatisfied. Also we can see that larger α, and smaller δ will give higher chance for multi - mode lasing.

APPENDIX B. DERIVATION OF THE STABILITY CONDITION

In this appendix, we derive the stability condition of Eq.(5.44) starting from the three coupled rate equations Eqs. (5.20)-(5.22). If we define the elements of the Jacobian matrix Eq.(5.41) as

$$F_{ij}\,|_s \equiv \frac{\partial F_i}{\partial X_j}\,|_s \tag{B.1}$$

where $X_1 = S_R$, $X_2 = N_R$, $X_3 = \Omega_R$, and subscript s denotes that partial derivatives are performed at the steady state equilibrium point (S_{RS}, N_{RS}, Ω_{RS}). Then, we obtain

$$F_{11}\,|_s = 0$$

$$F_{12}\,|_s = \frac{k_N S_{RS}}{1 + \frac{\tau}{\tau_{in}}[A - B]}$$

$$F_{13}\,|_s = \frac{2\frac{\tau_{ph}}{\tau_{in}} S_{RS}\left[\frac{dL}{d\Omega_R}\right]_s}{1 + \frac{\tau}{\tau_{in}}[A - B]}$$

$$F_{21}\,|_s = 1 - N_{RS} - \frac{1}{k_N}$$

$$F_{22}\,|_s = -\frac{\tau_{ph}}{\tau_s} - S_{RS}$$

$$F_{23}\,|_s = 0$$

$$F_{31}\,|_s = Y_S \cdot F_{21}\,|_s$$

$$F_{32}\,|_s = Y_S \cdot F_{22}\,|_s$$

$$F_{33}\,|_s = 0$$

where

$$Y_S \equiv \frac{\dot{\Omega}_R}{\dot{N}_R} \tag{B.2}$$

from Eq. (5.22).

To be dynamically stable, the real part of the eigenvalues of the Jacobian matrix should not have positive sign. Let p be the eigenvalues of **J**. The characteristic equation can be easily obtained as

$$p\,[\,p^2 - F_{22} \cdot p - F_{21} \cdot (F_{12} + F_{13} \cdot Y_S)\,] = 0 \tag{B.3}$$

Therefore, the eigenvalues are

$$p = 0 \ , \ \frac{F_{22} \pm [\, F_{22}^2 + 4\, F_{21}\, (F_{12} + F_{13}\, Y_S)\,]^{1/2}}{2} \tag{B.4}$$

Notice that

$$F_{22} = -S_{RS} - \frac{\tau_{ph}}{\tau_s} < 0$$

$$F_{21} < 0$$

The stability condition is reduced to

$$F_{12} + F_{13}\, Y_S > 0 \tag{B.5}$$

which will be reduced to the form in Eq. (5.44) after rearrangement.

$$p = 0 \ , \ \frac{F_{22} \pm [\, F_{22}^2 + 4\, F_{21}\, (F_{12} + F_{13}\, Y_S)\,]^{1/2}}{2} \tag{B.4}$$

Notice that

$$F_{22} = -S_{RS} - \frac{\tau_{ph}}{\tau_s} < 0$$

$$F_{21} < 0$$

The stability condition is reduced to

$$F_{12} + F_{13}\, Y_S > 0 \tag{B.5}$$

which will be reduced to the form in Eq. (5.44) after rearrangement.